

AD-750 902

INVESTIGATION OF DAMPING METHODS FOR  
AUGMENTOR COMBUSTION INSTABILITY

Gary D. Garrison, et al

Pratt and Whitney Aircraft

Prepared for:

Air Force Aero Propulsion Laboratory

October 1972

DISTRIBUTED BY:

**NTIS**

National Technical Information Service  
U. S. DEPARTMENT OF COMMERCE  
5285 Port Royal Road, Springfield Va. 22151

Reproduced From  
Best Available Copy

# INVESTIGATION OF DAMPING METHODS FOR AUGMENTOR COMBUSTION INSTABILITY

G. D. Garrison

P. L. Russell

J. Stettler

Pratt & Whitney Aircraft

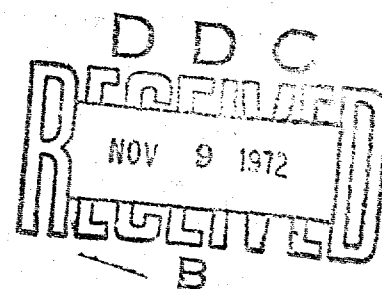
Division of United Aircraft Corporation  
Florida Research and Development Center

Technical Report AFAPL-TR-72-84  
October 1972

Approved for Public Release;  
Distribution Unlimited

NATIONAL TECHNICAL  
INFORMATION SERVICE

Air Force Aero Propulsion Laboratory  
Air Force Systems Command  
Wright-Patterson Air Force Base, Ohio



Reproduced From  
Best Available Copy

AD 750902

# NOTICE

When Government drawings, specifications, or other data are used for any purpose other than in connection with a definitely related Government procurement operation, the United States Government thereby incurs no responsibility nor any obligation whatsoever; and the fact that the Government may have formulated, furnished, or in any way supplied the said drawings, specifications, or other data, is not to be regarded by implication or otherwise as in any manner licensing the holder or any other person or corporation, or conveying any rights or permission to manufacture, use, or sell any patented invention that may in any way be related thereto.

|                                 |   |
|---------------------------------|---|
| ACCESSION No.                   |   |
| 1.5                             | White Section <input checked="" type="checkbox"/> |
| 000                             | Blue Section <input type="checkbox"/>             |
| UNAN. CODES                     | <input type="checkbox"/>                          |
| JUSTIFICATION                   |   |
| BY                              |   |
| DISTRIBUTION/AVAILABILITY CODES |   |
| Dist.                           | Avail. and/or SPECIAL                             |
|                                 |   |

Copies of this report should not be returned unless return is required by security considerations, contractual obligations, or notice on a specific document.

**Reproduced From  
Best Available Copy**

## **REPRODUCTION QUALITY NOTICE**

**This document is the best quality available. The copy furnished to DTIC contained pages that may have the following quality problems:**

- **Pages smaller or larger than normal.**
- **Pages with background color or light colored printing.**
- **Pages with small type or poor printing; and or**
- **Pages with continuous tone material or color photographs.**

**Due to various output media available these conditions may or may not cause poor legibility in the microfiche or hardcopy output you receive.**

☐ **If this block is checked, the copy furnished to DTIC contained pages with color printing, that when reproduced in Black and White, may change detail of the original copy.**

UNCLASSIFIED

Security Classification

## DOCUMENT CONTROL DATA - R &amp; D

(Security classification of title, body of abstract and indexing annotation must be entered when the overall report is classified)

|   |   |   |  |
|---|---|---|--|
| 1. ORIGINATING ACTIVITY (Corporate author)<br>Pratt & Whitney Aircraft<br>Division of United Aircraft Corporation<br>Florida Research and Development Center<br>West Palm Beach, Florida 33402  |   | 2a. REPORT SECURITY CLASSIFICATION<br>UNCLASSIFIED  |  |
|   |   | 2b. GROUP<br>N/A  |  |
| 3. REPORT TITLE<br>Investigation of Damping Methods for Augmentor Combustion Instability  |   |   |  |
| 4. DESCRIPTIVE NOTES (Type of report and inclusive dates)<br>Final Technical Report (71 March 01 to 72 October 31)  |   |   |  |
| 5. AUTHOR(S) (First name, middle initial, last name)<br>G. D. Garrison, P. L. Russell, and J. Stettler  |   |   |  |
| 6. REPORT DATE<br>October 1972  | 7a. TOTAL NO. OF PAGES<br>100 / 10 /  | 7b. NO. OF REFS<br>9  |  |
| 8a. CONTRACT OR GRANT NO<br>F33615-71-C-1361  | 9a. ORIGINATOR'S REPORT NUMBER(S)<br>FR-5163                                |   |  |
| b. PROJECT NO. 3066   |   |   |  |
| c. Task 05  | 9b. OTHER REPORT NO(S) (Any other numbers that may be assigned this report) |   |  |
| d. Work Unit 05   | AFAPL-TR-72-84  |   |  |
| 10. DISTRIBUTION STATEMENT<br>Approved for public release; distribution unlimited.  |   |   |  |
| 11. SUPPLEMENTARY NOTES   |   | 12. SPONSORING MILITARY ACTIVITY<br>Air Force Systems Command<br>Air Force Aero Propulsion Laboratory<br>Wright-Patterson AFB, Ohio 45433 |  |
| 13. ABSTRACT<br>Absorbing liners or "screech" liners are commonly used in the augmentors of turbo-propulsion systems to control combustion instability. Larger augmentors currently being proposed and developed can experience low frequency instabilities for which liners of conventional design are an impractical solution because of the unacceptably large volumes required for the liner resonator cavity. The objective of this program was to develop practical augmentor acoustic devices for controlling low frequency combustion instabilities. Analysis, supported by cold flow impedance experiments, indicated that (1) dimpled array liners, i.e., liners with punched and therefore lengthened apertures, (2) complex-porous liners having facings of two different porous materials in series, and (3) acoustic energy absorbing flameholders could provide sufficient absorption. To evaluate the effectiveness of candidate devices, a specially designed augmentor having inherent modes of low frequency instability was fabricated. Tests were conducted at fuel-air ratios of 0.05 and at stoichiometric; test sections consisted of a dimpled liner, a complex-porous liner, and three different absorbing flameholders. The augmentor was spontaneously unstable with frequencies less than 300 Hz when operated at design point conditions with no damping devices. Both liners reduced the amplitudes of the instability. The absorbing flameholders, however, were not found to be effective for suppressing the low frequency instability. From the results of the program it was concluded that dimpled array liners and complex-porous liners will suppress low frequency instability and can be designed with backing depths and facing thicknesses that are practical for augmentor installations. |   |   |  |

DD FORM 1473  
1 NOV 65

UNCLASSIFIED

Security Classification

I-A



# INVESTIGATION OF DAMPING METHODS FOR AUGMENTOR COMBUSTION INSTABILITY

G. D. Garrison  
P. L. Russell  
J. Stettler

Details of illustrations in  
this document may be better  
studied on microfiche

Approved for Public Release;  
Distribution Unlimited

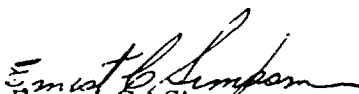
I-C

## FOREWORD

This report describes work accomplished in the program "Investigation of Damping Methods for Augmentor Combustor Instability," conducted under USAF Contract F33615-71-C-1361, Project 3066, Task 306605. The work was accomplished in the period from 1 March 1971 to 31 May 1972 by Pratt & Whitney Aircraft, Florida Research and Development Center, West Palm Beach, Florida. The report was submitted on 30 August 1972.

The program was sponsored by the Air Force Aero Propulsion Laboratory, Wright-Patterson Air Force Base, Ohio. The Air Force Project Engineer was Robert E. Henderson, Turbine Engine Division, and the Pratt & Whitney Aircraft Program Manager was Gary D. Garrison.

Publication of this report does not constitute Air Force approval of the report's findings or conclusions. It is published only for the exchange and stimulation of ideas.

  
Ernest C. Simpson

Director, Turbine Engine Division



## ABSTRACT

Absorbing liners or "screech" liners are commonly used in the augmentors of turbopropulsion systems to control combustion instability. Larger augmentors currently being proposed and developed can experience low frequency instabilities for which liners of conventional design are an impractical solution because of the unacceptably large volumes required for the liner resonator cavity. The objective of this program was to develop practical augmentor acoustic devices for controlling low frequency combustion instabilities. Analysis, supported by cold flow impedance experiments, indicated that (1) dimpled array liners, i. e., liners with punched and therefore lengthened apertures, (2) complex-porous liners having facings of two different porous materials in series, and (3) acoustic energy absorbing flameholders could provide sufficient absorption. To evaluate the effectiveness of candidate devices, a specially designed augmentor having inherent modes of low frequency instability was fabricated. Tests were conducted at fuel-air ratios of 0.05 and at stoichiometric; test sections consisted of a dimpled liner, a complex-porous liner, and three different absorbing flameholders. The augmentor was spontaneously unstable with frequencies less than 300 Hz when operated at design point conditions with no damping devices. Both liners reduced the amplitudes of the instability. The absorbing flameholders, however, were not found to be effective for suppressing the low frequency instability. From the results of the program, it was concluded that dimpled array liners and complex-porous liners will suppress low frequency instability and can be designed with backing depths and facing thicknesses that are practical for augmentor installations.

## CONTENTS

| SECTION  | PAGE |
|--|------|
| NOMENCLATURE . . . . .                             | xi   |
| I      PROGRAM SUMMARY . . . . .                   | 1    |
| A.    Background . . . . .                         | 1    |
| B.    Objective . . . . .                          | 3    |
| C.    Approach . . . . .                           | 3    |
| D.    Conclusions and Recommendations . . . . .    | 4    |
| II      DESIGN ANALYSES . . . . .                  | 6    |
| A.    Design Theory . . . . .                      | 6    |
| B.    Design Considerations . . . . .              | 9    |
| C.    Results of Analyses . . . . .                | 13   |
| III     COLD FLOW ACOUSTIC EXPERIMENTS . . . . .   | 24   |
| A.    Apparatus . . . . .                          | 24   |
| B.    Porous Absorber Experiments . . . . .        | 24   |
| C.    Ceramic Honeycomb Experiments . . . . .      | 33   |
| D.    Conclusions . . . . .                        | 34   |
| IV      AUGMENTOR SIMULATOR TEST PROGRAM . . . . . | 35   |
| A.    Hardware . . . . .                           | 35   |
| B.    Simulator Tests . . . . .                    | 60   |
| C.    Analysis of Data . . . . .                   | 70   |
| REFERENCES . . . . .                               | 84   |

## ILLUSTRATIONS

| FIGURE |  | PAGE |
|--------|--|------|
| 1      | Acoustic Liner Function Is Analagous to That of Mechanical Mass-Spring-Dashpot System . . . . .                                  | 1    |
| 2      | Low Frequency Combustion Instability Detected in Advanced Turbopropulsion System Augmentor Test . . . . .                        | 2    |
| 3      | Typical Resonant Absorber - An Array of Helmholtz-Type Resonators . . . . .  | 7    |
| 4      | Porous Absorber Configuration . . . . .  | 8    |
| 5      | Flow Resistance of Three Different Fibermetal Porous Facings . . . . .   | 10   |
| 6      | Wide Band Absorption Characteristics Achieved by Parametric Optimization . . . . .   | 11   |
| 7      | Liner Aperture and Cavity Gas Temperatures From Stable Rocket Chamber Tests . . . . .  | 12   |
| 8      | Cavity Gas Temperature vs Time for 15K LO <sub>2</sub> /LH <sub>2</sub> Rocket Chamber With 5% and 50% Absorption Coefficients . | 13   |
| 9      | Results of Porous Absorber Analysis, Effects of Variation in Cavity Depth. . . . .   | 14   |
| 10     | Results of Porous Absorber Analysis, Effect of Variation in Facing Flow Resistance . . . . .                                     | 15   |
| 11     | Results of Porous Absorber Analysis, Effect of Variation in Facing Thickness . . . . .   | 15   |
| 12     | Results of Porous Absorber Analysis, Effect of Variation in Facing Porosity . . . . .  | 16   |
| 13     | Dimpled Resonator Configuration . . . . .  | 16   |
| 14     | Absorption Characteristics of Dimpled Array Liner . . . . .  | 17   |
| 15     | Predicted Absorption Characteristics of Helmholtz-Type Acoustic Flameholder . . . . .  | 18   |
| 16     | Absorption Characteristics of Porous Resonator Flameholder . . . . .   | 19   |
| 17     | Absorption Characteristics of Porous Flameholder . . . . .   | 19   |

# ILLUSTRATIONS (Continued)

| FIGURE |  | PAGE |
|--------|--|------|
| 18     | Double Resonator in Series . . . . .   | 20   |
| 19     | Typical Absorption Curve for a Series Resonator Array<br>With Widely Separated Resonant Frequencies . . . . .                        | 21   |
| 20     | Typical Absorption Curve for a Series Resonator Array<br>With Narrow Separation of Resonant Frequencies . . . . .                    | 21   |
| 21     | Double Resonator in Parallel . . . . .   | 22   |
| 22     | Typical Absorption Curve for a Parallel Resonator Array .  | 22   |
| 23     | Low Frequency Impedance Tube . . . . .   | 25   |
| 24     | High Frequency Impedance Tube . . . . .  | 26   |
| 25     | Comparison of Predicted Absorption With Experiments<br>for Rigimesh Samples . . . . .  | 27   |
| 26     | Experimental Absorption Coefficients of Porous Inner<br>Material . . . . .   | 27   |
| 27     | Comparison of Experimental and Theoretical Absorption<br>Characteristics of 25% Porous, 0.9-in. Thick Rigimesh<br>Samples . . . . .  | 29   |
| 28     | Comparison of Experimental and Theoretical Absorption<br>Characteristics of 50% Porous, 0.9-in. Thick Rigimesh<br>Samples . . . . .  | 29   |
| 29     | Comparison of Experimental and Theoretical Absorption<br>Characteristics of 50% Porous, 1.25-in. Thick Rigimesh<br>Samples . . . . . | 30   |
| 30     | Complex-Porous Sample Absorption Characteristics . . . .   | 30   |
| 31     | Measured Absorption Characteristics of Cer-Vit<br>Porous Sample. . . . .   | 33   |
| 32     | Augmentor Simulator Schematic . . . . .  | 36   |
| 33     | Augmentor Simulator, Test Section Side . . . . .   | 37   |
| 34     | Augmentor Simulator, Nozzle End . . . . .  | 37   |

# ILLUSTRATIONS (Continued)

| FIGURE |  | PAGE |
|--------|--|------|
| 35     | Oscillatory Pressure Distributions (First Traverse Mode) in Annular Combustion Chamber and One With Splitter Plate . . . . . | 38   |
| 36     | Fuel Sprayring Design . . . . .  | 39   |
| 37     | Exhaust Nozzle Plate . . . . .   | 40   |
| 38     | Standard V-Gutter Flameholder . . . . .  | 41   |
| 39     | Cross Section of Augmentor Combustion Zone . . . . .   | 42   |
| 40     | Splitter Plate Hardware . . . . .  | 42   |
| 41     | Centerbody Cooling System . . . . .  | 44   |
| 42     | Liner Mounting Design Showing Dimpled Liner Installed . . . . .  | 45   |
| 43     | Design Sketch of Dimpled Liner Test Section . . . . .  | 46   |
| 44     | Design Sketch of Complex Porous Test Section . . . . .   | 47   |
| 45     | Assembled Dimpled Liner . . . . .  | 47   |
| 46     | Assembled Complex-Porous Liner . . . . .   | 48   |
| 47     | Porous Flameholder . . . . .   | 48   |
| 48     | Complex-Porous Flameholder . . . . .   | 49   |
| 49     | Acoustic Flameholder . . . . .   | 49   |
| 50     | Design Sketches of Flameholders Fabricated for Testing in Augmentor Simulator . . . . .                                      | 50   |
| 51     | Cross-Sectional Sketch of Pulse Gun Design . . . . .   | 51   |
| 52     | Pulse Gun . . . . .  | 52   |
| 53     | Dynamic Pressure Transducer and Pulse Gun Locations on Augmentor Simulator Rig . . . . .                                     | 52   |
| 54     | Sketch of Bomb Design . . . . .  | 53   |
| 55     | Water-Cooled Kistler Adapter . . . . .   | 54   |

# ILLUSTRATIONS (Continued)

| FIGURE |   | PAGE |
|--------|---|------|
| 56     | Modified Kulite Adapter . . . . .   | 55   |
| 57     | Instrumentation Diagram Showing Signal Conditioning<br>and Recording Channels . . . . .                                       | 56   |
| 58     | B-2 Test Stand Schematic . . . . .  | 57   |
| 59     | Schematic of Test Stand Fuel Supply System . . . . .  | 58   |
| 60     | Schematic of Test Stand TEB Supply System . . . . .   | 59   |
| 61     | Kistler Oscillograph Trace of Pulse Gun Firing,<br>Test 17 . . . . .  | 66   |
| 62     | Oscillograph Trace of Kulite and Kistler Dynamic<br>Pressure Data From Static Pulse Firing Test . . . . .                     | 67   |
| 63     | Oscillograph Trace of Static Bomb Firing Test . . . . .   | 68   |
| 64     | Typical Results From Real Time Spectrum Analysis -<br>Frequency Range 0-500 Hz, Kistler No. 1 . . . . .                       | 71   |
| 65     | Method for Determining Experimental Damping<br>Coefficient ( $\lambda D$ ) From the Dynamic Pressure<br>Decay Trace . . . . . | 72   |
| 66     | Maximum Low Frequency Amplitudes Measured With<br>Each Augmentor Configuration . . . . .                                      | 75   |
| 67     | Average Low Frequency Instability Data From Liner<br>and Baseline Tests . . . . .   | 75   |
| 68     | Comparison of Low Frequency Instability Data From<br>Absorbing Flameholder Tests With Baseline Results . . .                  | 76   |
| 69     | Comparison of Low Frequency Instability Data From<br>Porous Flameholder Tests . . . . .                                       | 77   |
| 70     | Typical Oscillograph Traces of Pulse Gun Firings . . . . .  | 78   |
| 71     | Comparison of Effects of Frequency Filtering on Decay<br>Time and Peak Amplitude . . . . .                                    | 81   |
| 72     | Comparison of Liner Cavity Gas Temperature . . . . .  | 82   |

# TABLES

| TABLE |  | PAGE |
|-------|--|------|
| 1     | Simulator Nominal Operating Conditions . . . . .                     | 14   |
| 2     | Rigimesh Samples - Low Frequency Tests . . . . .                     | 28   |
| 3     | Design Point Operating Conditions . . . . .                          | 60   |
| 4     | Augmentor Simulator Test Procedure . . . . .                         | 61   |
| 5     | Measured Augmentor Simulator Operating Conditions . . . .            | 62   |
| 6     | Augmentor Simulator Instability Data . . . . .                       | 73   |
| 7     | Augmentor Pressure Decay Data . . . . .                              | 79   |
| 8     | Average Damping Coefficients From Perturbation<br>Analysis . . . . . | 82   |

# NOMENCLATURE

| <u>Symbol</u>  | <u>Description</u>                         | <u>Units</u>  |
|----------------|--|---|
| A              | Aperture Area                              | in <sup>2</sup>   |
| c              | Sonic Velocity                             | ft/sec  |
| C <sub>f</sub> | Aperture Flow Coefficient                  |   |
| d              | Aperture Diameter                          | in.   |
| f              | Frequency                                  | Hz  |
| i              | $\sqrt{-1}$                                |   |
| k              | Wave Number                                | ft <sup>-1</sup>  |
| L              | Cavity Depth                               | in.   |
| ℓ              | Effective Aperture Length                  | in.   |
| M              | Mach Number                                |   |
| P              | Pressure Amplitude (Peak Value)            | lb <sub>f</sub> /in <sup>2</sup> , db*,<br>lb <sub>f</sub> /ft <sup>2</sup> |
| P <sub>c</sub> | Combustion Pressure, Static                | lb <sub>f</sub> /in <sup>2</sup>  |
| p              | Porosity of Porous Material                |   |
| Q              | Quality Factor                             |   |
| t              | Facing Thickness                           | in.   |
| T              | Temperature                                | deg R   |
| R              | Flow Resistance                            | lb <sub>m</sub> /ft <sup>3</sup> -sec                                       |
| S              | Surface Area                               | in <sup>2</sup>   |
| u              | Particle Velocity in Aperture (Peak Value) | ft/sec  |
| V              | Volume                                     | in <sup>3</sup>   |
| W <sub>v</sub> | Viscous Losses                             | lb <sub>m</sub> /ft <sup>2</sup> /sec <sup>4</sup>                          |
| Z              | Specific Acoustic Impedance                |   |

---

\*Reference: 0.0002 microbar



# NOMENCLATURE (Continued)

| <u>Symbol</u> | <u>Description</u>                       | <u>Units</u>                     |
|---------------|--|----------------------------------|
| $\alpha$      | Absorption Coefficient                   |                                  |
| $\eta_c$      | Combustion Efficiency                    |                                  |
| $\tau$        | Time                                     | sec                              |
| $\theta$      | Specific Acoustic Resistance Ratio       |                                  |
| $\rho$        | Aperture Gas Density                     | lb <sub>m</sub> /ft <sup>3</sup> |
| $\rho_c$      | Effective Gas Density in Porous Material | lb <sub>m</sub> /ft <sup>3</sup> |
| $\sigma$      | Open Area Ratio                          |                                  |
| $\epsilon$    | $(P_c/\rho_c)^{1/2}$                     | ft/sec                           |
| $\omega$      | Angular Frequency                        | sec <sup>-1</sup>                |
| $\chi$        | Specific Acoustic Reactance Ratio        |                                  |
| $\delta$      | Effective Length Correction Factor       |                                  |
| $\mu$         | Viscosity                                | lb <sub>m</sub> /ft-sec          |
| $\lambda_D$   | Damping Coefficient                      |                                  |

## Subscripts

|   |                                  |
|---|----------------------------------|
| 0 | Resonance                        |
| 1 | At Liner Facing                  |
| 2 | In Liner Cavity                  |
| a | Conditions in Aperture           |
| c | Conditions in Combustion Chamber |
| i | Conditions in Impedance Tube     |
| n | No Flow                          |
| p | Past Flow                        |

## NOMENCLATURE (Continued)

| <u>Symbol</u>                 | <u>Description</u>       | <u>Units</u> |
|-------------------------------|--------------------------|--------------|
| <u>Subscripts (Continued)</u> |                          |              |
| r                             | Simulator Rig Conditions |              |
| s                             | At Boundary Surface      |              |
| t                             | Through Flow             |              |

## SECTION I

### PROGRAM SUMMARY

#### A. BACKGROUND

The phenomenon of combustion instability has plagued all types of high heat-release combustors from industrial furnaces to rocket engines. In general, however, the problem has been most severe in flight propulsion systems, such as turbojets, ramjets, and rockets, where weight considerations dictate highly efficient structures. In such applications, the pressure, vibration, and heat loads resulting from combustion instability, superimposed on the normal loading, are usually destructive.

In airbreathing engines, solutions to high frequency combustion instability problems were first sought through mathematical modeling and analytical studies directed toward an understanding of the phenomenon. These proved inadequate, and "cut and try" empirical approaches involving changes in flameholders, combustion chamber shape, fuel injection, velocity profiles, and flame piloting were attempted. Fuel additives and combustion chamber baffles were also tested. Although some of these approaches, notably baffles, produced marginal improvement, the problem was not solved until damping devices in the form of acoustical absorbers (screech liners) were introduced. Screech liners are now used routinely, and high frequency instability is no longer regarded as a problem.

The success of screech liners results from the fact that combustion instability is a regular cyclic oscillation, usually correlatable with one of the principal acoustic modes of the combustion chamber. This indicates a feedback mechanism where each new cycle is triggered by the reflection of a previous cycle pressure wave from the chamber wall. Screech liners eliminate or reduce the reflection of pressure waves from any surface. As shown in figure 1, the theory of operation is analogous to that of the mechanical mass-spring system; that is, the mass of gas oscillating in the liner apertures corresponding to a mechanical mass sliding over a resistive surface and the compressibility of the gas in the resonator cavity acting like the spring in the mechanical system.

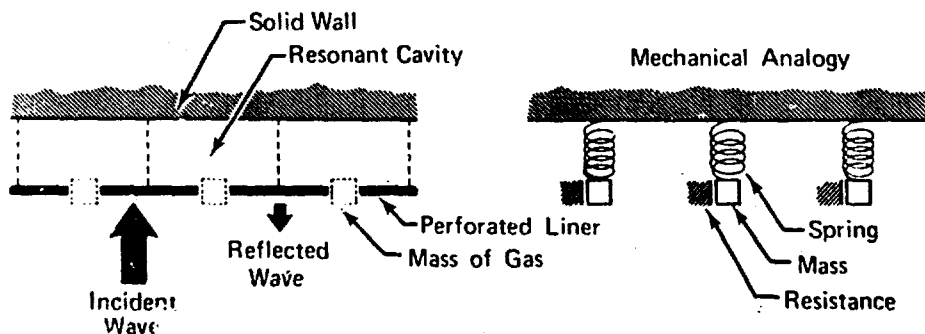


Figure 1. Acoustic Liner Function Is Analogous to That of Mechanical Mass-Spring-Dashpot System

FD 65583

For future applications, larger and more powerful turbopropulsion systems are presently being designed and developed. Because of the large physical dimensions of augmentors used in these systems, their natural acoustic modes have correspondingly long wave lengths; therefore, combustion instability can occur at very low frequencies, i. e., approximately 200 Hz or less. Evidence of low frequency combustion instability occurrence is presented in figure 2; the augmentor combustor pressure oscillations shown were recorded during a recent test of an advanced turbopropulsion system at FRDC.

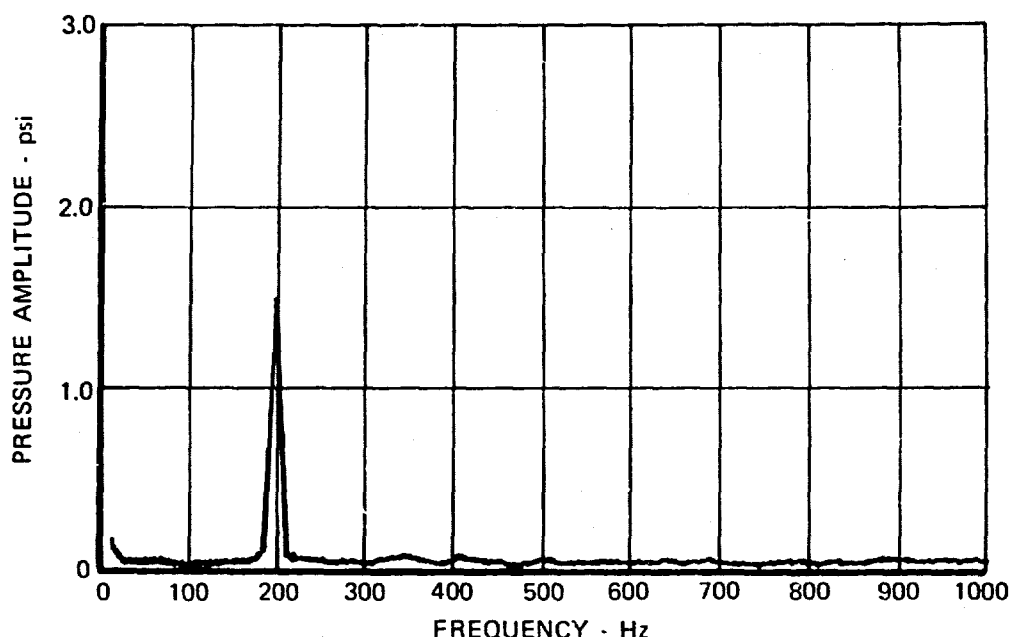


Figure 2. Low Frequency Combustion Instability  
Detected in Advanced Turbopropulsion  
System Augmentor Test

FD 65584

The occurrence of instability at lower frequencies makes use of the perforated liners of conventional design difficult. To obtain adequate damping, the absorbing devices are designed so that the frequency of resonance corresponds to the frequency of the expected mode of instability. The resonance frequency of conventional acoustic absorbers, which are typically arrays of Helmholtz-type resonators, is dependent upon the geometry of the system according to:

$$f_o = \frac{c}{2\pi} \sqrt{\frac{A}{Vl}} \quad (1)$$

where

$f_o$  = Resonance frequency

$A$  = Cross-sectional area of apertures

$V$  = Resonator cavity volume

$l$  = Effective length of apertures (approximately the thickness of the facing)

$c$  = Sonic velocity of media

Inspection of equation (1) reveals that the required cavity volume and effective aperture length are proportional to the resonance frequency that causes practical application problems for low frequencies. Good absorption characteristics can theoretically be obtained if the required cavity volume is provided; however, great volumes result in large augmentor envelopes, which increase engine weight. Similarly, use of smaller cavities with increased effective aperture length would require a thicker liner facing, which would impose a weight penalty as well as introducing complex cooling requirements.

## B. OBJECTIVE

The objective of the work reported herein was the development of acoustic damping techniques and devices for suppressing low frequency combustion instability that are not necessarily restricted to the dimensional limitations of conventional liners and are practical for turbopropulsion augmentor installations.

## C. APPROACH

To meet the objective, a program consisting of three separate tasks was conducted. In the first task, an analysis of potential low frequency damping devices was performed consisting of, where possible, calculations of the absorption coefficient of candidate configurations for frequencies from 50 to 300 Hz. The results of the analysis indicated that two different types of combustion chamber liners would produce adequate absorption, with facing thickness and cavity volumes that would be reasonable for flightweight augmentor installations. The types of liners were dimpled arrays, i.e., thin facings consisting of arrays of apertures formed by a dimpling process to lengthen the aperture neck and liners with porous facings made from materials such as Rigimesh\* and/or Feltmetal.\*\* The absorption coefficients of dimpled arrays were predicted using Helmholtz resonator theory modified to account for long apertures and the flow of combustion gases past the liner. The Beranek theory, Reference 1, was used to predict the absorption of porous liner configurations.

The high energy release region in the vicinity of the augmentor flameholder is a primary source of combustion instability. An acoustic absorber incorporated within the flameholder might be an effective damping device because of its close proximity to the instability source. The analysis required for the design of absorbing flameholders was included in the Task I effort. It was found that resonators having satisfactory absorption at low frequencies could be incorporated in conventional V-gutter flameholders by installing a facing across the downstream side so that the resulting enclosed volume can act as a resonator cavity. Use of a porous material for the facing, or one or more rows of apertures in a solid facing, would then cause the assembly to have acoustic characteristics typical of Helmholtz-type arrays.

Other types of devices that were considered for use as low frequency instability suppressors were baffles, quarter wave length cavities, and complex resonators, i.e., series and parallel combinations of Helmholtz-type arrays.

---

\*Rigimesh is the trade name of a porous, sintered wire mesh material manufactured by Aircraft Porous Media, Long Island, New York.

\*\*Feltmetal is the trade name of a porous fibermetal manufactured by Huych Metals Company, Milford, Connecticut.

Under Task II, cold-flow acoustic experiments were conducted to verify, where necessary, the predicted absorbing characteristics of the devices studied in Task I, to determine the absorption of candidate materials for which no theory exists, and to provide data for improvement of the theories. An existing ASTM-type impedance tube was modified for use at low frequencies and used to obtain the acoustic data. With this apparatus, it was possible to inexpensively reproduce the oscillation pressure amplitudes and frequencies experienced in large augmentors and to measure the acoustical parameters associated with the design of a particular damping device while it is subject to those conditions.

The results of the first two tasks indicated that dimpled liners, complex-porous liners, and absorbing flameholders could be designed for adequate acoustic absorption at frequencies below 300 Hz with configurations practical for augmentor installations. To evaluate the effectiveness of the devices for suppressing low frequency combustion instability, a boilerplate augmentor simulator in which the devices could be tested was fabricated. Air for the augmentor, a specially designed annular combustor, was bled from the compressor of a slave turbojet engine. The combustion chamber was designed so that the path length for pressure perturbations produced by explosive pulse guns would have a corresponding frequency of approximately 100 Hz, and the natural frequency of the tangential mode would be approximately 200 Hz. In addition to the dimpled and complex-porous liners, which were one-quarter annular sections, three different absorbing flameholders were fabricated for the augmentor.

Sixty tests of 13.5-sec duration were conducted at two fuel-air ratios, 0.05 and stoichiometric. Baseline tests, i.e., with no damping devices installed, showed that combustion at the lower mixture ratio was spontaneously unstable with frequencies from 210 to 290 Hz; at stoichiometric conditions, high frequency instability also occurred with nominal frequencies of 1100, 1470, and 5400 Hz. Similar tests were conducted with each of the five damping devices installed; their effect on the combustion instability was determined by comparing dynamic pressure amplitudes with those from the baseline tests and by computing decay coefficients from perturbation decay data.

#### D. CONCLUSIONS AND RECOMMENDATIONS

From the results of this program, the following conclusions were made:

1. Both the dimpled liner and the complex-porous liner were effective in suppressing low frequency combustion instability.
2. If the liners had been full annular sections, instead of quarter annular sections, low frequency instability would have been essentially eliminated.
3. All three absorbing flameholders had an adverse effect on the low frequency instability, i.e., amplitude levels were higher than those of the baseline tests.
4. Each of the absorbing flameholders completely eliminated the high frequency instability.

5. Dimpled array liners and complex-porous liners, which suppress low frequency instability, can be designed with backing depths and facing thicknesses that are practical for augmentor installations.
6. Effective dimpled array and complex-porous liners require no supplementary cooling.

The following recommendations are made:

1. Additional development of the absorbing flameholder concept should be conducted; the devices could be used in conjunction with liners to produce extremely wide-band damping systems.
2. The results of this program have demonstrated that porous liners, if properly designed, can suppress combustion instability over a wide range of frequencies; however, the design of such liners requires cold flow experimental data for selection of configurations and scaling of the data to the desired hot test conditions. Additional porous liner development should be conducted, consisting of cold flow impedance experiments and the formulation of more effective porous liner design theory.
3. The effects of centrifugal force fields on augmentor combustion stability should be investigated.
4. Additional augmentor tests should be conducted with a choked nozzle at a chamber pressure of 30 psia to investigate combustion stability characteristics under sea level augmentor operating conditions.

## SECTION II

### DESIGN ANALYSES

Analyses were conducted to determine the types of damping devices that would provide good absorption of low frequency pressure oscillations with minimum volume and weight requirements. Included in the following paragraphs are discussions of the acoustic theory used, descriptions of damping devices studied, and results of the analyses.

#### A. DESIGN THEORY

##### 1. Helmholtz-Type Resonant Absorbers

As shown by theory developed in Reference 2, the absorption coefficient of resonant absorbing devices, i. e., arrays of Helmholtz-type resonators with a common cavity volume, figure 3, is computed from

$$\alpha = \frac{4\theta}{(\theta + 1)^2 + \chi^2} \quad (1)$$

where the specific reactance ratio,  $\chi$ , is computed from

$$\chi = \frac{2\pi f_0 \ell}{12c\sigma} (f/f_0 - f_0/f) \quad (2)$$

In these equations the specific resistance ratio,  $\theta$ , and the effective aperture length,  $\ell$ , are functions of the particular flow environment to which the absorber is subjected. If there is no net flow through or past the facing, the effective length is computed from

$$\ell = t + \delta d \quad (3)$$

Where the effective length correction factor,  $\delta$ , is

$$\delta = 0.85d (1 - 0.7 \sqrt{\sigma}) \quad (4)$$

and the specific resistance ratio from

$$\theta = 0.37 u/c C_f^2 \sigma \quad (5)$$

where the amplitude of oscillations in the apertures,  $u$ , or particle velocity, is found by solving

$$u^4 + (2.7 \sigma c C_f^2 u \chi)^2 \left( \frac{P_1 C_f^2 g}{0.37 \rho} \right)^2 \quad (6)$$



In equation (6),  $P_1$ , the pressure amplitude at the liner facing (in units of  $\text{lb}_f/\text{ft}^2$ ), is the highest amplitude permitted for combustion to be considered stable, e. g., 5% of combustion pressure.

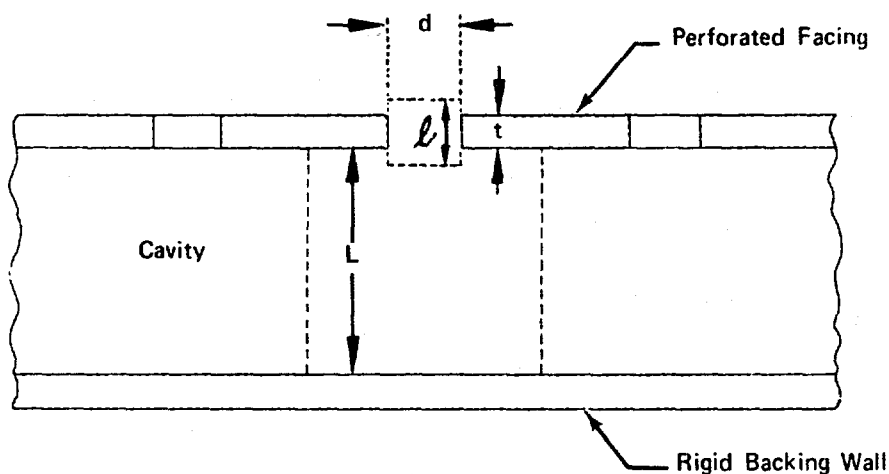


Figure 3. Typical Resonant Absorber - An Array of Helmholtz-Type Resonators

FD 65585

If there is flow past the absorber facing, all of the above equations are used except the effective length, which is computed from

$$l = t + 0.38 \delta d \quad (7)$$

and if

$$\frac{cM_p}{u} \left( \frac{\rho}{\rho_c} \right)^{3/2} > 1.5 \quad (8)$$

where  $M_p$  is the parallel net flow Mach number and  $\rho_c$  is the density of the combustion chamber gas, the resistance ratio should be calculated using

$$\theta = \frac{0.123}{C_f^2} \left[ M_p \left( \frac{\rho}{\rho_c} \right)^{3/2} + \frac{1.5 u}{c} \right] \quad (9)$$

If the inequality (8) is not satisfied, the effects of past flow on resistance can be ignored.

For a situation in which there is net flow through the apertures so that

$$M_t > u/2c \quad (10)$$

the resistance ratio is found from

$$\theta = \frac{M_t}{\sigma C_f^3} \quad (11)$$

If  $M_t < u/2c$ , the effects of through-flow on absorption are negligible.

In equation (2), the frequency at which the term in parenthesis becomes zero (thus causing the reactance to vanish) is the resonance frequency; for arrays, it is computed from

$$f_0 = \frac{c}{2\pi} \sqrt{\frac{144\sigma}{Ll}} \quad (12)$$

where  $L$  is the backing cavity depth.

## 2. Porous Absorbers

If the facing of a damping device is composed of a porous material, the acoustic impedance of the device will be dependent on the flow resistance and porosity of the facing, the effective dynamic mass of the enclosed gas, and the geometry of the system.

For example, the low frequency impedance of the configuration shown in figure 4 is according to Reference 1.

$$Z = \left[ \frac{Rt}{3} + \frac{R\rho_e \epsilon^2 L}{3\rho_p c^2} \right] + i \left[ \omega \left( \frac{\rho_e t}{3} + \frac{\rho_e^2 \epsilon^2 L}{3\rho_p c^2} \right) - \frac{1}{\omega \left( \frac{\rho_e t}{3} + \frac{L}{\rho_p c^2} \right)} \right] \quad (13)$$

For a rigid porous material, i.e., one in which the individual fibers cannot deflect, the cavity density,  $\rho$ , will be equal to the effective density,  $\rho_e$ , of the gas in the porous material.

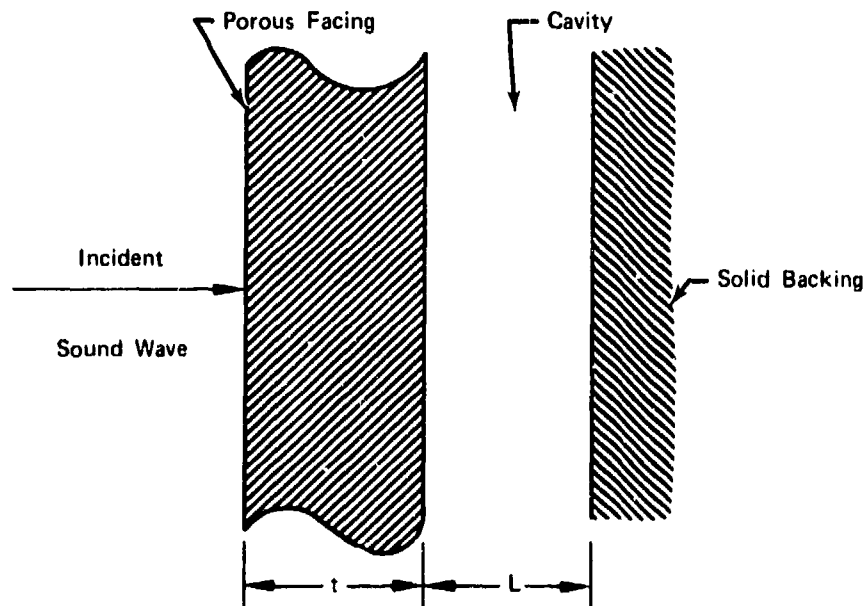


Figure 4. Porous Absorber Configuration

FD 65586

As with the conventional resonator, the acoustic resistance of the device is the real part of the impedance, equation (13), and the reactance is the imaginary part, i.e.,

$$\theta = \frac{Rt}{3} + \frac{R \rho_e \epsilon^2 L}{3 \rho_c^2 p} \quad (14)$$

$$\chi = \omega \left( \frac{\rho_e t}{3} + \frac{\rho_e^2 \epsilon^2 L}{3 p \rho_c^2} \right) - \frac{1}{\omega \left( \frac{pt}{\rho_e \epsilon^2} + \frac{L}{\rho_c^2} \right)} \quad (15)$$

The resonance frequency of the system may be found by setting equation (15) equal to zero and simplifying it to produce

$$\omega_o = \left[ \frac{pt^2 \rho_e}{3 P_c} + \frac{2 \rho_e t L}{3 \rho_c^2} + \frac{\rho_e P_c L^2}{3 p \rho_c^4} \right]^{-1/2} \quad (16)$$

A study of equation (16) indicates that, for resonance at low frequencies, the material thickness, the backing cavity depth, and the porosity should be high.

The acoustic resistance, which controls energy dissipation, of porous facings may be regulated by several parameters, as seen in equation (14). The most important of these parameters, the flow resistance,  $R$ , is a function of the structural composition of porous material and, as discussed in Reference 3, is dependent on sound pressure level. Typical flow resistance as a function of sound pressure level for three different porous samples is shown in figure 5.

The absorption of any device is defined as that portion of the incident sound pressure level for three different porous samples is shown in figure 5.

The absorption of any device is defined as that portion of the incident sound energy that is transmitted, rather than reflected, through the facing. Thus, the absorption coefficient of a porous absorber can be computed by substituting the resistance and reactance determined by equations (14) and (15) into equation (1).

## B. DESIGN CONSIDERATIONS

### 1. Effects of Liner Geometry

The selection of an absorber for a given application requires within the geometric limitations of the system a compromise between absorption coefficient and frequency bandwidth. The geometric variables for Helmholtz-type liners are aperture diameter, liner thickness, backing cavity depth and open area ratio. Open area ratio, liner thickness, and backing depth have more of an effect on

acoustic properties than aperture diameter, but in most practical liner designs, the backing distance and the liner thickness are generally fixed from considerations of strength and cooling requirements. Limitations on the values of aperture diameter that can be tolerated are set by the diameter of holes that can be conveniently machined and cooling flow requirements. For these reasons it is usually better to use the open area ratio as the liner design variable.

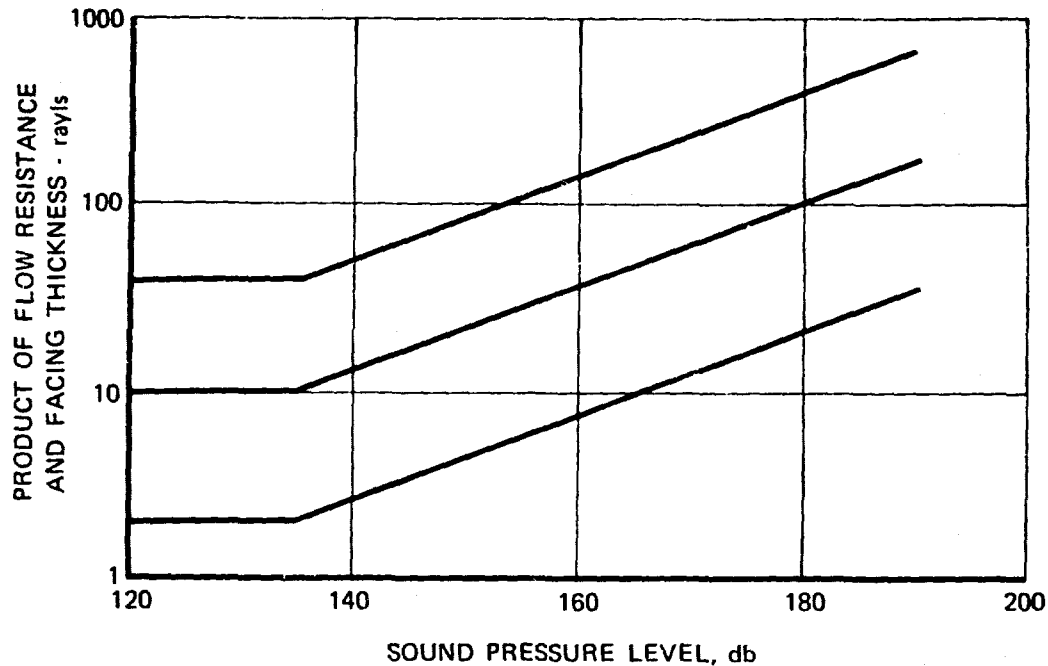


Figure 5. Flow Resistance of Three Different Fibermetal Porous Facings

FD 65587

The open area ratio,  $\sigma$ , is based only on the area of the combustion chamber that is backed by the liner cavity, i.e.,

$$\sigma = N \frac{\pi}{4} (d)^2 / S \quad (17)$$

where

$N$  = total number of holes

$S$  = surface area of combustion chamber backed by liner cavity

If wide supporting struts, partitions, or individual resonator cavities are used, the area should be corrected to account for only the surface area of the cavity.

An optimum  $\sigma$  can be determined by computing the absorption coefficient as a function of frequency,  $f$ , with  $\sigma$  as a parameter. The optimum  $\sigma$  is that value which gives the maximum value of the absorption coefficient over the widest band of frequencies. The same procedure can be followed to optimize aperture diameter, facing thickness, and backing depth if there are sufficient variations allowable to warrant the added difficulty.

In cases where the absorption bandwidth is too narrow, it will be necessary to change the bandwidth factor,  $Q$ , of the system. The  $Q$  value is the inverse of the damping coefficient and is a measure of the absorption bandwidth. Systems

having high Q values absorb very selectively and have narrow bandwidths. Systems with low Q values usually have less peak absorption, but absorb over a wider range of frequencies. Unfortunately, it is not possible to specify a maximum value for Q; therefore, some judgment must be exercised to achieve good absorption characteristics over the anticipated range of the instability. Variations in Q can best be achieved by varying the aperture diameter,  $d$ ; both  $\sigma$  and  $d$  must be optimized if adequate bandwidth performance cannot be achieved by optimizing  $\sigma$  alone. In figure 6 the calculated absorption-frequency characteristics of a liner have been graphed to illustrate the results that can be achieved through parametric optimization.

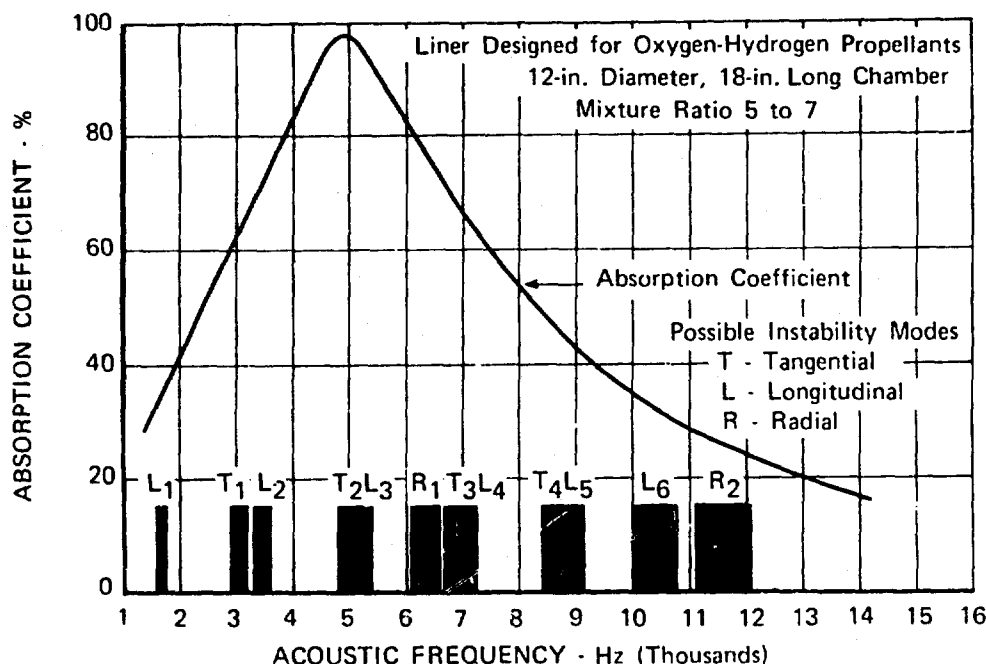


Figure 6. Wide Band Absorption Characteristics  
Achieved by Parametric Optimization

FD 65588

## 2. Amount of Absorption Required

The amount of absorption required to damp an unstable combustion process cannot be determined from theoretical considerations alone. However, it is possible to install absorbing liners in a combustion system having a known record of instability and record the amplitude of the resulting pressure oscillations. Experiments of this type were conducted on a rocket chamber by Pratt & Whitney Aircraft for NASA-MSFC under Contract NAS8-11038 (Reference 4). Full chamber length absorbing liners with design absorption coefficients from 0% to 70% were used in the series of tests. The results showed that all of the liners with coefficients of 20% or greater damped the combustion process so that the oscillations were less than the background noise level of the data recording system. Unfortunately, no extensive programs have been conducted to determine the minimum absorption coefficient required for airbreathing systems; however, full-length liners with 10% to 20% absorption coefficients have been successful in suppressing high frequency combustion instability in most augmentors.

### 3. Absorber Location

An absorbing liner may be installed on any of the combustion chamber surfaces; however, experimental studies at Pratt & Whitney Aircraft (Reference 5) have determined that a sensitive stability area exists near the region of highest energy release, e.g., near the flameholder or injector face. For maximum effectiveness, damping devices must be located in this vicinity.

### 4. Aperture and Cavity Gas Temperature

The temperature of the gas in the apertures and cavities of the absorber must be known so that the properties (density and sonic velocity) can be correctly specified for the design analysis. As was the case with the required absorption coefficient, the temperatures usually cannot be calculated and must be measured or assumed. Some experimental data from the test of absorbing liners are available (References 4 and 5). A summary of the data is shown in figure 7.

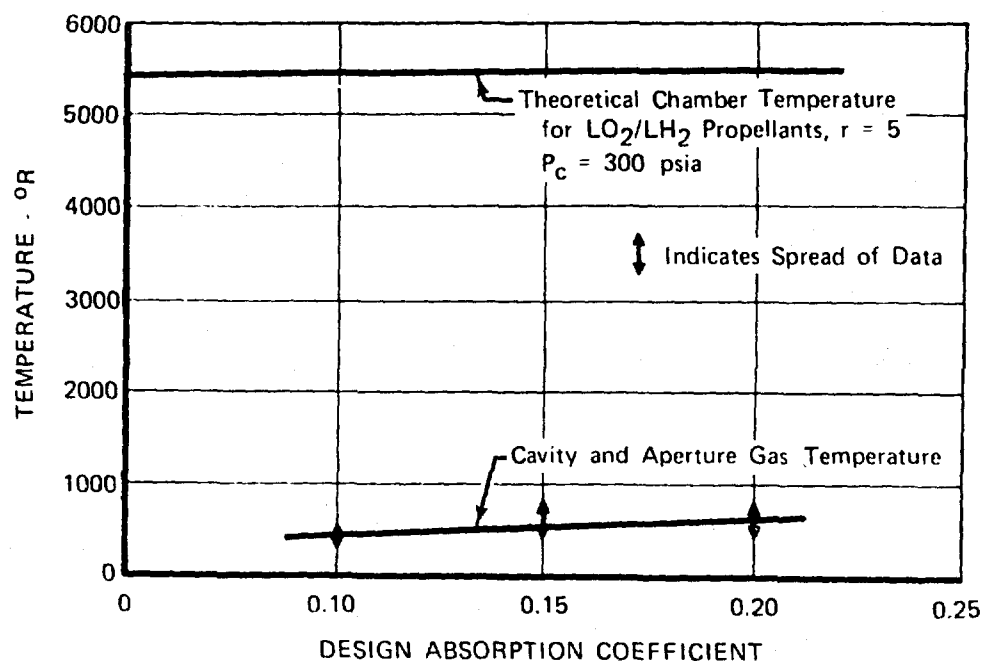


Figure 7. Liner Aperture and Cavity Gas Temperatures From Stable Rocket Chamber Tests

FD 65589

In addition, when combustion is stable, the cavity gas temperatures have been found to be significantly lower than when instabilities are present. (See figure 8.) It is recommended that if no experimental aperture gas temperature data are available for a particular augmentor configuration, an assumed value of from 1000°R to 2000°R be used for design purposes. For cooled-wall liners, where the gas pumped into the cavity is temperature conditioned by passing the cooled wall, a temperature below 1500°R can be assumed; uncooled liner temperature assumptions would be above 1500°R. A further refinement of the assumption is based on open area ratio. Low open area ratio liners (less than 5%) allow such a small percentage of hot gas to enter the cavity that the temperature is moderated, whereas radiation from the flame and pumping of larger

quantities of hot gas influences the cavity temperature with moderate to high open area ratio liners. Thus a temperature assumption of approximately  $2000^{\circ}\text{R}$  would be used for a high open area ratio, uncooled liner, while  $1000^{\circ}\text{R}$  would be used for a low open area ratio, cooled liner.

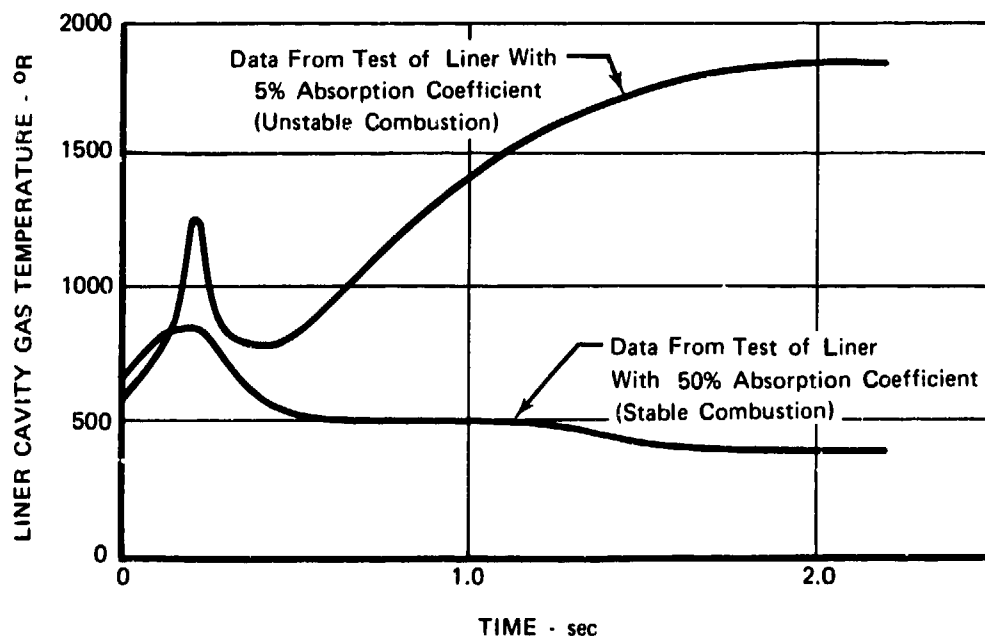


Figure 8. Cavity Gas Temperature vs Time for 15K  $\text{LO}_2/\text{LH}_2$  Rocket Chamber With 5% and 50% Absorption Coefficients

FD 65590

## 5. Effects of Gas Flow

An absorbing liner designed for a combustion chamber could encounter one of several flow situations. Parallel flow on the chamber side of the liner would always be present. There would also be flow through the aperture if (1) airflow was required to transpiration-cool the liner and/or (2) the resonator cavity was not partitioned, thus allowing flow along the cavity in the axial direction. Usually either parallel or through flow is assumed to be controlling, depending upon the relative momentum of the streams.

## C. RESULTS OF ANALYSES

### 1. Porous Absorbers

A porous absorber having an air space behind the facing is similar to a conventional array, except that the perforated facing is replaced by an unperforated porous material. A parametric analysis of configurations similar to the absorber shown in figure 4 was conducted for the design point operating conditions of table 1; the effects on absorption of variations in porosity, flow resistance, thickness, and backing depth were studied. Typical results are shown in figures 9 through 12. The resonant frequency of each configuration occurred in the 500 to 4000 Hz range, with highest absorption predicted near resonance. Good

absorption characteristics were also predicted at frequencies far from resonance, which indicates that porous absorbers, unlike Helmholtz resonators, are not necessarily restricted to operation near the frequency of resonance; therefore, a single porous liner configuration could theoretically be used to suppress instabilities over a wide range of frequencies.

Table 1. Simulator Nominal Operating Conditions

|                                    |      |
|------------------------------------|------|
| Inlet Air Temperature, °F          | 1000 |
| Airflow Rate, lb <sub>m</sub> /sec | 26   |
| Fuel-Air Ratio                     | 0.05 |
| Static Pressure, psia              | 17.6 |
| Mach No. in Combustion Zone        | 0.15 |
| Combustion Temperature, °F         | 3000 |

Because the porous theory had not yet been verified by experimental data, it was necessary to fabricate and test porous resonator samples before configurations could be selected for the simulator test program. The results of these experiments are discussed in Section III.

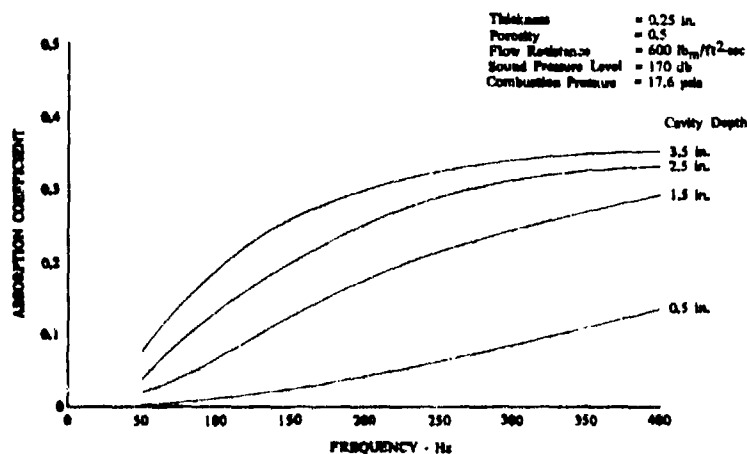


Figure 9. Results of Porous Absorber Analysis,  
Effects of Variation in Cavity Depth

DF 92923



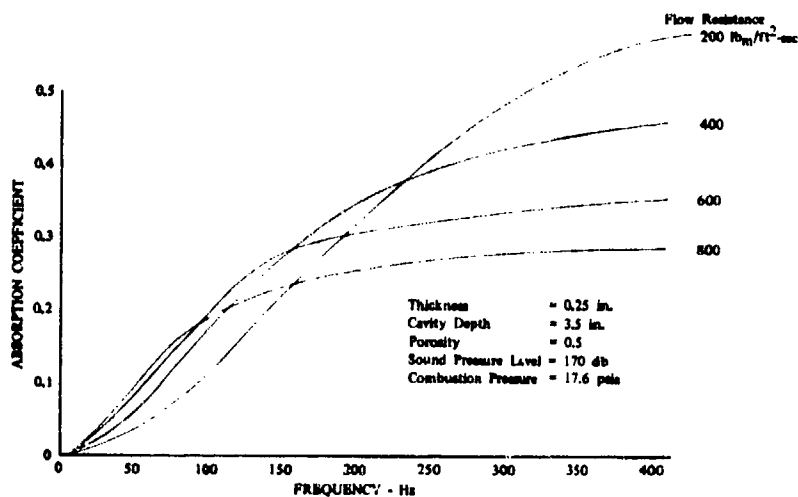


Figure 10. Results of Porous Absorber Analysis,  
Effect of Variation in Facing Flow  
Resistance

DF 92924

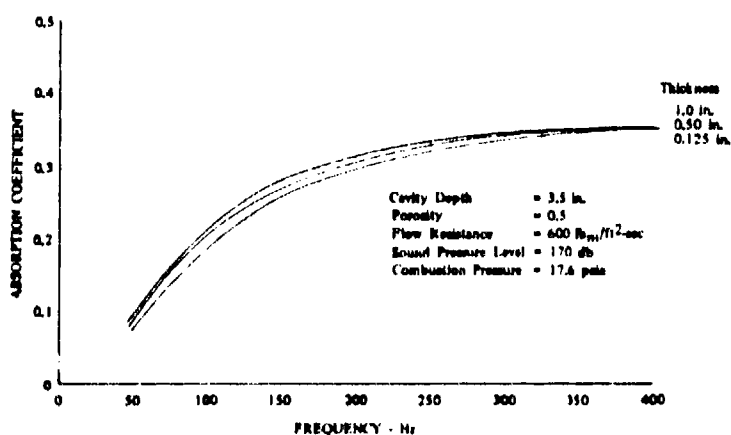


Figure 11. Results of Porous Absorber Analysis,  
Effect of Variation in Facing Thickness

DF 92925

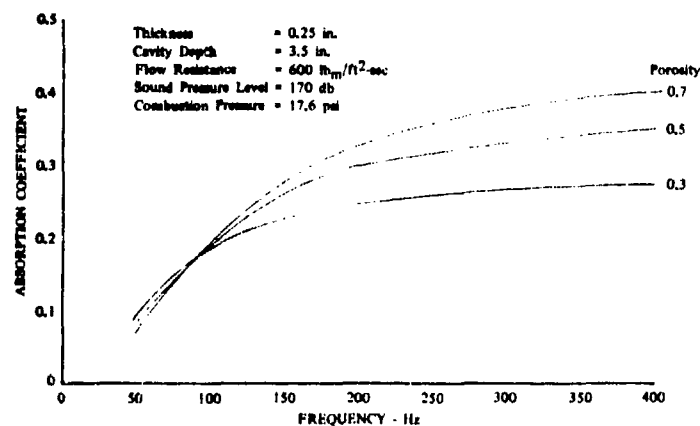


Figure 12. Results of Porous Absorber Analysis,  
 Effect of Variation in Facing Porosity

DF 92926

## 2. Dimpled Resonator Absorbers

A dimpled resonator is a conventional resonator in which the apertures have been punched or otherwise lengthened to increase the effective aperture length without increasing the basic liner facing thickness. (See figure 13.) Because the effective length is approximately proportional to the aperture length, the resonance frequency of a liner can be significantly lowered by using dimpled apertures. The analysis for the dimpled array was performed for the conditions of table 1 using the Helmholtz resonator theory.

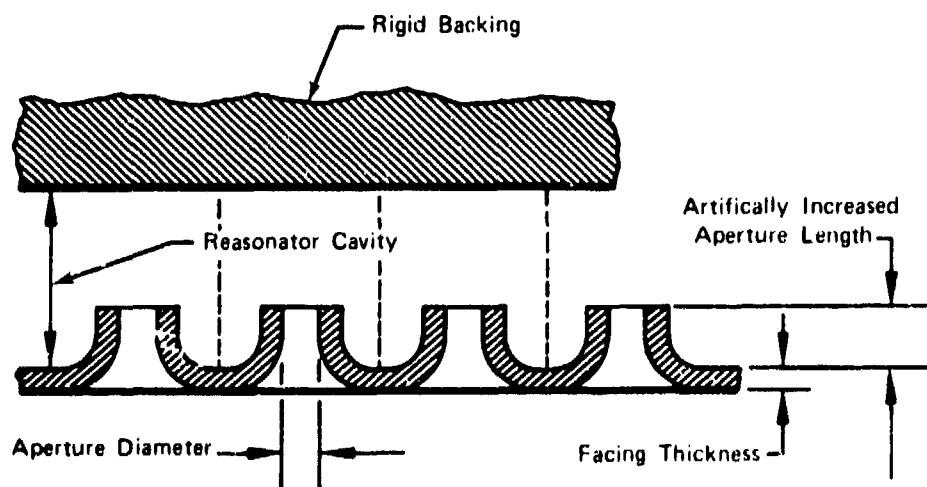


Figure 13. Dimpled Resonator Configuration

FD 65591

It was assumed for the analysis that a maximum cavity depth of 3.0 inches was reasonable and that apertures with diameters of up to 0.5 inch could be used. Past experience with dimpling processes indicated that an aperture depth slightly larger than the diameter can be obtained; hence, the maximum aperture length was assumed to be 0.5 inch. To further lower the resonance frequency and increase the low frequency absorption characteristics, the apertures could be further lengthened by welding tubular extensions to each aperture. However, this type of operation was not considered for this program because of the excessive fabrication costs involved.

The results of the analysis indicated that the best absorption characteristics were obtained with a 1.0% open area array, producing, as shown in figure 14, a maximum absorption coefficient of 26%. A considerable amount of data previously obtained for arrays of Helmholtz resonators, Reference 6, indicated that good agreement with theory should be expected; therefore, no additional cold flow experiments were considered necessary prior to fabrication of such a device.

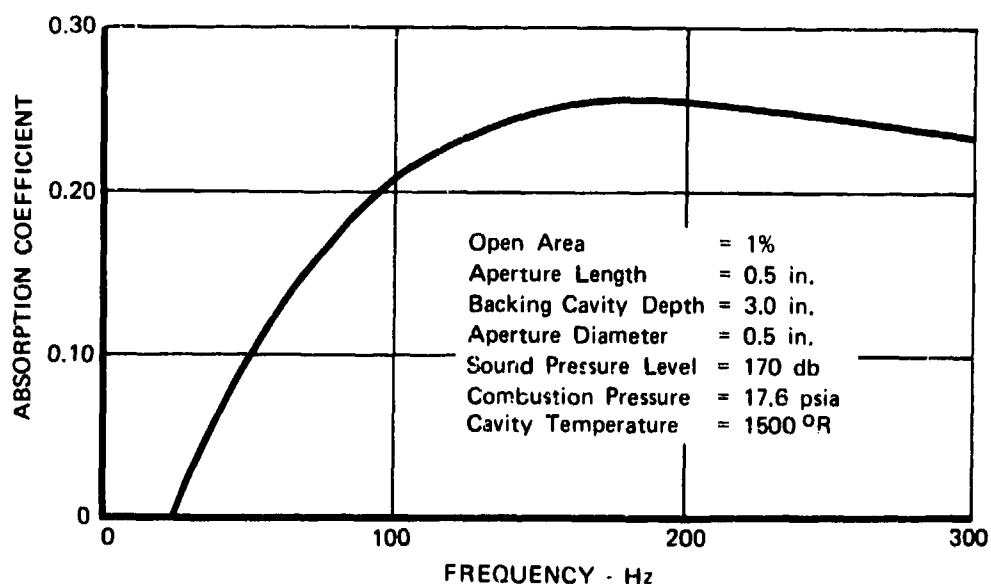


Figure 14. Absorption Characteristics of Dimpled Array Liner

FD 65592

### 3. Absorbing Flameholders

Several concepts for acoustic absorbing flameholders were analyzed. Because of the proximity to the most sensitive, highest energy release zone, it was believed that an absorber in this region would not need to be as efficient (or operate as near resonance) to have the same effect as a larger device with more absorption located elsewhere.

The first flameholder concept involved enclosing a portion of the region that is already partially enclosed by the concave side of the flameholder and using this volume as the backing cavity for a simple Helmholtz resonator or a porous resonator.

The results of the Helmholtz resonator analysis, figure 15, indicated that a 0.9% open area array facing of 0.125 inch thickness and a cavity volume of 3.9 in<sup>3</sup> per aperture would provide 14% and 23% absorption coefficient at 100 and 300 Hz, respectively.

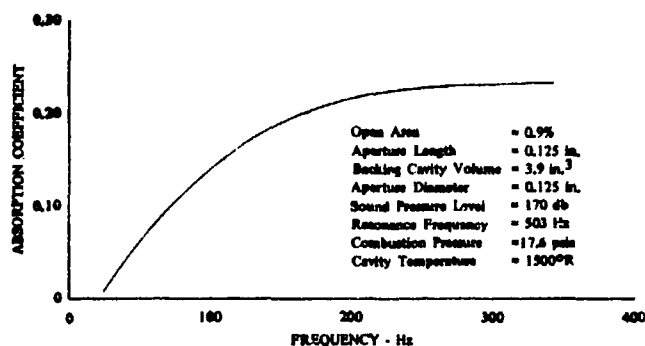


Figure 15. Predicted Absorption Characteristics of Helmholtz-Type Acoustic Flameholder

DF 92927

The results of the porous resonator analysis, figure 16, indicated that a facing of 30% porosity with a 200 CGS Rayl flow resistance and a 0.25 inch facing thickness and a cavity depth of 2.5 inches would provide 13% and 31% absorption coefficient at 100 and 300 Hz, respectively.

The second absorbing flameholder concept involved using a "V" gutter flameholder made from a porous material. This type absorber does not have an enclosed backing cavity and depends only on the impedance of the material for its damping characteristics. Analysis was based on the porous absorber theory, with the backing volume assumed to be very large to produce negligible cavity impedance. The results, figure 17, indicated that a "V" gutter facing of 0.125 inch thickness with a porosity of 50% and a 140 CGS Rayl flow resistance would provide 57% and 36% absorption coefficient at 100 and 300 Hz, respectively.

#### 4. Complex Resonators

Complex resonators can be of two basic forms, series or parallel. The facings of the resonator can be perforated or porous, but because no information was available on porous resonators in series or parallel, the analysis was postponed until the basic porous theory could be verified by cold flow experiments. For results of the experiments, see Section III.

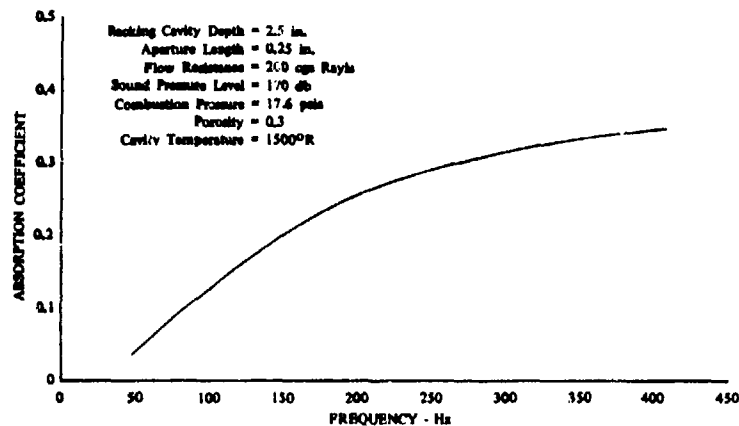


Figure 16. Absorption Characteristics of Porous Resonator Flameholder

DF 92928

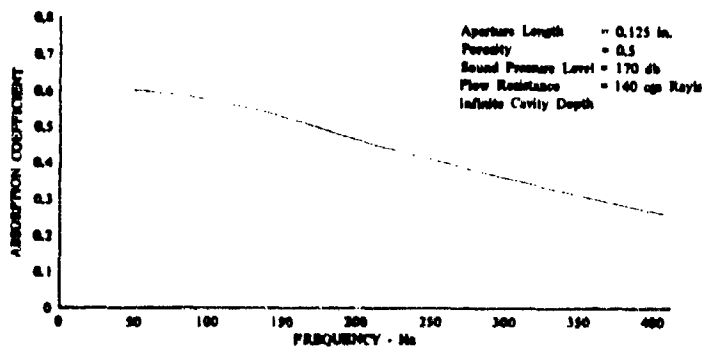


Figure 17. Absorption Characteristics of Porous Flameholder

DF 92929

The complex Helmholtz resonator has been previously studied (Reference 7); the results indicated that these types of devices could be used to improve bandwidth characteristics of an array liner design. It was found that the double resonator in series (figure 18) was characterized by two natural frequencies, and that they correspond to the individual resonance frequencies of the component resonators. Figures 19 and 20 illustrate typical absorption characteristics. The relative proximity of the two natural frequencies dictates the absorption characteristics of the resonator system; i.e., if the two frequencies are close together, the absorber will have good wide band absorption; but, if the frequencies are far apart, the absorption coefficient curve tends to sag between the resonant points.

The double resonator in parallel (figure 21) exhibits the same type of absorption characteristics as those of the resonators in series, with the primary difference concerning resonance of the system. The lower frequency of resonance corresponds to that of the resonator having the lowest natural frequency. The highest resonance of the system corresponds to a value determined by averaging the geometric variables and gas properties for the two components.

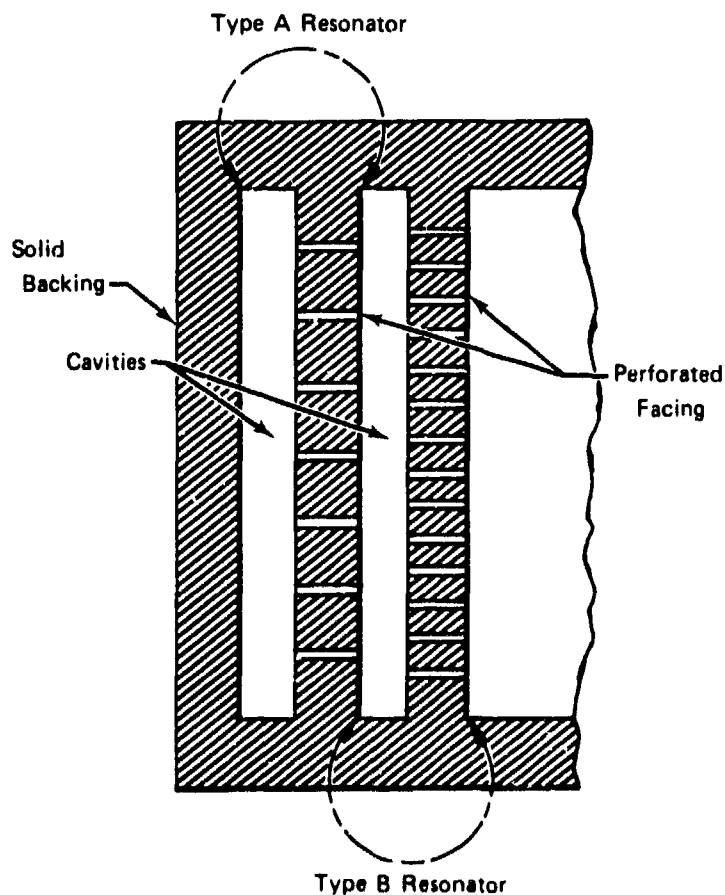


Figure 18. Double Resonator in Series

FD 65593

The result is that the higher system resonance lies between the two individual frequencies of resonance; the effect is illustrated in figure 22. Analysis showed that the major advantage to complex resonators is their improved bandwidth characteristics, and that neither the parallel nor the series systems have lower resonance frequencies than their individual resonators. It was concluded that complex Helmholtz-type resonator systems would not provide low frequency absorption superior to conventional liners.

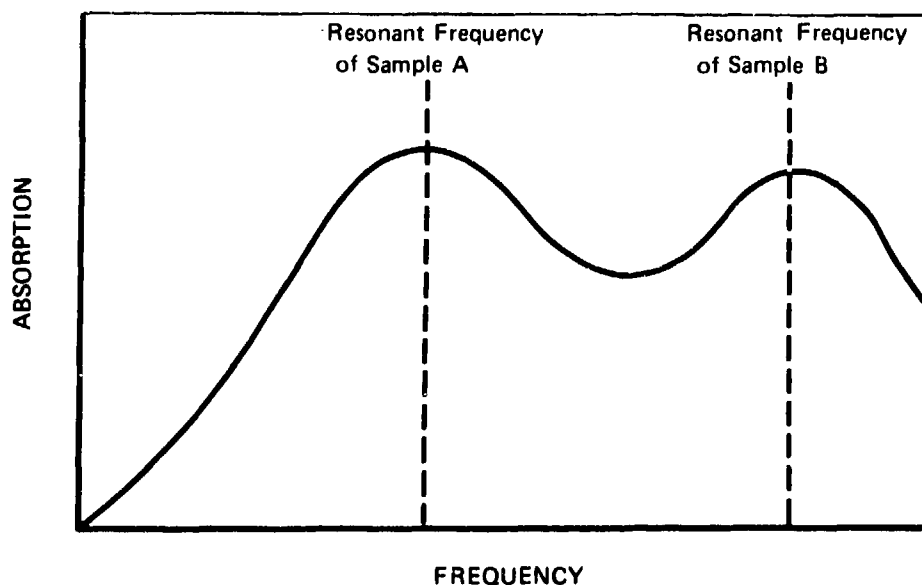


Figure 19. Typical Absorption Curve for a Series Resonator Array With Widely Separated Resonant Frequencies

FD 65594

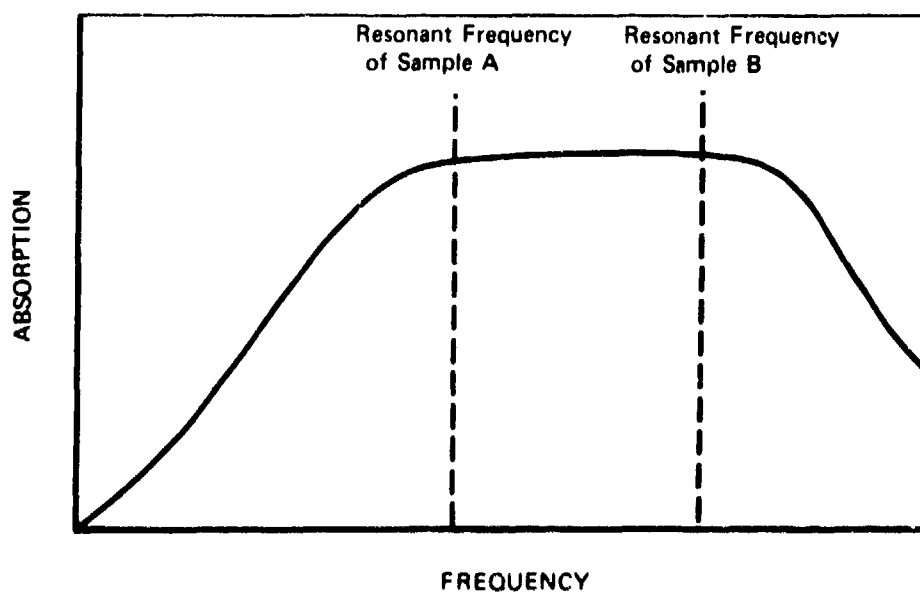


Figure 20. Typical Absorption Curve for a Series Resonator Array With Narrow Separation of Resonant Frequencies

FD 65595

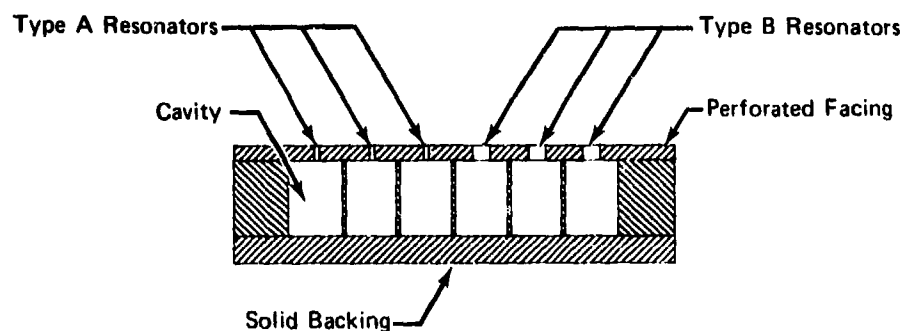


Figure 21. Double Resonator in Parallel

FD 65596

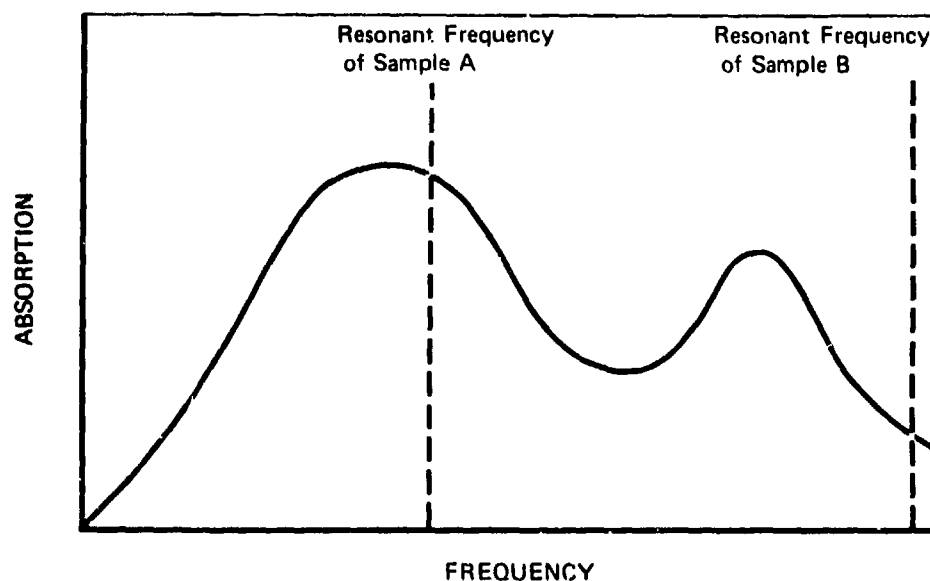


Figure 22. Typical Absorption Curve for a Parallel Resonator Array

FD 65597

## 5. Acoustical Cavities

Acoustical cavities, i.e., quarter wave tubes or slots, normally are used in combustion chambers with limited surface areas. These devices consist of a tube or a slot whose length is one-fourth the wavelength of the oscillations to be damped, with one end closed by a flat reflector plate and the other end opening to the region of instability. Their damping characteristics are quite sensitive to their resonance frequency; thus, they must be carefully tuned to obtain maximum damping at the frequency of the potential instability. For the conditions of table 1, a cavity depth of 2.0 feet is required to damp 200 Hz oscillations with a quarter wave tube.

A study recently completed on quarter wave tubes and quarter wave cavities, Reference 8, showed that when compared to a conventional Helmholtz resonator of the same cavity volume and aperture area the acoustic cavity



(1) could absorb only 50% as much acoustical energy and (2) would have a bandwidth of only 75% of the Helmholtz resonator. It was, therefore, concluded that acoustical cavities would not be more practical than conventional resonators for low frequency application.

## 6. Baffles

The natural frequencies of acoustic modes within a volume are inversely proportional to the linear dimensions; therefore, it is possible to increase these frequencies by using baffles to divide the volume into smaller units. This can have two beneficial effects with regard to stabilizing augmentor combustion. One effect is to remove the pressure wave coupling mechanism which sustains an instability, by disorganizing the modes associated with the original unstable augmentor geometry, and replacing them with modes that do not couple with the driving force of the instability. The second effect is to raise the frequency of the oscillations to a value for which a practical conventional screech liner can be designed. However, to be effective, baffles must extend well into the combustion zone, which introduces a complex cooling problem. It is for this reason that they were not considered for further evaluation in this program.

### SECTION III

#### COLD FLOW ACOUSTIC EXPERIMENTS

##### A. APPARATUS

Acoustic cold flow experiments were conducted to investigate the low frequency acoustic characteristics of porous materials and to verify the analytical formulations discussed in Section II. Two impedance tubes were used to obtain the acoustic data. The device used to obtain low frequency data is shown in figure 23; the standing wave method is used in this apparatus to measure the acoustical characteristics of facing samples. The basic principles of the technique are described in ASTM Standard C384-58. The essential equipment consists of (1) a Ling EPT-94-B air modulating sound source, (2) a long tube of fixed length and uniform cross section, with rigid walls that transmit negligible sound energy, and (3) an Altec-type 2 BR-180 microphone mounted to a traversable probe to measure the standing wave. The system was modified for the test series by the addition of two microphones; one located on the incident sound side of the test facing, and the second located in the back wall of the cavity so that pressure-phase data could be obtained. The pressure-phase techniques of data management are described in Reference 8.

High frequency data were obtained with the impedance device shown in figure 24. The pressure phase method and/or the standing wave method of data reduction can be used with this apparatus.

##### B. POROUS ABSORBER EXPERIMENTS

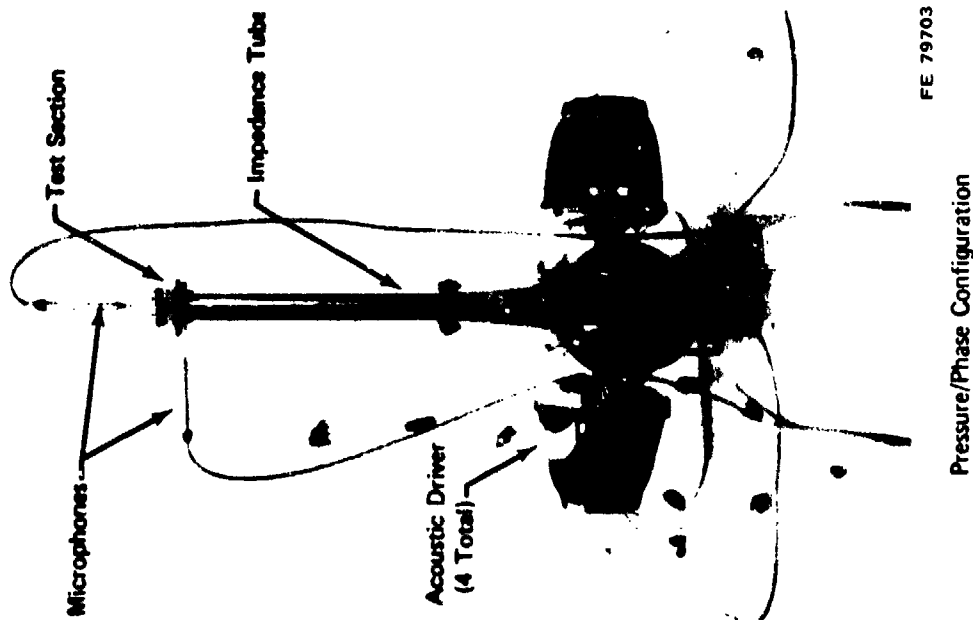
The objective of the porous absorber experiments was to obtain data for verification and/or improvement of the porous theory. The absorbers used were porous facing samples fabricated from Rigimesh and Feltmetal. The first series of experiments was conducted with the high frequency impedance tube at frequencies from 1750 to 3300 Hz with two Rigimesh samples, each with a 0.30 inch backing depth. The results, figure 25, showed good agreement with theory.

The second series of tests was conducted with the low frequency impedance tube at frequencies from 50 to 200 Hz with one Rigimesh facing and three different Feltmetal facings. The Rigimesh sample was 0.25 inch thick with a 2000-SCFM flow rating; one Feltmetal sample was 0.062 inch thick and 20% dense; the two others were 10% dense and 0.125 and 0.25 inch thick. All tests were conducted with a 0.75 inch backing depth. The results of the tests are shown in figure 26; a maximum of 13% absorption coefficient was obtained, indicating that configurations with higher absorption coefficients would be required to properly evaluate the theory.

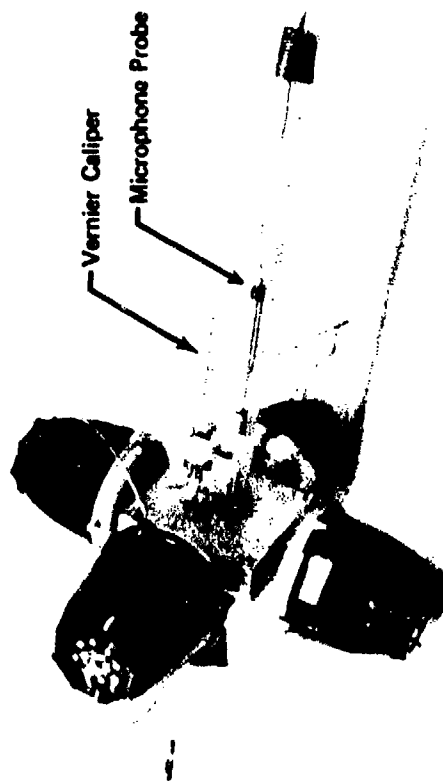


Figure 23. Low Frequency Impedance Tube

FC 25377A



Pressure/Phase Configuration



Standing Wave Configuration

FD 65598

Figure 24. High Frequency Impedance Tube

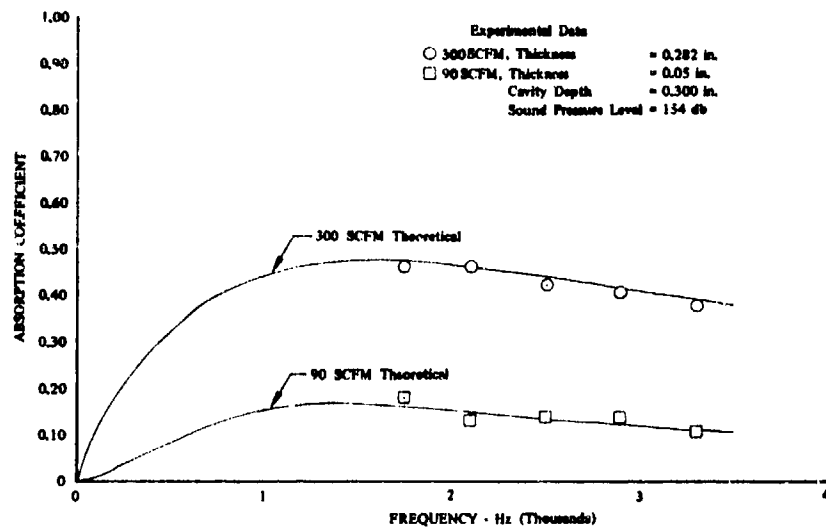


Figure 25. Comparison of Predicted Absorption With Experiments for Rigimesh Samples

DF 92930

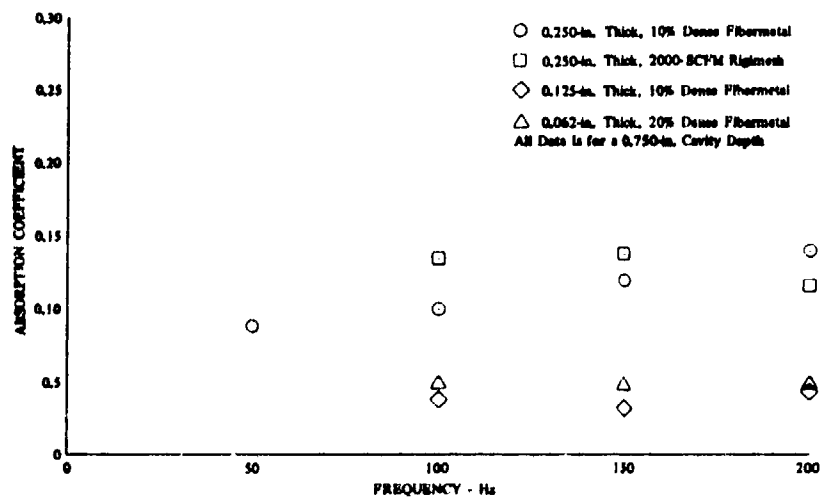


Figure 26. Experimental Absorption Coefficients of Porous Liner Material

DF 92931

A series of experiments was conducted with the nine Rigimesh samples described in table 2. Data from the 75% dense samples (porosity 25%), as shown in figure 27, near 100 Hz agreed with the porous theory; however, data from the 50% dense samples, figures 28 and 29, were found to be in poor agreement. The experimental absorption coefficient at 100 Hz for the 50% density sample was similar to the data from the 75% density sample; theory indicates the values should be approximately three times greater. Because the results showed that the porous theory was not suitable for use in designing low frequency absorbing devices, it was necessary to supplement the theory with empirical correlations, i.e., cold flow data would be used to determine the absorption characteristics of a candidate porous absorber in air and empirical scaling techniques used to predict the values at the simulator test conditions.

Table 2. Rigimesh Samples - Low Frequency Tests

| Class | Thickness, in. | Flow Rating,<br>SCFM at 2 psid | Porosity |
|-------|----------------|--------------------------------|----------|
| 1     | 0.9            | 70                             | 0.25     |
| 2     | 0.9            | 90                             | 0.25     |
| 3     | 0.9            | 110                            | 0.25     |
| 4     | 0.9            | 70                             | 0.5      |
| 5     | 0.9            | 90                             | 0.5      |
| 6     | 0.9            | 110                            | 0.5      |
| 7     | 1.25           | 70                             | 0.5      |
| 8     | 1.25           | 90                             | 0.5      |
| 9     | 1.25           | 110                            | 0.5      |

Additional tests were conducted using Rigimesh facings with flow resistances of 300, 1000, and 2000 SCFM in series with Feltmetal sheets of 10%, 20%, and 30% density. The tests were conducted to determine the proper selection of materials for a complex porous acoustic liner for the simulator test program. It was found that the configuration that had the higher flow resistance immediately behind a facing of lower resistance provided the highest absorption; the 2000-SCFM Rigimesh facing in series with a 0.25 inch thick, 10% dense Feltmetal sheet with a backing cavity of 0.75 inch provided 10% and 22% absorption coefficient at 150 and 250 Hz, respectively. The results of the tests are shown in figure 30 for a nominal sound pressure level of 165 db.

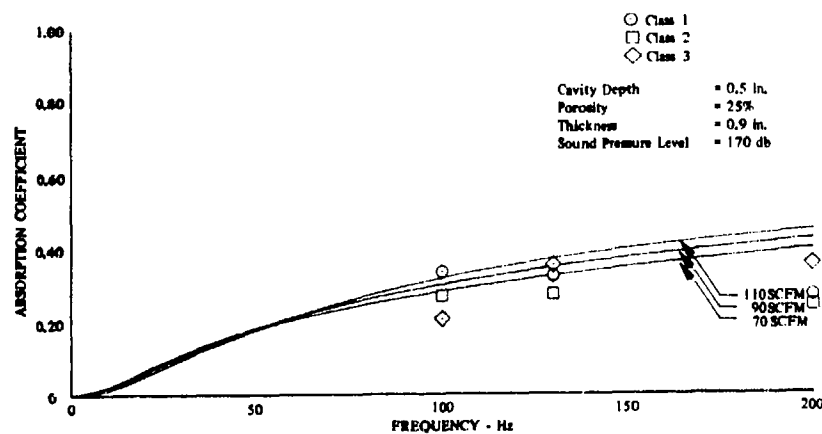


Figure 27. Comparison of Experimental and Theoretical Absorption Characteristics of 25% Porous, 0.9-in. Thick Rigimesh Samples

DF 92932

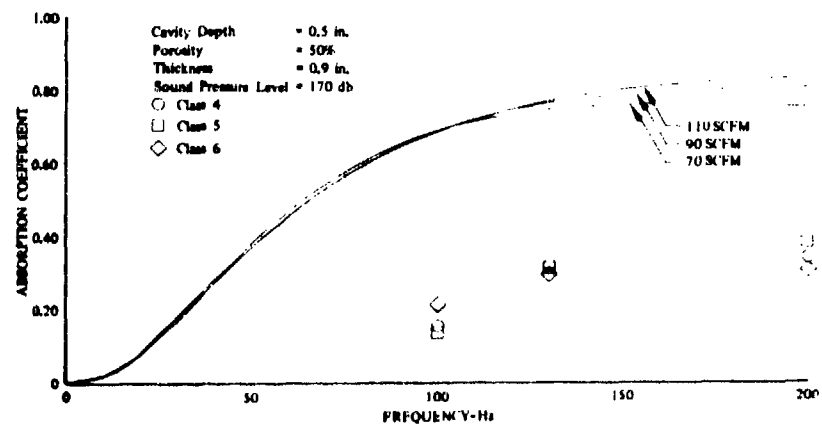


Figure 28. Comparison of Experimental and Theoretical Absorption Characteristics of 50% Porous, 0.9-in. Thick Rigimesh Samples

DF 92933

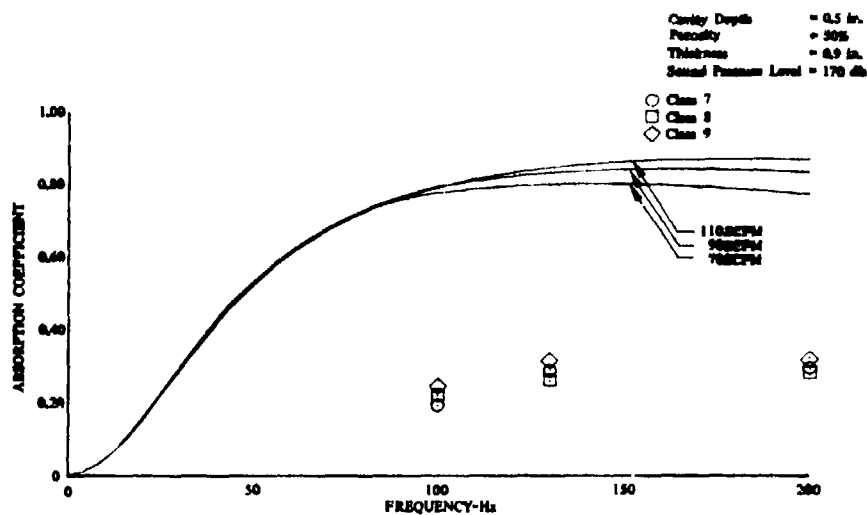


Figure 29. Comparison of Experimental and Theoretical Absorption Characteristics of 50% Porous, 1.25-in. Thick Rigmesh Samples

DF 92934

Reproduced from best available copy.

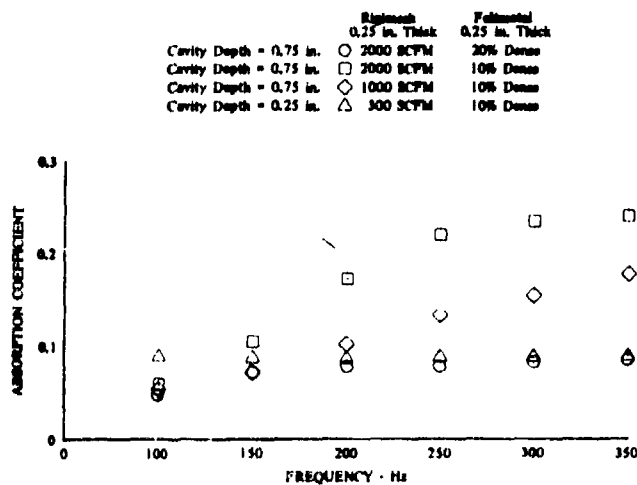


Figure 30. Complex-Porous Sample Absorption Characteristics

DF 92935



The absorption characteristics of the complex porous configuration at the simulator test conditions were then predicted using the following technique. For a porous material, it can be assumed that the dissipation resistance is controlled by viscous losses, where the viscous losses are given by

$$W_v = \int R_s u^2 dS \quad (18)$$

where

$S$  = surface area  
 $R_s$  = boundary layer friction coefficient  
 $u$  = particle velocity.

A good approximation for the viscous resistance is (Reference 9)

$$R_s \cong 1/2 (2\rho\mu\omega)^{1/2} \quad (19)$$

where

$\mu$  = viscosity  
 $\rho$  = density  
 $\omega$  = angular frequency

For the gases, it is known that the proportionality between viscosity and absolute temperature,  $T$ , is of the form

$$\mu \propto \sqrt{T}. \quad (20)$$

Thus, equation (19) can be written as

$$R_s \propto T^{1/4} \rho^{1/2} \omega^{1/2} \quad (21)$$

and because the viscous resistance is assumed to be controlling, the normalized value becomes the specific acoustic resistance, i.e.,

$$\theta = \frac{R_s}{\rho c} \quad (22)$$

where  $c$ , the sonic velocity, is proportional to  $T^{1/2}$ .

Using equation (21) in equation (22) produces

$$\theta \propto \omega^{1/2} \rho^{-1/2} T^{1/4}. \quad (23)$$

The absorption coefficient at resonance can be written as

$$\alpha = \frac{4\theta}{(\theta+1)^2} \quad (24)$$

but for porous absorbers

$\theta \gg 1$ ; therefore,

$$\alpha \cong \frac{4\theta}{\theta^2} \cong \frac{4}{\theta} \quad (25)$$

Substituting the value of resistance from equation (23) the absorption coefficient becomes

$$\alpha \propto \frac{\rho^{1/2} T^{1/4}}{\omega^{1/2}} \quad (26)$$

If  $\alpha_i$  is the absorption in the impedance tube and  $\alpha_r$  the absorption at simulator design conditions, then

$$\frac{\alpha_r}{\alpha_i} = \frac{\rho_r^{1/2} T_r^{1/4} \omega_i^{1/2}}{\rho_i^{1/2} T_i^{1/4} \omega_r^{1/2}} \quad (27)$$

Since a particular frequency is of interest  $\omega_i = \omega_r$  and equation (27) becomes

$$\frac{\alpha_r}{\alpha_i} = \frac{\rho_r^{1/2} T_r^{1/4}}{\rho_i^{1/2} T_i^{1/4}} \quad (28)$$

With the assumption that the operating pressure of the simulator is near ambient and that the gas constants  $R_r$  and  $R_i$  are the same, equation (28) becomes

$$\frac{\alpha_r}{\alpha_i} = \left( \frac{T_i}{T_r} \right)^{1/4}$$

or

$$\alpha_r = \alpha_i \left( \frac{T_i}{T_r} \right)^{1/4} \quad (29)$$

For the operating condition of the simulator (table 1) the gas temperature in the porous liner would be approximately one-half that of the mainstream gas temperature, or approximately 2000°F; the gas temperature of the cold flow tests was 520°F. Thus, the absorption at the simulator conditions would be

$$\alpha_r = \alpha_i \left( \frac{520}{2000} \right)^{1/4} = 0.714 \alpha_i \quad (30)$$

The results of applying equation (30) to the value of absorption from the cold flow tests indicate 7.1% and 15.7% absorption coefficient would be obtained at 150 and 250 Hz, respectively.

### C. CERAMIC HONEYCOMB EXPERIMENTS

The objective of the honeycomb experiments was to investigate the low frequency acoustic characteristics of the structure and to evaluate their usefulness for the simulator test program. The experiments were conducted on the low frequency impedance tube with three samples of Cer-Vit\* material. The configurations tested were 1-inch thick facings, with pore sizes of 0.025, 0.063, and 0.090 inch ID and a backing cavity depth of 0.5 inch. The tests were conducted over a frequency range of 50 to 300 Hz. The results indicated that less than 5% absorption was obtained. The 0.025-inch pore size sample was again tested at frequencies from 1400 Hz to 2000 Hz. The data showed that resonance occurred at approximately 1600 Hz, and that excellent, wide band absorbing characteristics were obtained with this material. (See figure 31.)

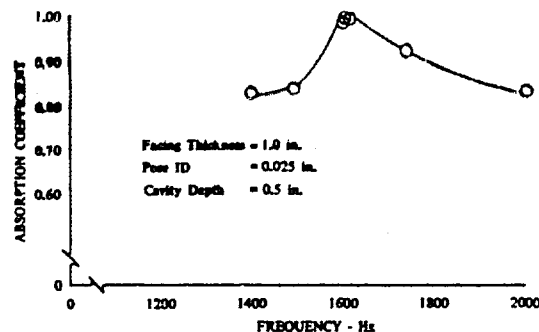


Figure 31. Measured Absorption Characteristics  
of Cer-Vit Porous Sample

DF 92936

\*Cer-Vit is a ceramic honeycomb material manufactured by the Owens-Illinois Corporation, Toledo, Ohio.

#### D. CONCLUSIONS

Results of the cold flow tests showed that the porous theory was useful for prediction of absorption at frequencies from 1000 to 3000 Hz. Experimental data and empirical scaling techniques were necessary to predict low frequency absorption characteristics. The ceramic honeycomb was found to have excellent wide band absorption characteristics, but was not practical for low frequency application without a large backing cavity volume.

A complex-porous configuration was found to have absorption characteristics that warranted further evaluation as a test section for the augmentor simulator.

## SECTION IV

### AUGMENTOR SIMULATOR TEST PROGRAM

#### A. HARDWARE

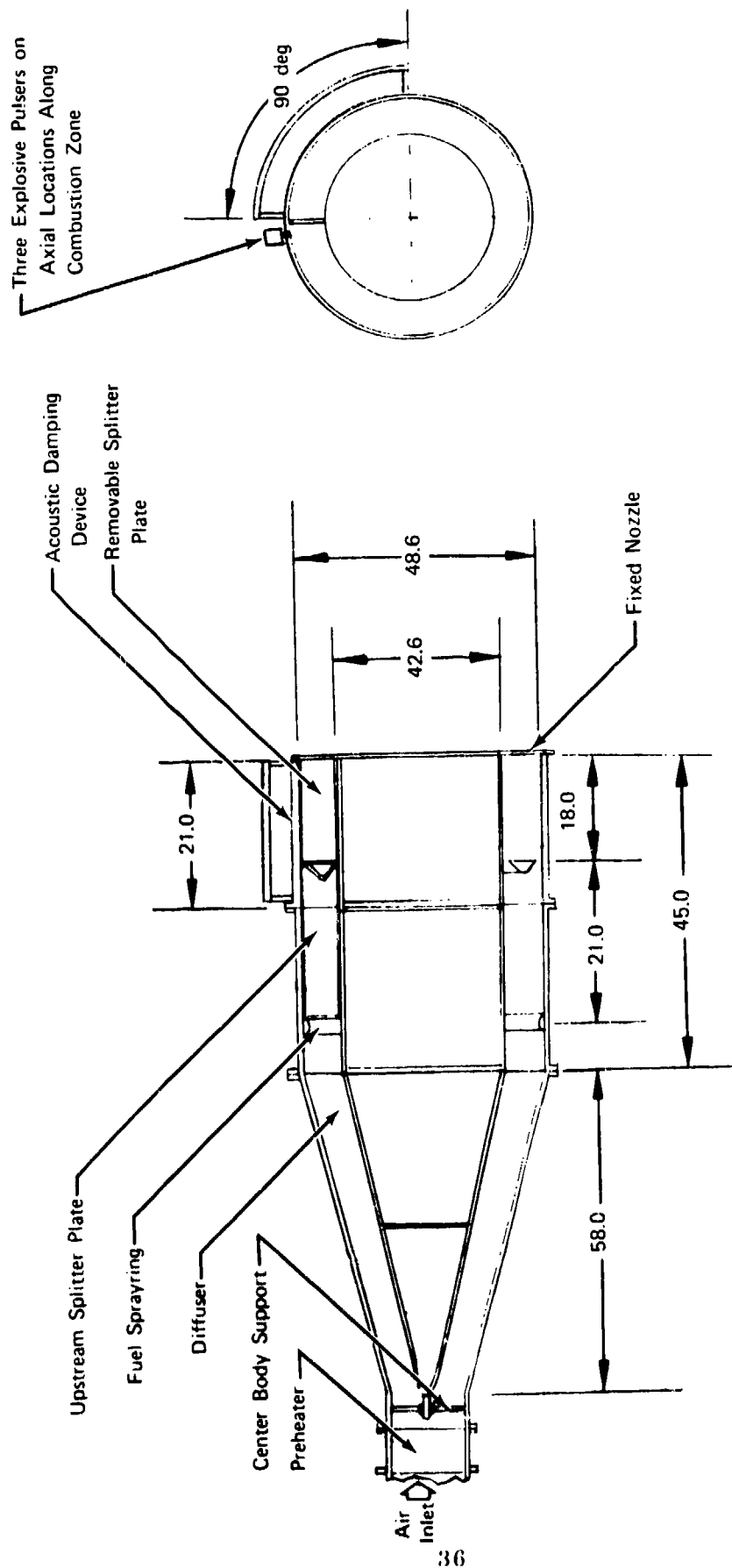
A workhorse combustion chamber in which the pressures, temperatures, gas flows, and modes of instability of a large augmentor could be simulated was designed and fabricated. A discussion of the rig, facilities, and ancillary equipment follows.

##### 1. Augmentor Simulator Rig

The augmentor simulator tests were conducted using a rig with a modified annular combustion chamber designed to have a natural transverse (tangential) mode with a frequency of 100 Hz. A rig schematic is shown in figure 32, and figures 33 and 34 show the rig mounted on the test stand.

The modified annular configuration has a natural transverse mode occurring at a much lower frequency than any other type of combustion chamber of the same flow area. It is essentially a standard annular chamber with a fin or splitter plate extending axially in the annular chamber from the zone of fuel injection to the exhaust nozzle. By adding the splitter plate in the annulus, the frequency of the first tangential mode becomes one-half that of a full annular chamber of the same radii. This may be explained by the following: As shown in figure 35, the maximum path length, i. e., wavelength, for a perturbation occurring in a full annulus is the circumferential distance about the mean diameter of the annular gap; a disturbance occurring at  $-360$  deg travels in both directions to  $180$  deg, where it is reflected and travels back to the source. If a splitter plate is added so that the perturbation can occur on one side only, the path length is then doubled; a disturbance occurring at  $0$  deg must travel (in a clockwise direction in this example) to  $360$  deg before it is reflected and returned. The frequency of the first transverse mode is inversely proportional to the wavelength; hence, the natural frequency for the modified annulus is one-half that of the full annulus.

The modified annular chamber has other advantages over cylindrical, slab, and other configurations. To have the same frequency for the first transverse mode, a cylindrical chamber would have a diameter approximately three and a half times larger than the mean diameter of the modified annulus. For example, for a 100-Hz first tangential mode, the mean diameter of the modified annulus is approximately 4 feet, as compared to 14 feet for a cylindrical chamber. Thus, a cylindrical chamber is impractical for economical low frequency simulation because of the extremely high flowrates that would be required. A slab augmentor section of a small flow area could be used; however, a longitudinal mode having a frequency of 100 Hz would require a chamber length of approximately 13 feet. Finally, a small combustion chamber could be constantly driven at a low frequency with an oscillating piston or acoustic transducer, but this type of experiment is not a true simulation of an unstable combustion process because the source of instability, the combustion process, and the test sections (damping devices), are not directly coupled as they are in a natural mode experiment.



Note: All dimension shown are in inches.

FD 65599

Figure 32. Augmentor Simulator Schematic

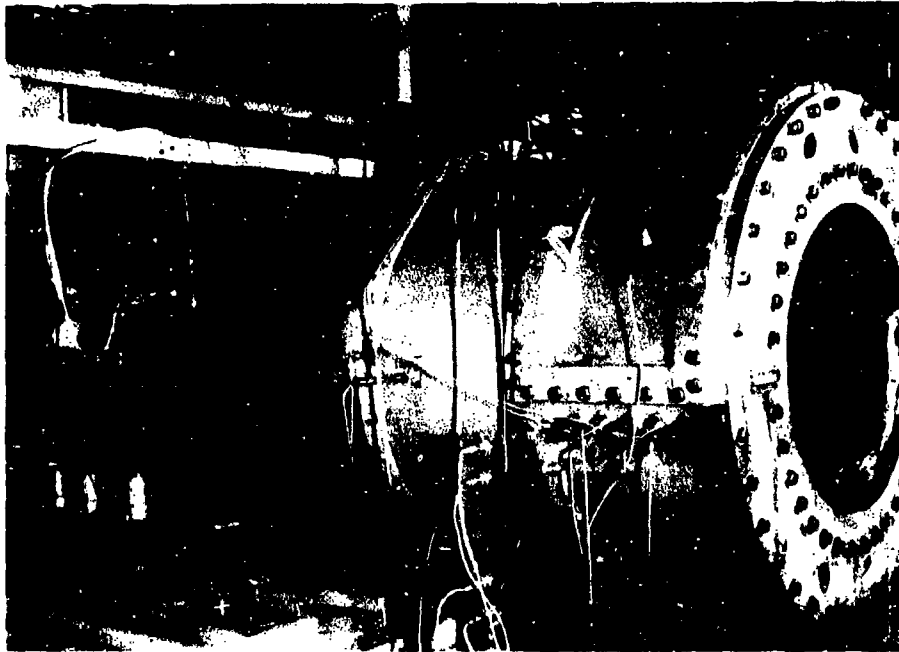


Figure 33. Augmentor Simulator, Test Section Side FE 116547

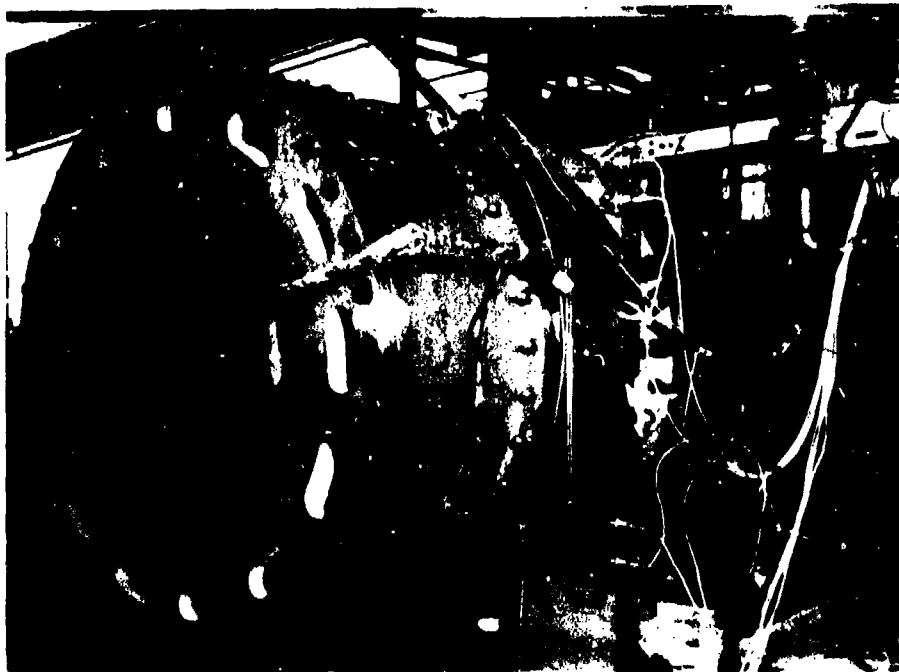


Figure 34. Augmentor Simulator, Nozzle End FE 116545

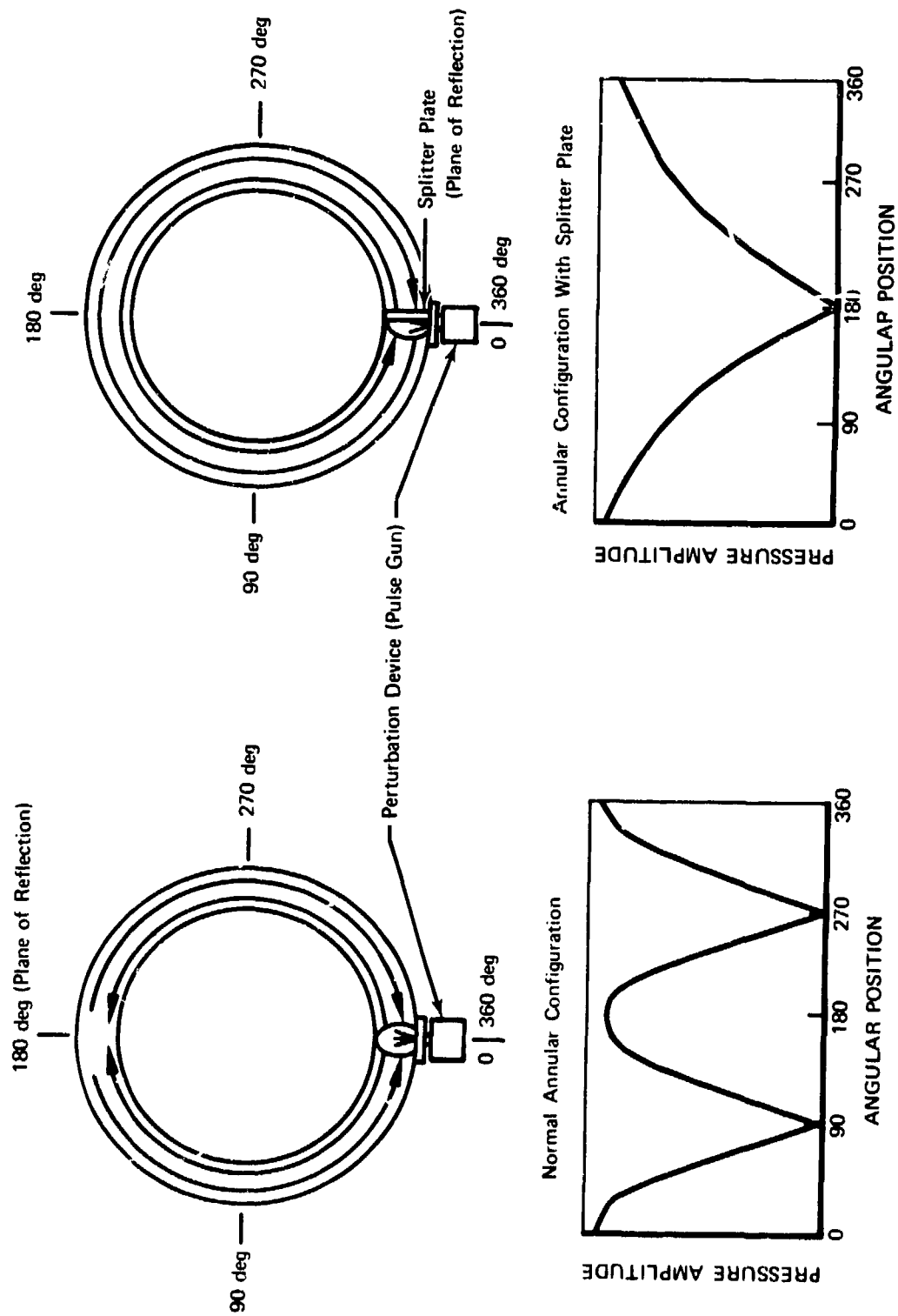


Figure 35. Oscillatory Pressure Distributions (First Traverse Mode) in Annular Combustion Chamber and One With Splitter Plate

FD 65600



The augmentor simulator rig consisted of five basic sections: diffuser, fuel injection section, liner housing section, centerbody section, and nozzle. The diffuser section is used to divert the air from stand plumbing to the combustion chamber. The diffuser consists of an 18 inch-long, cylindrical, flow-straightening section of 17.75-inch internal diameter and a 58-inch conical section that increases to a diameter of 48.6 inches at the point of fuel injection. A diffusion angle of 30 deg was used to prevent flow separation. The type 316 stainless steel walls were 1/4 inch thick.

The fuel injection section is a cylinder of 48.6-inch internal diameter and 24 inches long with 1/4-inch thick walls. JP-5 fuel is injected into the rig in this section through four equally spaced sprayrings mounted 6 inches downstream of the fuel injection section inlet plane. The sprayrings were made of 3/8-inch diameter, 0.035-inch wall tubing; the design is shown in figure 36. Each ring covers an 88 deg segment of the combustion chamber (2 deg growth allowance) and is mounted in the annulus such that there is equal flow area around the sprayring. The fuel is injected perpendicular to the direction of airflow through eighteen 0.036-inch diameter holes spaced equally and alternately on the top and bottom of the sprayring. A rectangular tab was welded behind each hole to improve droplet atomization by increasing turbulence. Fuel is plumbed to the rig in two stages; the first stage consisting of segments in the 90 and 270 deg quadrants and the second stage the remaining two segments. Rig ignition is timed with fuel flow through the first stage only to permit easier starting at a lower fuel-air ratio.

The liner housing section makes up the outer hot wall of the annular combustion chamber. It has a 48.6-inch ID, is 21 inches long, and constructed of 1/2-inch thick, type 316 stainless steel. A 90 deg segment of this section is removable, providing an installation location for acoustic liners. A compressed asbestos gasket provides the seal between the liners and the rig.

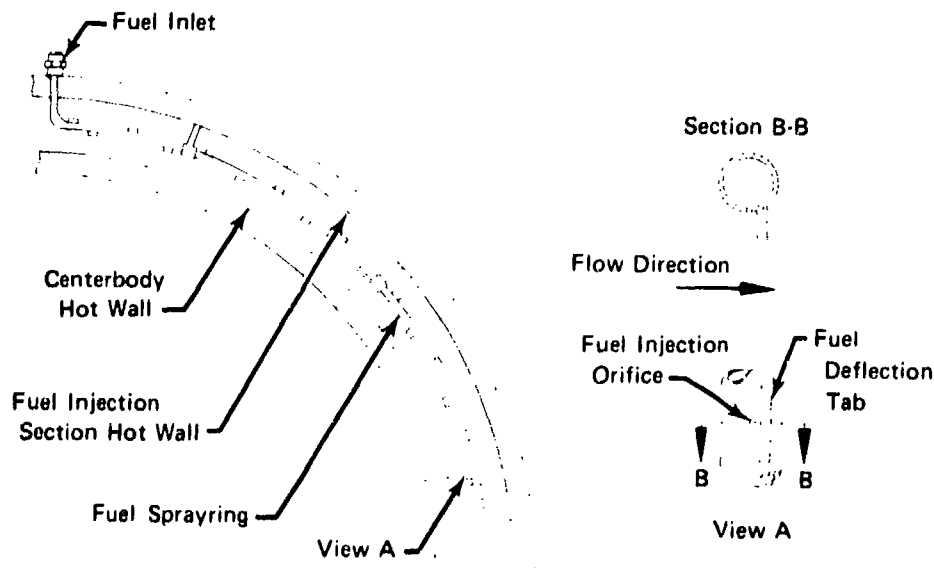


Figure 36. Fuel Sprayring Design

FD 65601

The rig exhausts to ambient conditions through the fixed geometry nozzle shown in figure 37. The nozzle was designed to operate unchoked, allowing a higher Mach No. in the combustion zone that more closely simulated actual augmentor conditions and, in addition, helped prevent longitudinal modes of instability upstream of the flameholder. The total nozzle exit area is 247 square inches, resulting in an exit Mach No. of 0.54 and a combustion zone Mach No. of 0.275.

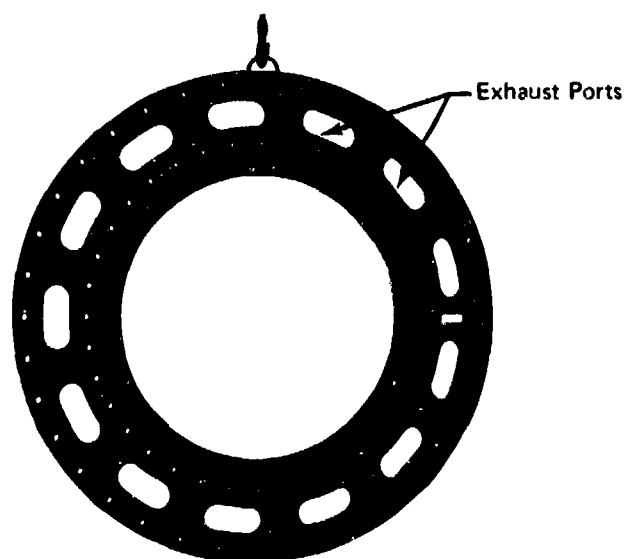


Figure 37. Exhaust Nozzle Plate

FE 116393A

The centerbody is cantilevered off the nozzle and is constructed in two sections. The upstream section, 82 inches long and made of 1/4-inch thick, type 316 stainless steel, extends from the diffuser inlet to the fuel injection exit, providing a constant expansion area in the diffusion section of the rig. A 1-inch diameter, 5.5-inch long rod attached to the centerbody nose cone provides a sliding fit through an aerodynamically contoured support welded to the diffuser section. This support design allows for centerbody growth during hot firing and minimizes centerbody vibrations.

The second centerbody section makes up the inner hot wall of the annular combustion chamber and is 21 inches long, has a 42.6-inch OD, and is made of 1/2-inch thick, type 316 stainless steel. Standard V gutter flameholders are mounted on this section; the flameholder exit plate is 3 inches downstream of the centerbody section 2 inlet plane, which produces a 21-inch long mixing zone between the fuel sprayings and the flameholder, and an 18-inch long combustion zone between the flameholder and the exhaust nozzle.

The standard V gutter flameholder shown in figure 38 is made in four 88 deg segments, each 1.9 inches long and 1.9 inches wide. The 1.9-inch V gutter width results in a 63% annulus blockage. A smaller 1.75-inch long by 1.6-inch wide V gutter is welded on one end of each segment and slides inside the adjacent V gutter to permit expansion while eliminating uneven flow distribution through voids between the flameholders. The flameholder mounting is designed to give equal flow area on each side of the V gutter.

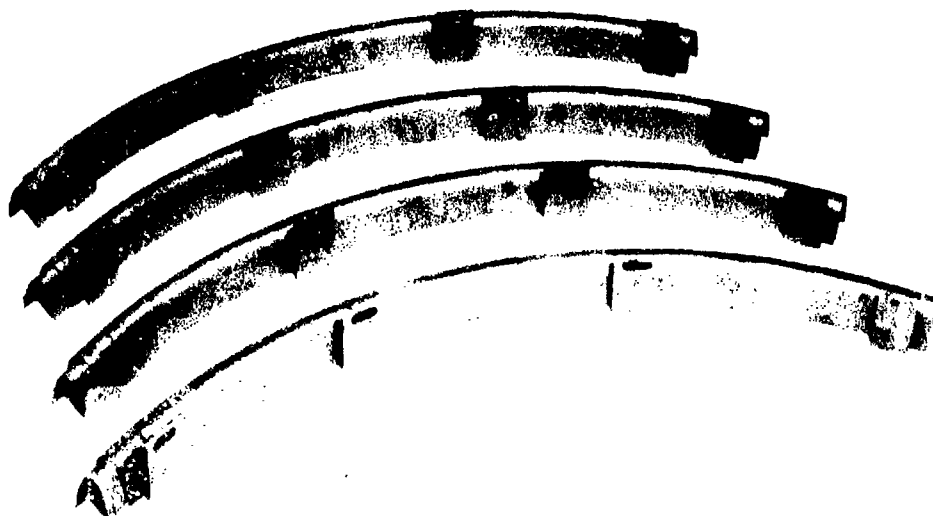


Figure 38. Standard V-Gutter Flameholder

FE 116207

The splitter plate used to obtain the 100-Hz tangential mode in the rig is designed in two sections, as illustrated in figure 39. The upstream section fits between the fuel sprayring and the flameholder with a fixed mount fastening to the ID of the fuel injection assembly and a sliding mount (for growth allowance) fastening to the OD of centerbody section 1. The downstream section fits through a slot in the nozzle and extends to the flameholder with a fixed mount on the OD of centerbody section 2. The downstream splitter is removable to modify the rig to the 250-Hz configuration; figure 40 shows the actual hardware.

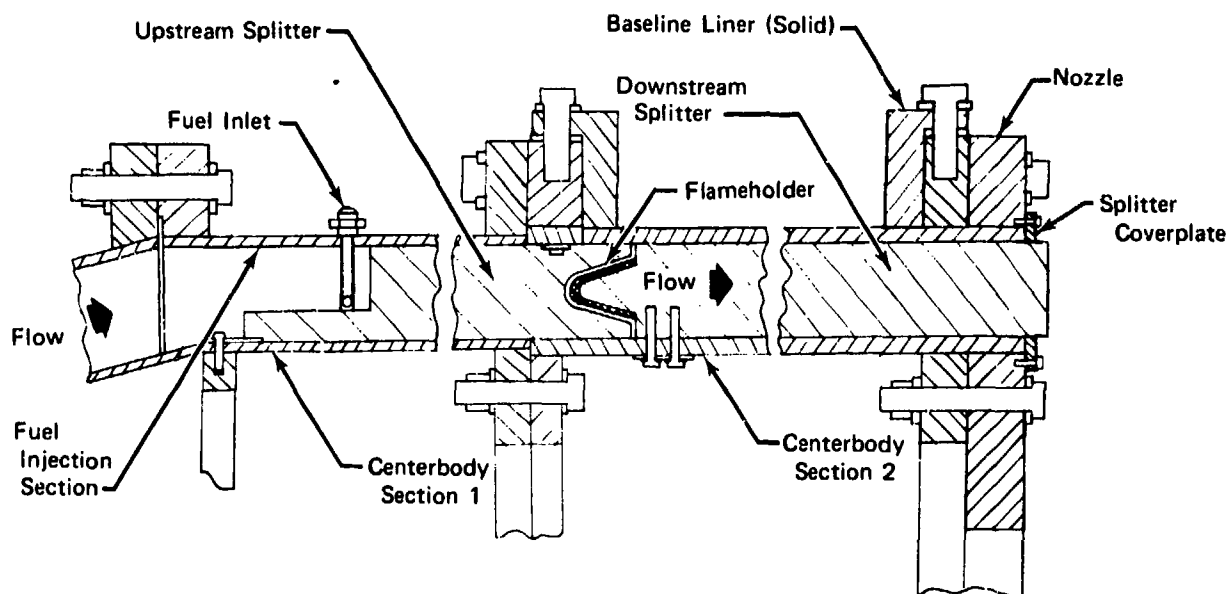


Figure 39. Cross Section of Augmentor Combustion Zone

FD 65602

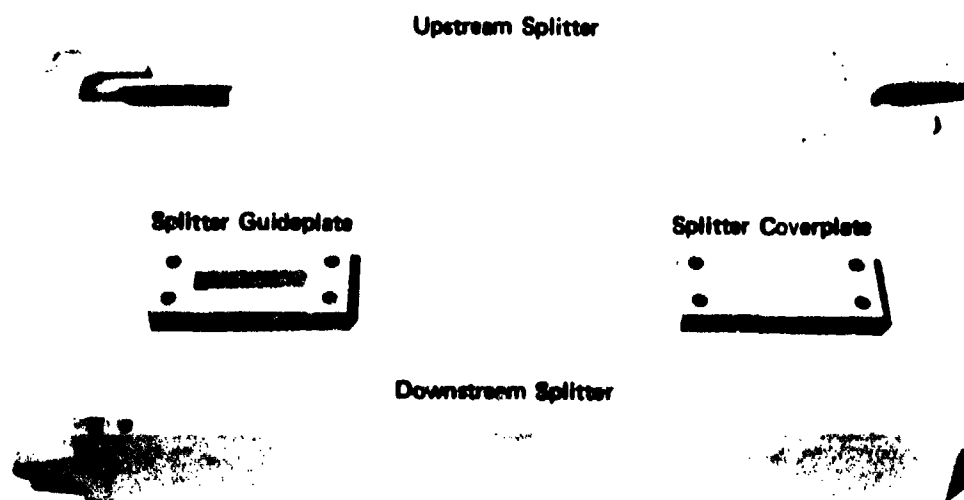


Figure 40. Splitter Plate Hardware

FE 116205A

For duration tests (10 seconds) all walls of the augmentor simulator need no cooling except the natural convection and radiation to the atmosphere. For combustion zone heat shielding, a refractory coating of magnesium zirconate was applied to the nozzle, splitters, baseline flameholder, ID of the liner housing section, and the OD of centerbody section 2. Heat transfer analysis indicated that, if longer duration tests, i. e., over 10 seconds, were attempted, the absence of an adequate heat sink could result in destructive temperatures within the combustion zone section of the centerbody. To provide sufficient cooling for longer tests, a water fog nozzle (4 gpm at 100 psi) mounted on the centerbody axial centerline and discharging water directly into the centerbody was installed, as shown in figure 41.

## 2. Damping Devices

The test sections fabricated for evaluation as low frequency damping devices were a dimpled liner, a complex-porous liner, an acoustic flameholder, a porous flameholder, and a complex-porous flameholder. The design of these test sections was based on the analysis and cold flow experiments as described in Sections II and III.

Both liner test sections were mounted in the liner housing section with the liner facing fitting flush to the adjacent hot wall of the housing section. Figure 42 shows a detail of the installation. The liners extend axially from 1.5 inches upstream of the flameholder exit plane to 1.5 inches upstream of the exhaust nozzle.

As shown in figure 43, the dimpled liner consisted of 24 equally spaced, 1/2-inch diameter apertures with a thickness of 1/2 inch and a backing cavity depth of 3 inches. The liner hot wall was coated with a 0.010-inch thickness of magnesium zirconate. As shown in figure 44, the complex porous test section consisted of a 1/4-inch thick, 2000-SCFM Rigimesh facing backed by 1/4-inch thick, 10% dense Feltmetal section with a 3/4-inch cavity depth. Both liners have 680 square inches of absorbing surface area; figures 45 and 46 show the dimpled liner and complex porous liner, respectively.

All flameholder test sections were similar to the standard V gutter (baseline) flameholder in that each consisted of four 88 deg segments (2 deg growth allowance) that mounted on the centerbody using the baseline flameholder installation locations. In figures 47, 48, and 49 the porous, complex-porous, and acoustic flameholder hardware, respectively, are shown. All of these flameholders have the same exit as the baseline flameholder to obtain the same blockage of the annulus (63%). As shown in figure 50, the porous and complex-porous flameholders also have the same length and contour as the baseline flameholder. The porous flameholder was made of 1/8-inch thick, 2000-SCFM Rigimesh. The complex-porous flameholder was a solid V gutter with a facing of 1/4-inch thick, 2000-SCFM Rigimesh backed with 1/4-inch thick, 10% dense Feltmetal attached inside of the V gutter to form an enclosed volume. The Rigimesh/Feltmetal facing is recessed 0.25 inch to prevent interference with the flame recirculation zone. The ratio of cavity volume to surface area of the complex-porous flameholder is the same as that of the complex-porous liner. The acoustic flameholder design is based on Helmholtz resonator theory. A plate with 41 equally spaced, 0.125-inch diameter holes was inserted into each V gutter

segment to form an enclosed cavity. The flameholder was elongated to 5.8 inches to increase the volume of the cavity and thus bring the resonance frequency of the device into the desired low frequency range. The absorbing surface areas of the complex porous flameholder and the acoustic flameholder are 203 square inches and 215 square inches, respectively.

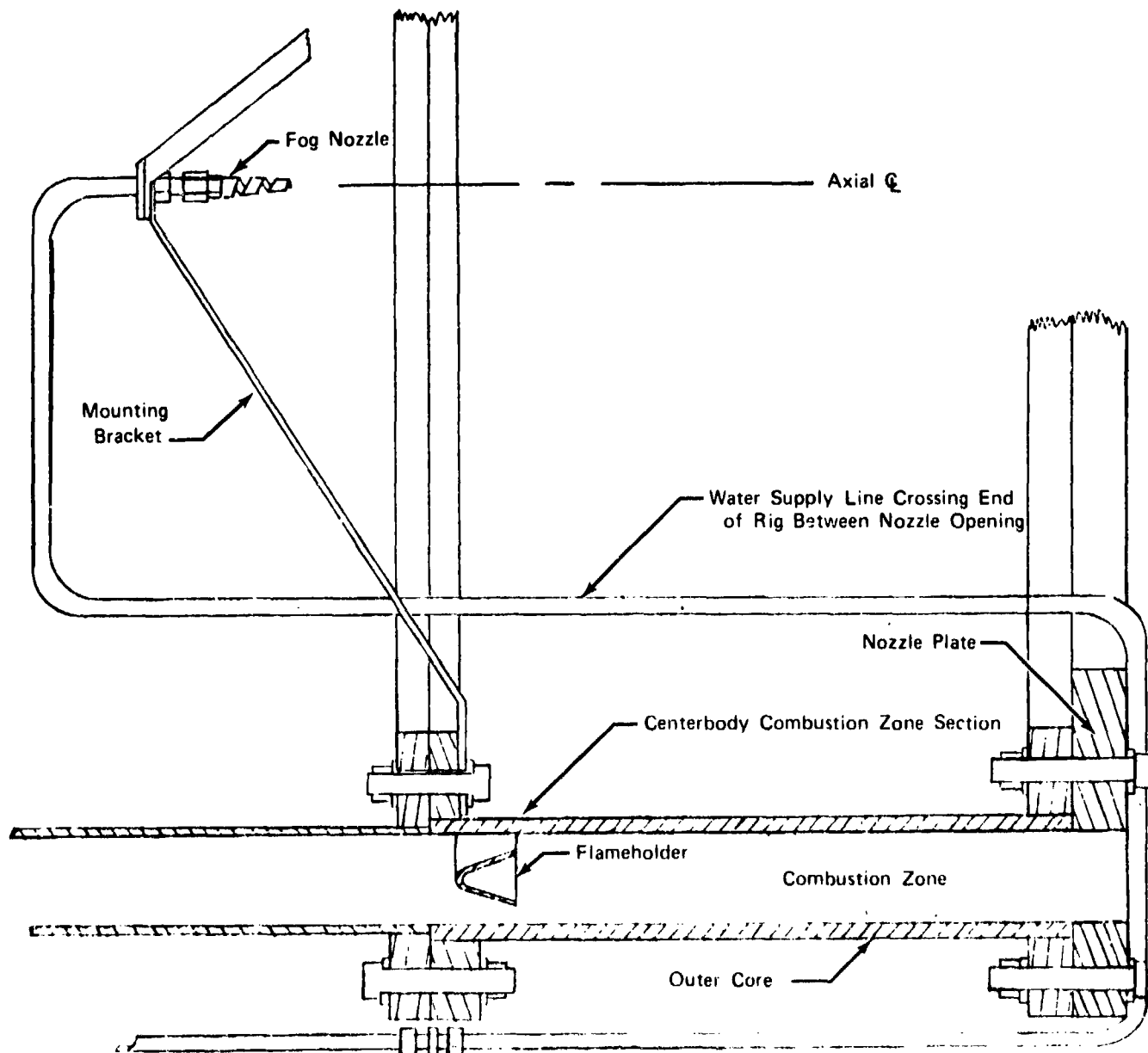


Figure 41. Centerbody Cooling System

FD 65603

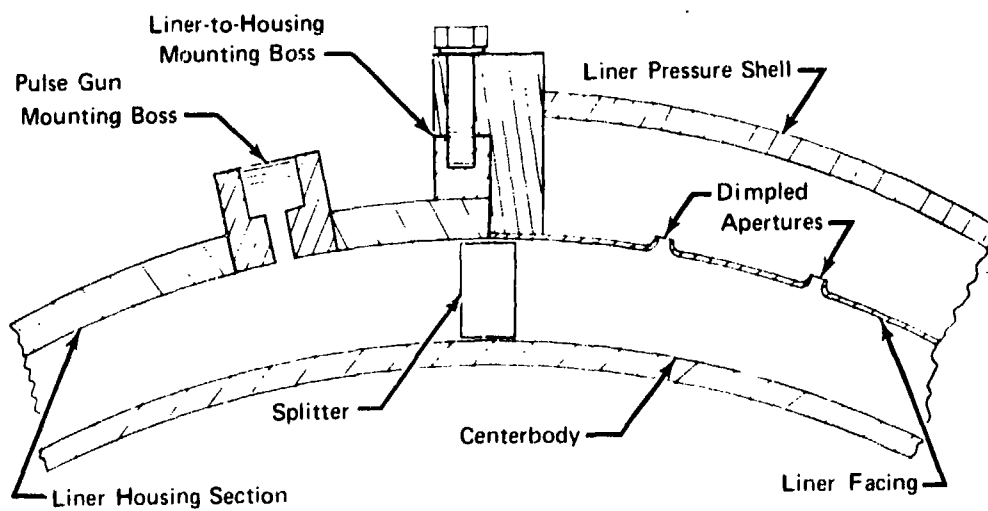
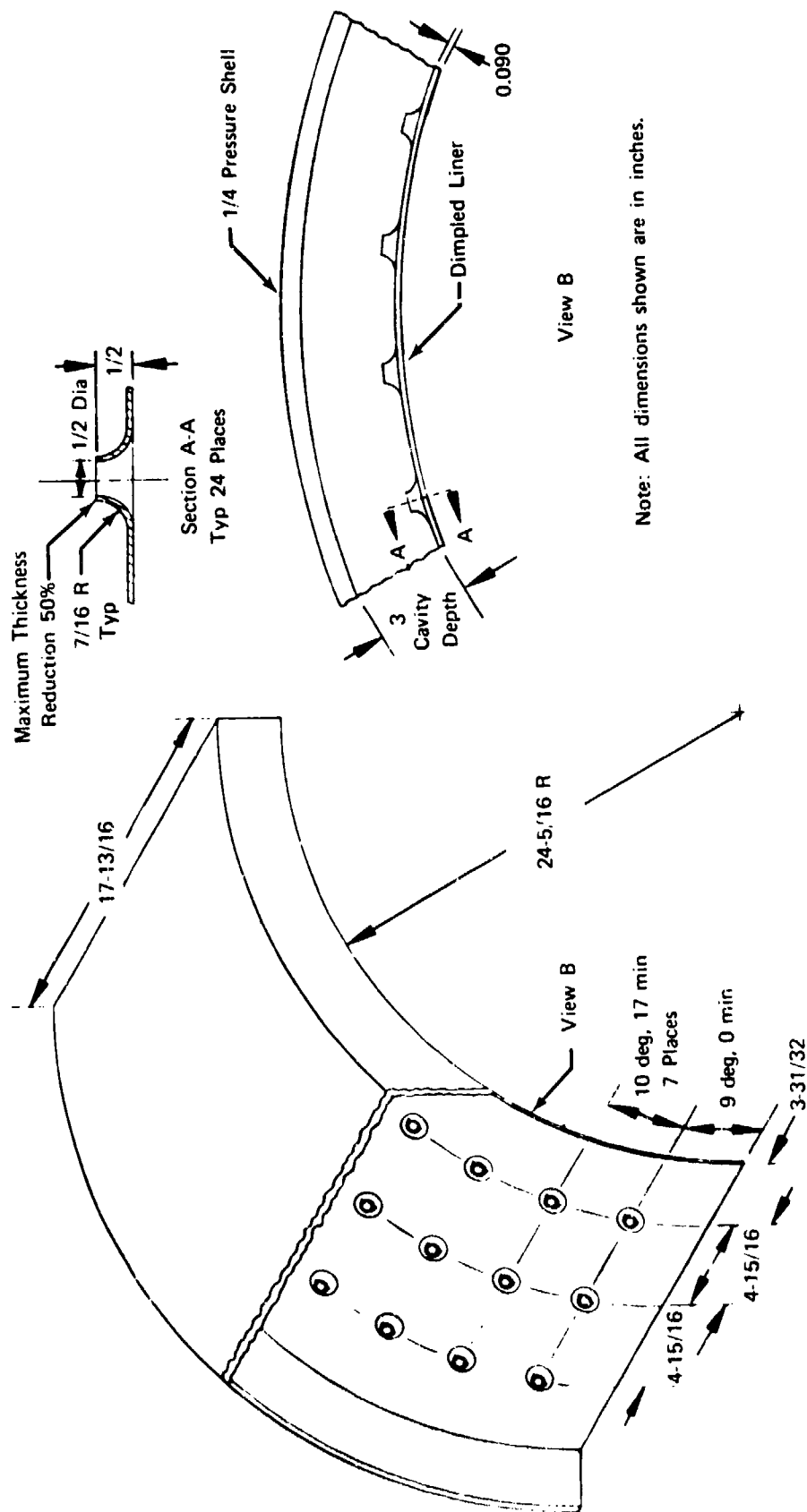


Figure 42. Liner Mounting Design Showing Dimpled Liner Installed

FD 65605



FD 65606

Figure 43. Design Sketch of Dimpled Liner Test Section



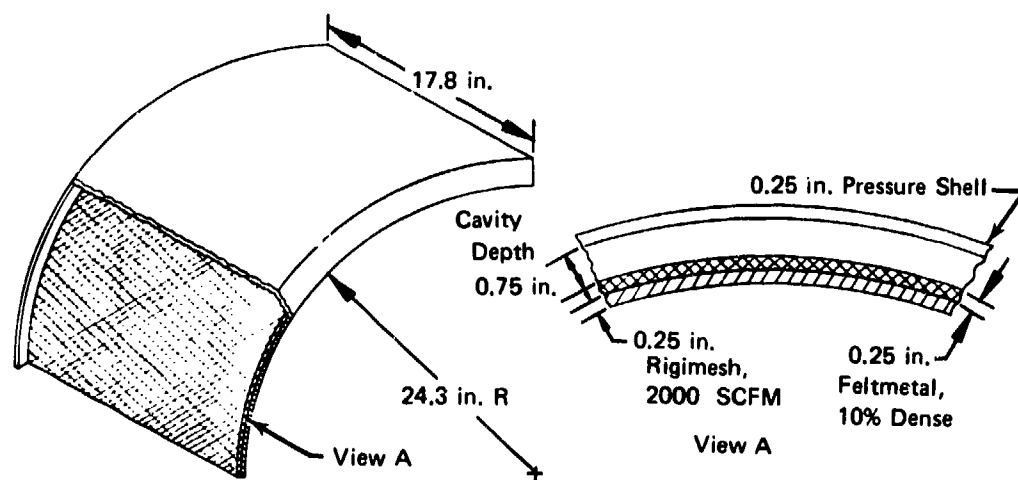


Figure 44. Design Sketch of Complex Porous Test Section

FD 65607



Figure 45. Assembled Dimpled Liner

FE 116174



Reproduced from  
best available copy.



Figure 46. Assembled Complex-Porous Liner

FE 114782

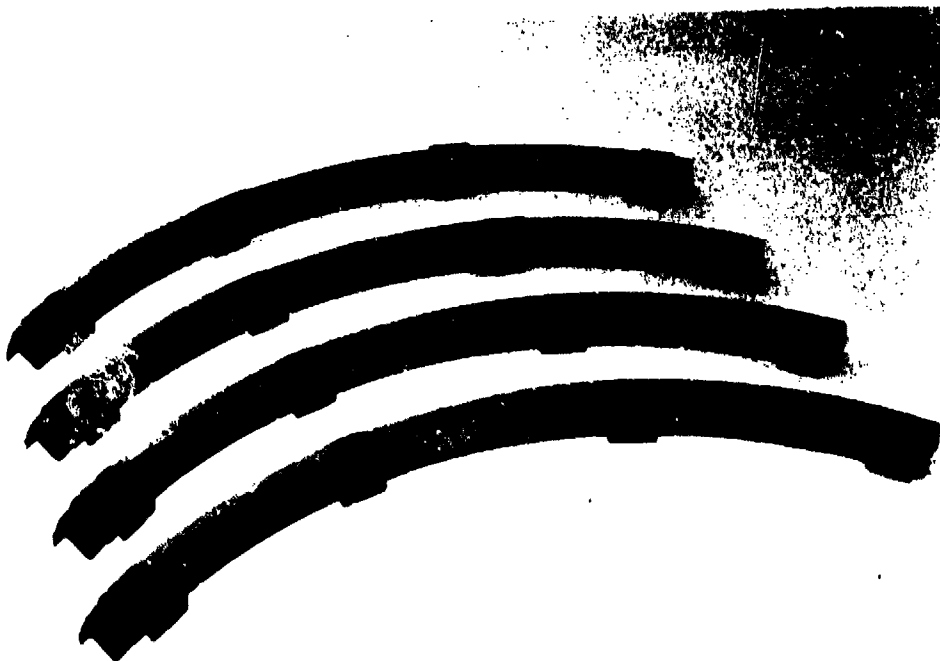


Figure 47. Porous Flameholder

FE 116208

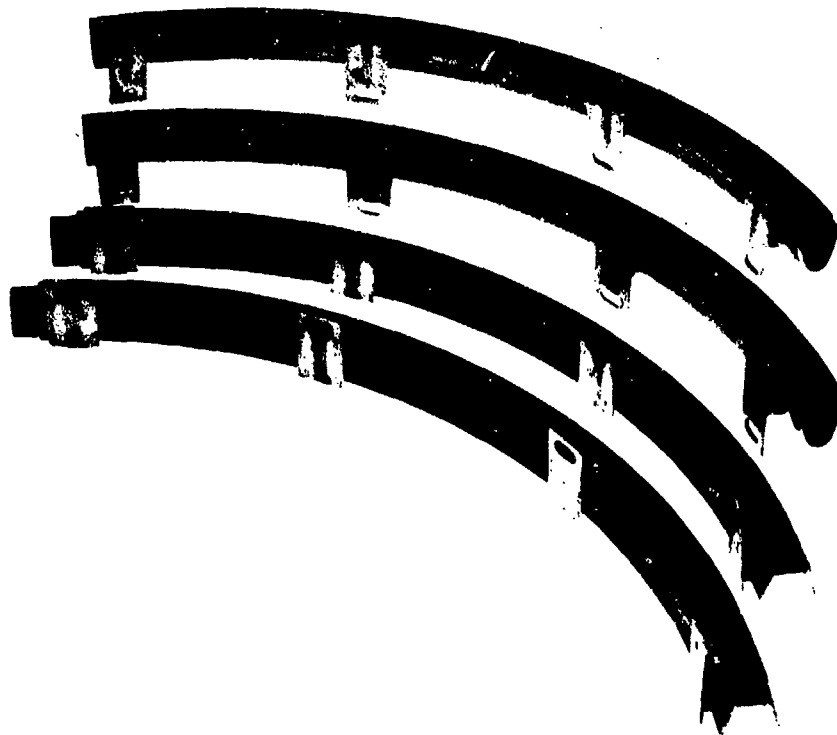


Figure 48. Complex-Porous Flameholder

FE 120402



Figure 49. Acoustic Flameholder

FE 114781

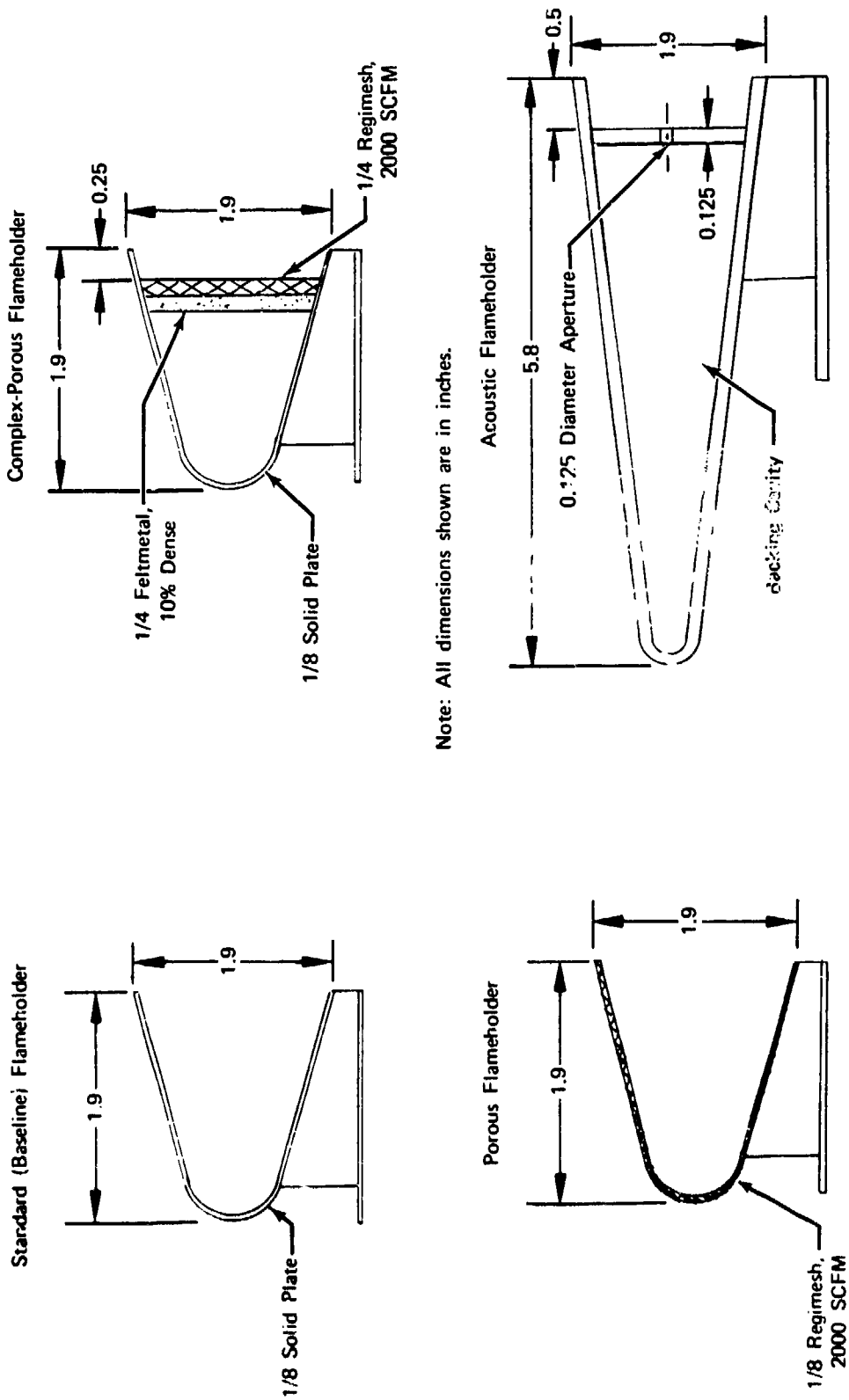


Figure 50. Design Sketches of Flameholders Fabricated for Testing in Augmentor Simulator

FD 65608

### 3. Combustion Perturbation Devices

Provisions were incorporated in the rig design to introduce pressure perturbations with explosive charges fired in wall-mounted pulse guns. A cross-sectional sketch of the pulse gun design is shown in figure 51 and the actual hardware is pictured in figure 52. The pulse gun body consisted of a nickel inner cylinder and an Inconel outer jacket. The jacket is shrunk-fit over the cylinder to help resist the extremely large tensile stresses produced when the charge fires. A threaded cap fastened over the outer jacket provided support for the Conax fitting to prevent it from being blown off when the gun detonated. The gun was loaded with C-4 explosive and detonated electrically with a 6-grain blasting cap. The charge weight could be varied from 6 grains to 95 grains.

Three pulse gun mounting bosses were provided on the liner housing section located angularly 10 deg from the splitter on the side opposite the liner and axially 2, 8, and 14 inches from the flameholder exit plane (figure 53). One, two, or three pulse guns could be fired simultaneously.

An alternate type of explosive device, a nondirectional bomb, was used on two occasions during the test program. The bomb, shown in figure 54, also used C-4 high explosive detonated electrically with a 6-grain blasting cap.

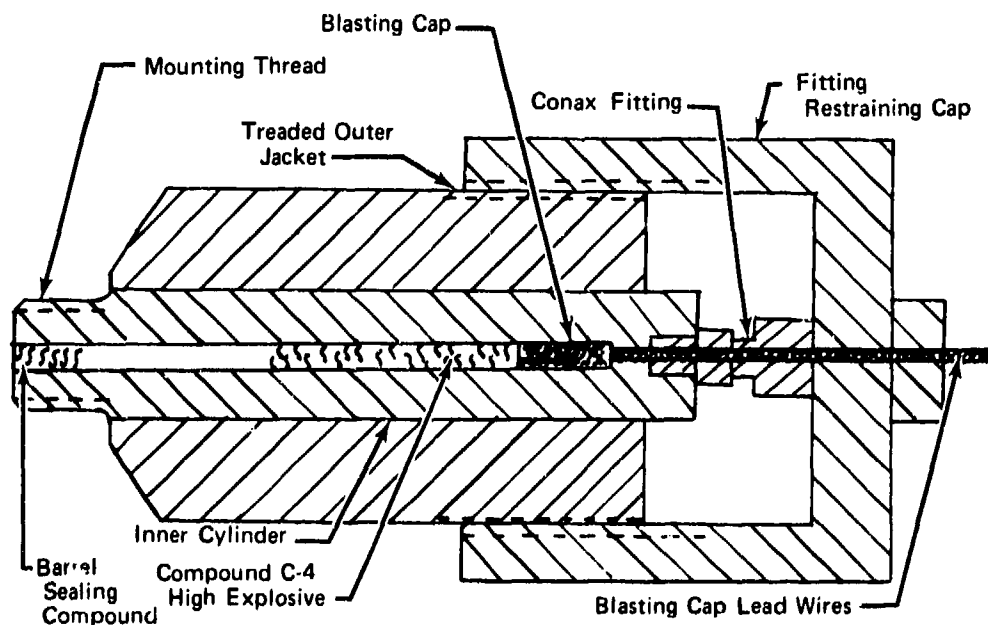


Figure 51. Cross-Sectional Sketch of Pulse Gun Design

FD 65609



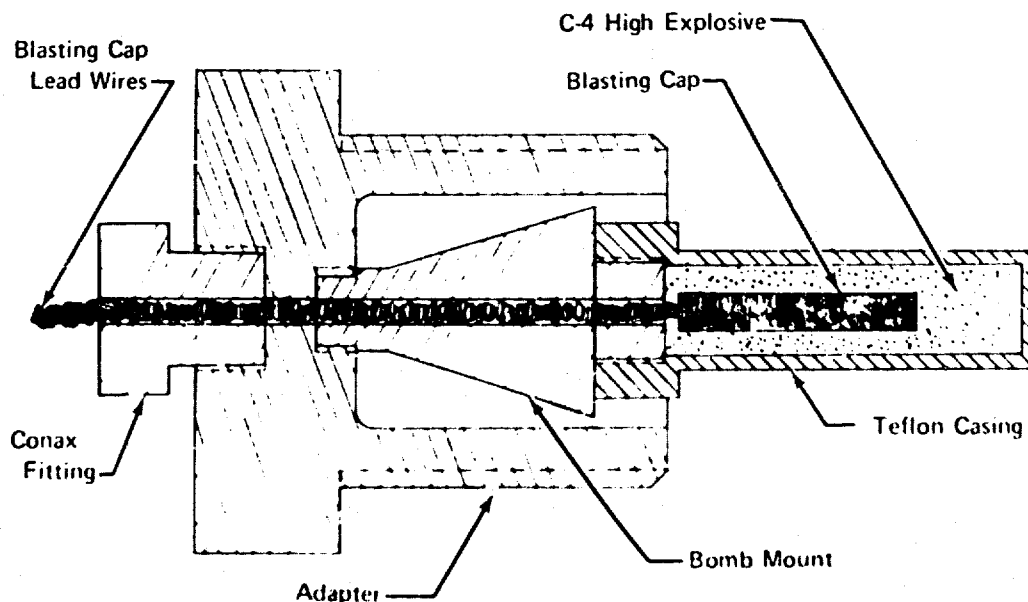


Figure 54. Sketch of Bomb Design

FD 65611

#### 4. Instrumentation

Operating conditions of the augmentor simulator rig were monitored using instrumentation mounted in the diffuser inlet and liner housing. Air inlet conditions were measured by pitot-static pressure probes and uncooled probe-type thermocouples mounted in the cylindrical flow-straightening section of the diffuser 10 inches from the inlet. Static pressure probes and uncooled probe thermocouples were mounted 11.5 inches downstream of the flameholder exit plane to measure combustion zone gas properties. Bare wire thermocouples were installed on the centerbody and liner housing backwalls to measure metal temperatures of combustion zone hardware.

Dynamic pressure transducers are necessary to measure the pressure oscillations resulting from combustion instabilities. Four transducer installation bosses were provided on the liner housing section, as shown in figure 53. The No. 1 and No. 2 transducers were mounted between the pulse gun bosses angularly 10 deg from the splitter and axially 5 and 11 inches, respectively, downstream of the flameholder exit plane. The No. 3 and No. 4 transducers were located angularly 90 and 135 deg from the No. 1 transducer, respectively; both are axially 5 inches from the flameholder exit plane.

Kistler Instrument Corporation Model 606A quartz dynamic pressure transducers were used to obtain electrical signals that are proportional to any pressure instability in the chamber. The Kistler transducers were mounted in water-cooled adapters, as shown in figure 55. The pressure signals were transmitted from the combustion chamber to the transducer through a 0.062-inch diameter passage filled with combustion gases. The passage acts as a resonator and is capable of amplifying dynamic pressure signals if the frequency of the signal is near the natural frequency of the passage. To determine the range over which meaningful data, i.e., unamplified by the resonance characteristics of

the passage, could be obtained, an analysis of the resonance characteristics of the passage was made. The analysis indicated that resonance occurred at 7050 Hz with signal amplification negligible below 5200 Hz.

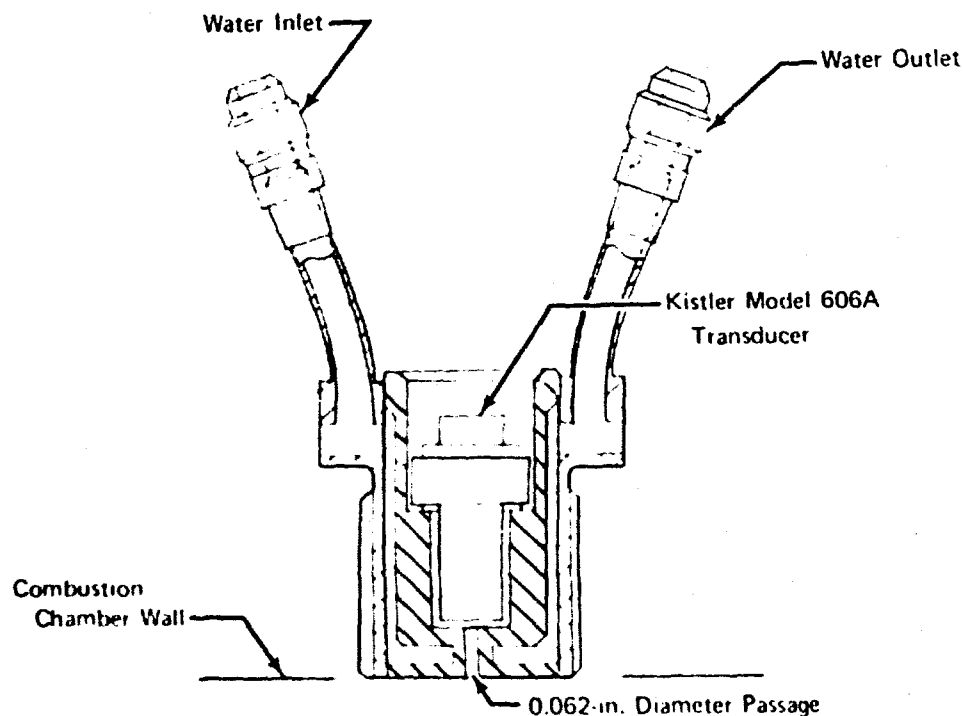


Figure 55. Water-Cooled Kistler Adapter

FD 65612

After the test program was underway it was discovered that the Kistler Model 606A transducers were sensitive to acceleration caused by the pulse gun firing, making pressure decay data unreliable. Model XTEI-190 semiconductor strain gage pressure transducers manufactured by Kulite Semiconductor Products, Inc. were found to be unaffected by acceleration because of the extremely small mass of the sensing element. The adapter shown in figure 56 was fabricated for mounting the Kulite transducers into the water-cooled adapters. Analysis of the modified adapter's resonance characteristics indicated resonance would occur at approximately 2800 Hz, with signal amplification being negligible below 1300 Hz.

Kistler Instrument Corporation Model 553B charge amplifiers were employed to convert the Kistler transducer charge output to a useable voltage level. The amplifiers were set for a gain of approximately 20 millivolts per picocoulomb. Electrical isolation and further amplification were obtained by using specially designed isolation amplifiers. Isolation of the grounded transducer from the grounded but remote recording system was necessary to eliminate ground loops and noise from the system. The additional gain was used to satisfy recording system sensitivity requirements. The Kulite transducers were excited by 10 volts DC from SRC Model 3564 constant voltage power supplies. The output signals were applied to 0.3 Hz high-pass R-C filters to eliminate any thermal drift effects. The filtered signals were then amplified to make the level compatible with calibration and recording systems by Astrodata Model 885 Wideband Differential DC Amplifiers prior to recording.



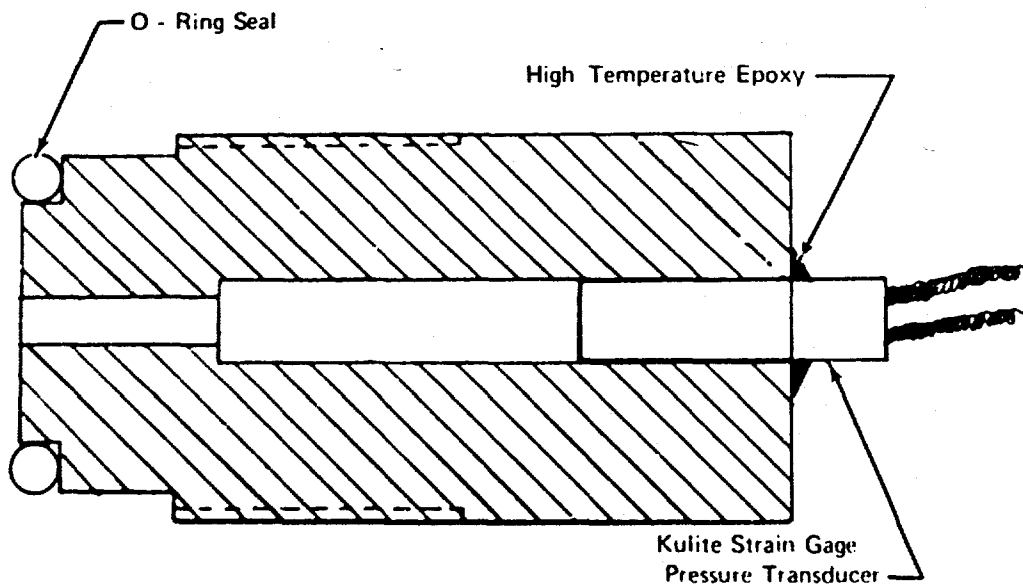


Figure 56. Modified Kulite Adapter

FD 65613

A CEC FR-2500 fourteen channel magnetic tape recorder was used to record the conditioned signals from the transducers. All data were recorded using the FM mode with a 27K Hz IRIG standard center frequency. Each dynamic pressure transducer signal was also parallel-recorded on a test stand oscillograph along with the static pressure and temperature probe data; typical channels are diagrammed in figure 57.

## 5. Test Facility

The turbojet component stand, designated B-2, was used to conduct the Task III test program. As shown in figure 58, the air supply was provided by airbleed from the compressor of a JT4 slave engine. Before entering the rig, the air passed through two orifices and a control valve. An existing heater consisting of a turbojet engine burner can and fuel nozzles was used for pre-heating the air to approximately 1000°F; it was located immediately upstream of the augmentor rig. Schematics of the stand fuel and TEB supply systems are shown in figures 59 and 60.

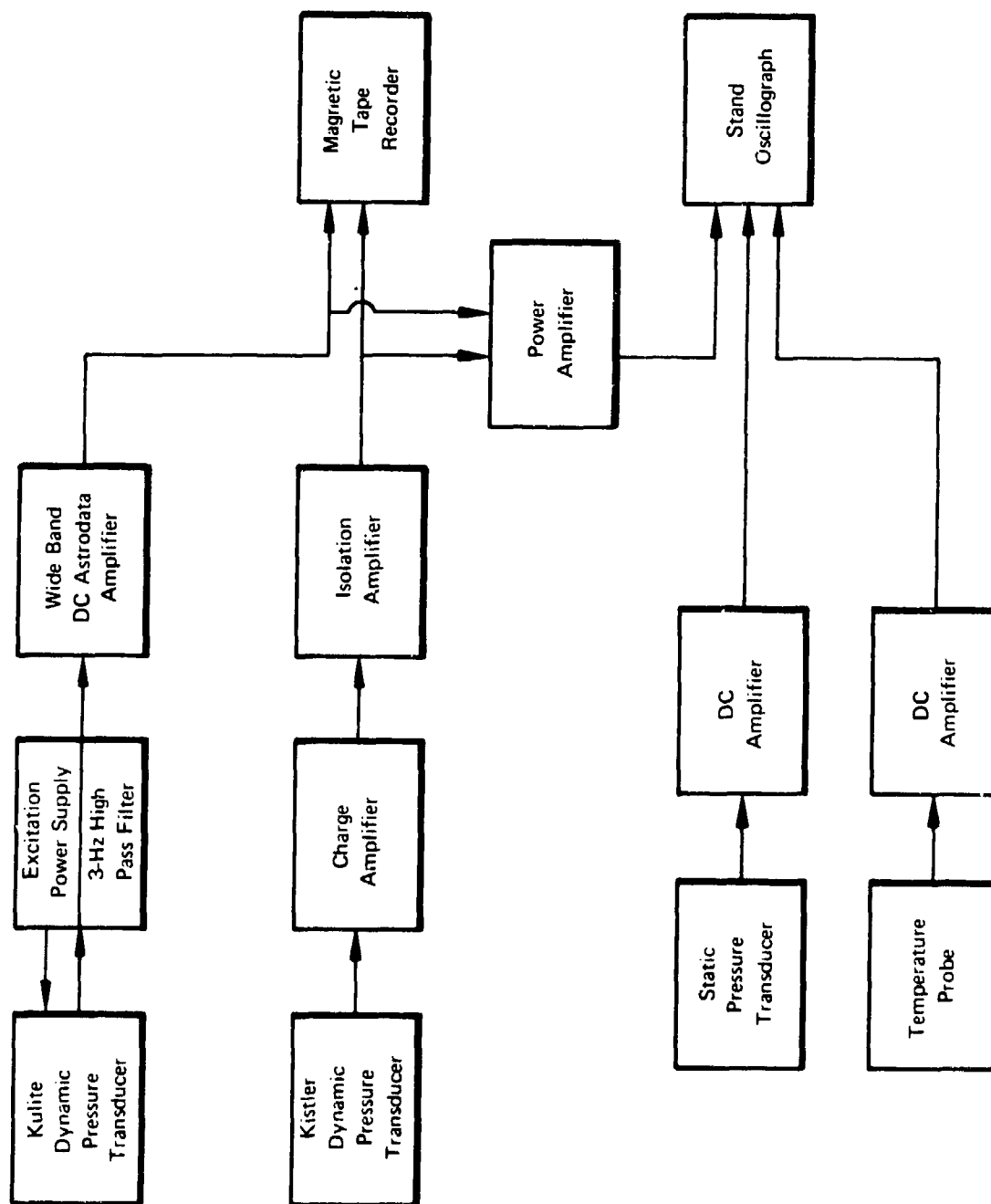


**Figure 57. Instrumentation Diagram Showing Signal Conditioning and Recording Channels**

FD 65614

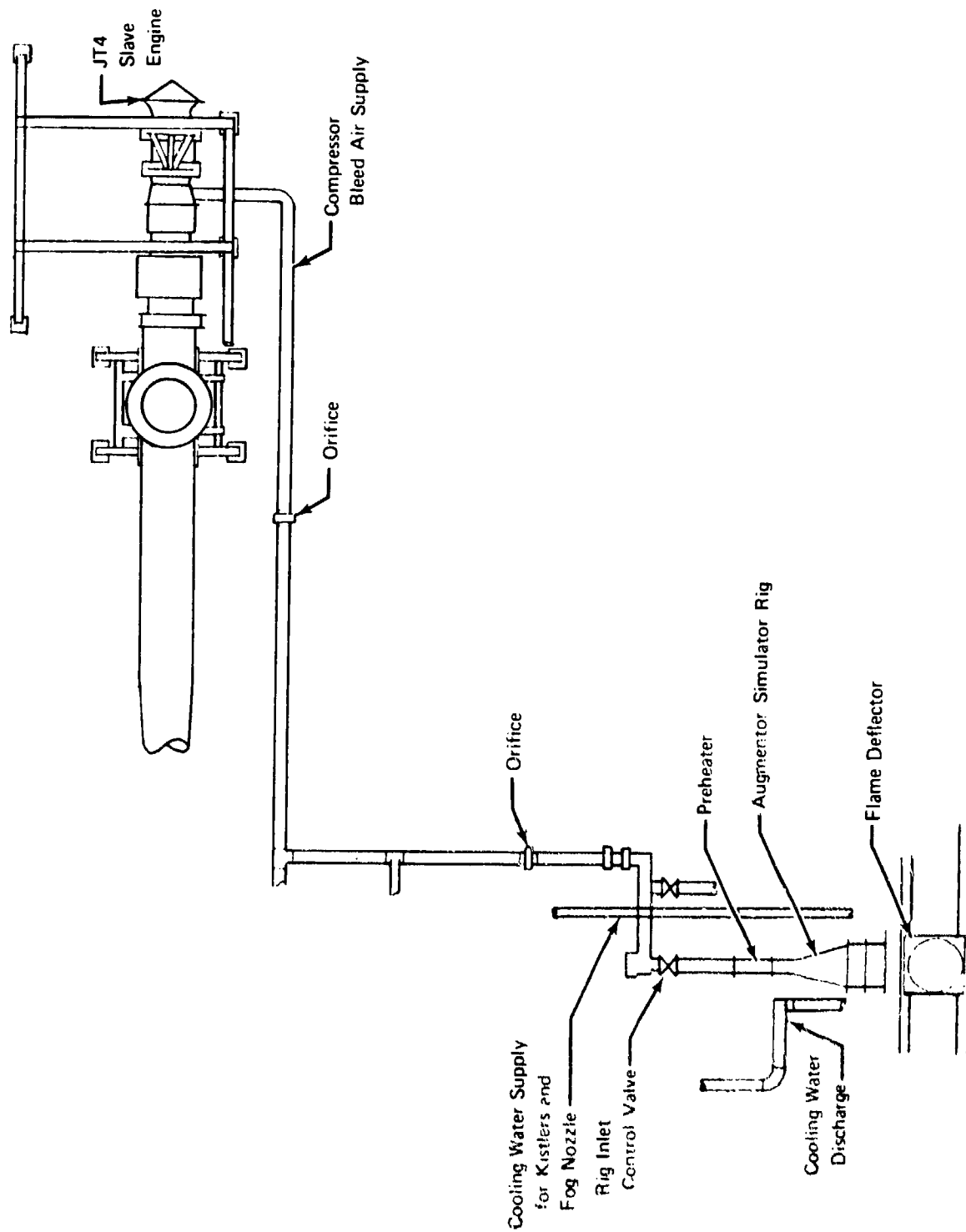
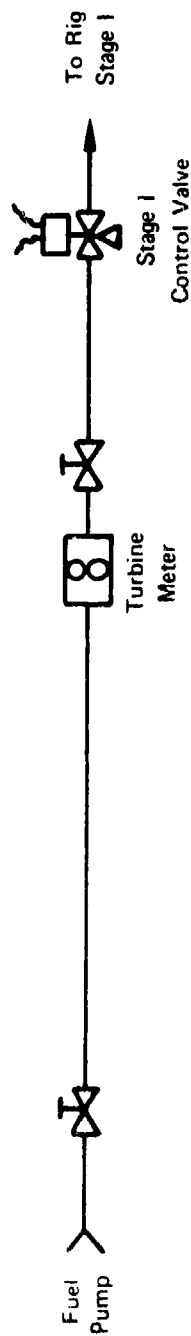


Figure 58. B-2 Test Stand Schematic

FD 65615



Hand Valve

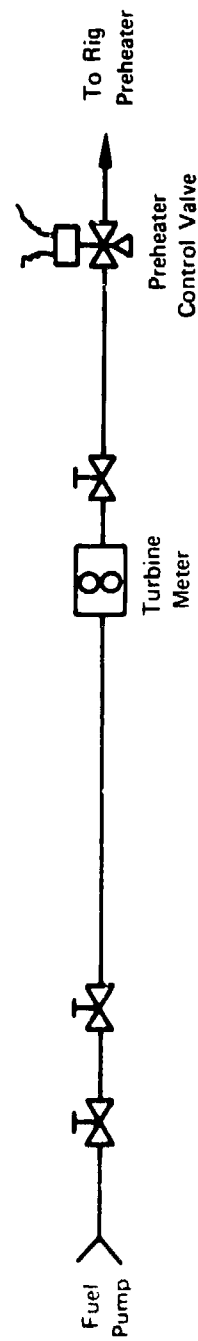
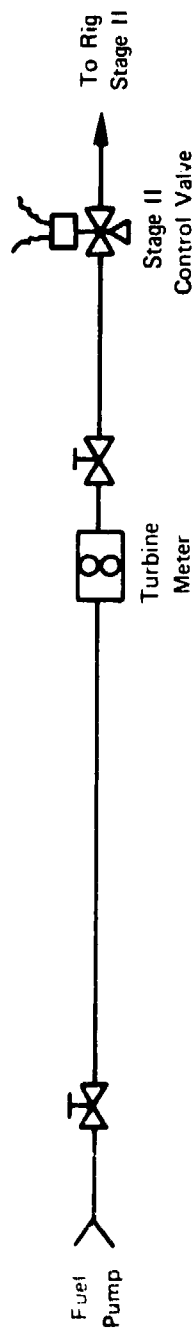


Figure 59. Schematic of Test Stand Fuel Supply System

FD 65616

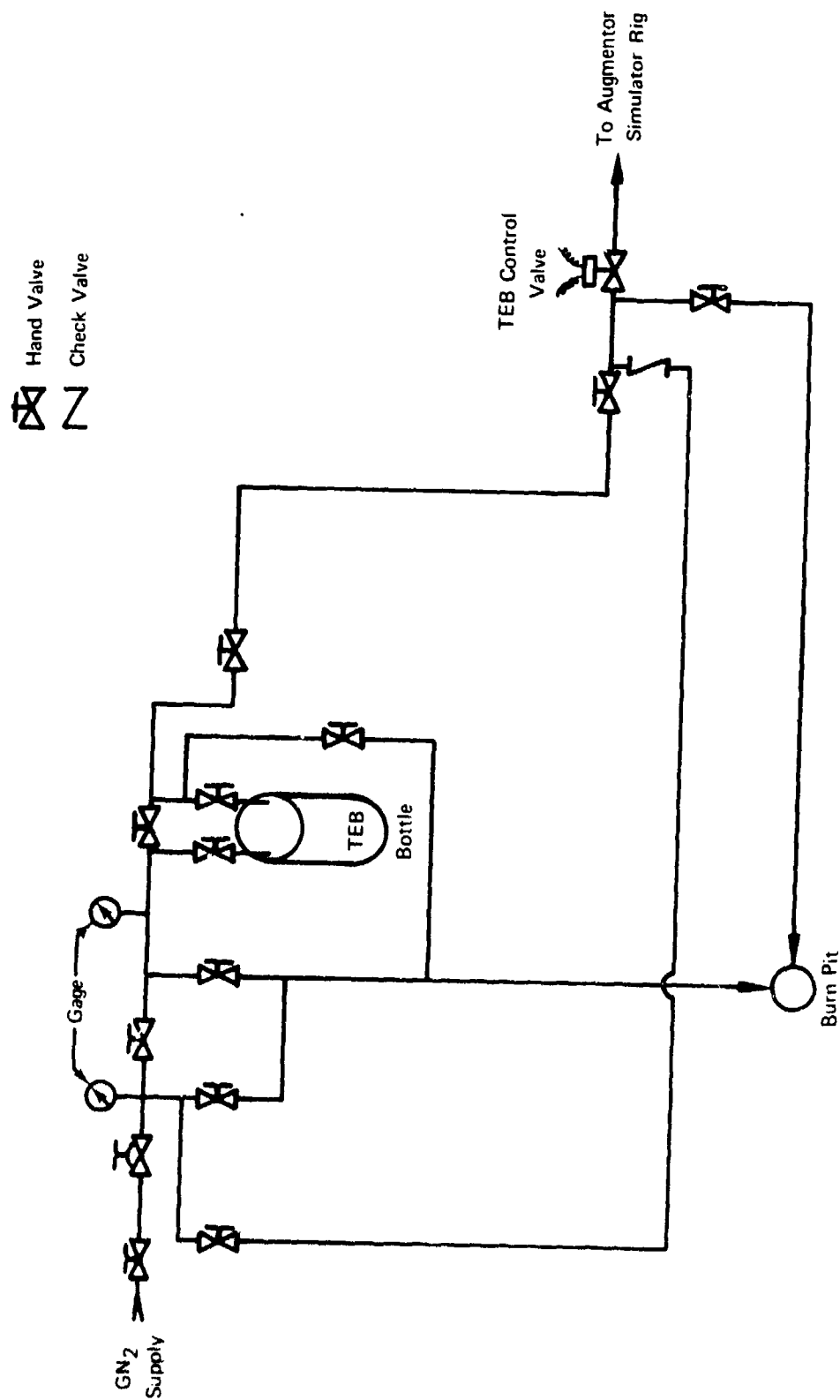


Figure 60. Schematic of Test Stand TEB Supply System

FD 65617

## B. SIMULATOR TESTS

### 1. Method of Test

To approximate augmentor operating conditions at altitude, a pressure of 17.5 psia was chosen as the nominal chamber pressure. To obtain the additional design point operating conditions summarized in table 3, the subsequent test procedures were followed:

- The slave engine was started and adjusted to approximately 50% power lever. The engine compressor bleed valve and stand dump valves were opened, and a blowdown was completed on stand plumbing up to the rig inlet to remove any condensed moisture and debris.
- Dump valves were closed and the rig inlet valve opened, allowing airflow through the preheater and rig. Airflow was then set by adjusting the position of the rig inlet valve to obtain 8-10 lb/sec, as measured by an instrumented orifice upstream of the preheater. Fuel pumps were started and preheater fuel flow, measured by a turbine meter, set at 1 gpm. Stage I and stage II rig fuel flows were also set for the desired fuel-air ratio at this time. The preheater fuel inlet valve was opened manually and a preselected volume of triethylborane (TEB) injected into the preheater for ignition. Rig inlet air temperature was monitored and airflow rate and preheater fuel flowrate were increased simultaneously to attain the desired inlet conditions of 26 lb/sec and 1000°F.
- With prerun setup completed, testing commenced by arming and starting the events sequencer, which operated the following controls in the sequence shown in table 4: preheater, stage I, and stage II fuel inlet valves; rig cooling water inlet valve, rig chemical igniter injection valve, No. 1, 2, and 3 pulse gun firing voltage circuits; and combustion zone temperature level (for aborting the test if ignition was unsuccessful). Test duration was 13.5 sec; however, the rig airflow was maintained for cooldown purposes until combustion zone metal temperatures decreased below 800°F.

Table 3. Design Point Operating Conditions

|                                       |             |
|---------------------------------------|-------------|
| Inlet Temperature, °F                 | 1000        |
| Airflow Rate, lb <sub>m</sub> /sec    | 26          |
| Fuel-Air Ratio                        | 0.05        |
| Combustion Zone Static Pressure, psia | 17          |
| Mean Combustion Zone Temperature, °F  | 3600        |
| Mach No. at Flameholder               | 0.453       |
| Mach No. in Combustion Zone           | 0.275       |
| Exhaust Back Pressure                 | Atmospheric |

Table 4. Augmentor Simulator Test Procedure

| Event   | Time, sec |
|---|-----------|
| First Stage Fuel Flow On                          | 0.0       |
| Injection of Chemical Igniter                     | +0.5      |
| Second Stage Fuel Flow On                         | +2.5      |
| Verification of Ignition                          | +5.5      |
| Fire Pulse Guns (1, 2, or 3 fired simultaneously) | +6.5      |
| Shut Down Fuel Flow                               | +13.5     |
| Shut Down Preheater                               | +13.5     |

## 2. Description of Tests

The objective of the first augmentor simulator test was to determine the amplitude and frequency of any spontaneous combustion instability encountered with the rig in the baseline configuration, i.e., with standard flameholders and no damping devices installed.

The rig was assembled with the splitter installed and with no pulse guns. The first two test attempts were made with an airflow of 26 lb<sub>m</sub>/sec and a fuel-air ratio of 0.05. The rig would not ignite at these conditions, hence the airflow was reduced to approximately 23 lb<sub>m</sub>/sec while maintaining the 0.05 fuel-air ratio. Ignition occurred at the lower airflow rate and a successful test (test number 3) of 7.5 sec duration was completed; a summary of the measured test conditions is given in table 5. Preliminary dynamic pressure data recorded on low speed (16 inches/sec) test stand oscillographs indicated that the rig was spontaneously unstable, with peak-to-peak amplitudes of 1 psi occurring at a frequency of 230 Hz.

At shutdown, maximum combustion zone backwall temperatures of both the centerbody and outer core were approximately 400 °F below the design limits of 1200 °F; therefore, the run duration of all subsequent tests was increased to 13.5 sec. Test 4 was conducted with the rig in the same configuration; the resulting frequency and amplitude of the spontaneous instability were essentially the same as that of the previous test. No overheating problems were encountered with the longer test duration.

A pulse gun, loaded with 34 grains of C-4 high explosive and a 6-grain blasting cap was fired at the No. 2 position (figure 53) 6.5 sec after rig ignition during test 6. The purpose of this test was to determine the baseline perturbation decay rate of the rig. Preliminary data indicated that the decay times were approximately 0.02 sec. The next test (test 7) was a repeat of test 6; similar results were obtained.

Table 5. Measured Augmentor Simulator Operating Conditions

| Test No. | Test Type                     | Airflow<br>Rate,<br>lb <sub>m</sub> /sec | Fuel<br>Flowrate,<br>lb <sub>m</sub> /sec | Combustion<br>Zone Static<br>Pressure,<br>psia | Inlet<br>Temp.,<br>°F | Combustion *<br>Zone Temp.,<br>°F | Liner<br>Cavity<br>Temp.,<br>°F | Centerbody<br>Backwall<br>Temp.,<br>°F |
|----------|-------------------------------|--|---|--|-----------------------|-----------------------------------|---------------------------------|--|
| 3        | Baseline                      | 21.2                                     | 1.30                                      | 16.9   | 985                   | 2700                              | ---                             | 700                                    |
| 4        | ↓                             | 22.6                                     | 1.30                                      | 17.6   | 977                   | 2740                              | ---                             | 820                                    |
| 6        | ↓                             | 24.6                                     | 1.31                                      | 17.8   | 962                   | 2550                              | ---                             | 800                                    |
| 7        | ↓                             | 21.3                                     | 1.30                                      | 17.0   | 988                   | 2590                              | ---                             | 800                                    |
| 8        | ↓                             | 24.0                                     | 1.31                                      | 17.5   | 926                   | 2570                              | ***                             | 820                                    |
| 9        | ↓                             | 24.3                                     | 1.31                                      | 17.8   | 927                   | 2550                              | ***                             | 790                                    |
| 10       | ↓                             | 23.8                                     | 1.30                                      | 17.5   | 927                   | 2580                              | 807                             | 770                                    |
| 13       | ↓                             | 22.8                                     | 1.29                                      | 17.6   | 984                   | 2580                              | 1220                            | 760                                    |
| 14       | ↓                             | 23.0                                     | 1.52                                      | 17.8   | 869                   | 2670                              | 1030                            | 800                                    |
| 17       | Baseline                      | 23.2                                     | 1.30                                      | **   | 997                   | 2550                              | ---                             | 790                                    |
| 18       | ↓                             | 23.7                                     | 1.51                                      | **   | 984                   | 2810                              | ---                             | 710                                    |
| 19       | ↓                             | 23.9                                     | 1.29                                      | **   | 950                   | 2540                              | ---                             | 710                                    |
| 20       | ↓                             | 23.4                                     | 1.50                                      | **   | 911                   | 2710                              | ---                             | 730                                    |
| 21       | ↓                             | 24.0                                     | 1.56                                      | **   | 913                   | 2710                              | ---                             | 760                                    |
| 22       | ↓                             | 23.3                                     | 1.28                                      | 17.4   | 1014                  | 2540                              | ---                             | 740                                    |
| 23       | ↓                             | 21.6                                     | 1.52                                      | 17.6   | 958                   | 2600                              | ---                             | 780                                    |
| 24       | ↓                             | 22.7                                     | 1.57                                      | 17.6   | 951                   | 2660                              | ---                             | 740                                    |
| 25       | ↓                             | 22.8                                     | 1.30                                      | 17.5   | 986                   | 2530                              | ---                             | 770                                    |
| 26       | ↓                             | 24.5                                     | 1.29                                      | 18.4   | 970                   | 2480                              | ---                             | 880                                    |
| 27       | ↓                             | 24.2                                     | 1.61                                      | 18.5   | 915                   | 2580                              | ---                             | 770                                    |
| 28       | ↓                             | 24.7                                     | 1.59                                      | 18.6   | 895                   | 2580                              | ---                             | 870                                    |
| 29       | ↓                             | 24.5                                     | 1.29                                      | 18.7   | 945                   | 2560                              | ---                             | 760                                    |
| 30       | Complex-Porous<br>Flameholder | 24.6                                     | 1.57                                      | 18.7   | 912                   | 2690                              | ---                             | 790                                    |
| 31       | ↓                             | 24.3                                     | 1.57                                      | 18.7   | 936                   | 2730                              | ---                             | 720                                    |
| 32       | ↓                             | 24.3                                     | 1.28                                      | 18.6   | 959                   | 2580                              | ---                             | 790                                    |
| 34       | ↓                             | 24.9                                     | 1.31                                      | 18.4   | 921                   | 2760                              | ---                             | 800                                    |
| 35       | ↓                             | 25.4                                     | 1.59                                      | 18.8   | 908                   | 2880                              | ---                             | 820                                    |
| 36       | ↓                             | 25.2                                     | 1.31                                      | 18.4   | 916                   | 2700                              | ---                             | 750                                    |
| 37       | ↓                             | 24.0                                     | 1.59                                      | 18.6   | 920                   | 2890                              | ---                             | 740                                    |



Table 5. Measured Augmentor Simulator Operating Conditions (Continued)

| Test No. | Test Type                                  | Airflow<br>Rate,<br>lbm/sec | Fuel<br>Flowrate,<br>lbm/sec | Combustion<br>Zone Static<br>Pressure,<br>psia | Inlet<br>Temp,<br>°F | Combustion *<br>Zone Temp,<br>°F | Liner<br>Cavity<br>Temp,<br>°F | Centerbody<br>Backwall<br>Temp,<br>°F |
|----------|--|-----------------------------|------------------------------|--|----------------------|----------------------------------|--------------------------------|---------------------------------------|
| 38       | Porous Flameholder<br>With Dimpled Liner   | 24.1                        | 1.30                         | 18.4   | 947                  | 2660                             | 1608                           | 880                                   |
| 40       |  | 23.2                        | 1.57                         | 18.6   | 966                  | 2810                             | 1410                           | 820                                   |
| 41       |  | 23.1                        | 1.29                         | 18.5   | 1010                 | 2630                             | 1558                           | 780                                   |
| 42       |  | 23.0                        | 1.57                         | 18.5   | 978                  | 2780                             | 1292                           | 840                                   |
| 45       | Baseline Flameholder<br>With Dimpled Liner | 25.3                        | 1.57                         | 18.7   | 890                  | 2700                             | 1197                           | 780                                   |
| 46       |  | 25.6                        | 1.30                         | 18.6   | 941                  | 2540                             | 1470                           | 750                                   |
| 47       |  | 24.8                        | 1.56                         | 18.7   | 942                  | 2930                             | 1323                           | 1036                                  |
| 48       |  | 25.1                        | 1.57                         | 19.2   | 949                  | 2821                             | 1431                           | 1051                                  |
| 49       |  | 25.6                        | 1.30                         | 19.0   | 978                  | 2689                             | 1567                           | 960                                   |
| 50       |  | 25.4                        | 1.28                         | 18.7   | 966                  | ***                              | N/A                            | 947                                   |
| 51       |  | 24.6                        | 1.30                         | 18.8   | 962                  | 2853                             | N/A                            | 866                                   |
| 52       |  | 24.5                        | 1.30                         | 18.7   | 952                  | 2866                             | N/A                            | 840                                   |
| 53       |  | 24.3                        | 1.56                         | 18.8   | 962                  | 2955                             | N/A                            | 907                                   |
| 54       |  | 24.8                        | 1.59                         | 19.0   | 943                  | 2934                             | N/A                            | 925                                   |
| 55       |  | 24.6                        | 1.31                         | 18.8   | 962                  | 2690                             | N/A                            | 979                                   |
| 56       |  | 24.6                        | 1.30                         | 18.4   | 964                  | ***                              | 909                            | 848                                   |
| 57       |  | 24.9                        | 1.56                         | 18.7   | 916                  | 2840                             | 842                            | 819                                   |
| 58       |  | 24.9                        | 1.29                         | 18.5   | 956                  | 2449                             | 842                            | 818                                   |
| 59       |  | 25.3                        | 1.57                         | 18.8   | 921                  | 2763                             | 809                            | 804                                   |
| 60       | Porous Liner                               | 24.8                        | 1.28                         | 18.7   | 1145                 | 2763                             | ***                            | ***                                   |

\* Temperature is in error by approximately 20% because of radiation losses from unshielded probe.

\*\* System leak resulted in incorrect readings.

\*\*\* Did not record properly.

The complex porous liner (1/4-inch thick, 2000-SCFM Rigimesh hotwall backed with 1/4-inch thick, 10% dense Feltmetal and a 3/4-inch deep cavity) was installed and three more tests were conducted. The first test (test 8) was made with no pulse gun, but each of the other tests (9 and 10) were made with 2 pulse guns located in the No. 1 and 2 positions. Preliminary data indicated that the peak-to-peak amplitude of the spontaneous instability was approximately 30% lower than that of the baseline configuration.

Spectrum analysis of dynamic pressure data from the above tests was completed that provided peak-to-peak amplitudes averaged from 1 sec of data over a frequency range of 0-500 Hz. The analysis revealed that the highest amplitudes occurred in a frequency range of 210 to 290 Hz, with the maximum occurring at 230 Hz. All amplitudes measured at this frequency were less than 5% of static chamber pressure, i. e., less than 0.87 psi. As the fuel-air ratio approaches stoichiometric, augmentor combustion usually becomes more unstable; thus, in an attempt to obtain data under the most unstable conditions, it was decided to conduct subsequent tests at both the original fuel-air ratio of 0.05 and at stoichiometric (fuel-air ratio of 0.067).

Tests 13 and 14, using the dimpled liner, were run at fuel-air ratios of 0.055 and 0.063, respectively. Test stand oscillograph data indicated a significantly higher instability on test 14; however, it occurred at a frequency of approximately 1400 Hz. The spectrum analysis range was increased to 0-2000 Hz and the data reduced. The analysis showed peak-to-peak amplitudes of 0.63 psi at 1100 Hz and 0.87 psi at 1400 Hz, while peak-to-peak amplitudes at 230 Hz decreased slightly from those obtained at baseline conditions.

The rig was changed back to the baseline configuration to determine if the high frequency instabilities were inherent at the higher fuel-air ratio or somehow caused by the dimpled liner. Tests 17 and 18 were run at fuel-air ratios of 0.055 and 0.062, respectively. The high frequency instability again occurred during test 18, with peak-to-peak amplitudes of 1.64 psi at 1100 Hz and 0.74 psi at 1470 Hz, which proved that the spontaneous high frequency instabilities were not caused by the dimpled liner.

The porous flameholder (2000-SCFM Rigimesh) was installed in the rig and three tests conducted; test 19 was run at a fuel-air ratio of 0.053, and tests 20 and 21 were run at fuel-air ratios of 0.063 and 0.064, respectively. The high frequency instabilities were not encountered at the high fuel-air ratios, and low frequency (230 Hz) amplitudes from all three tests were significantly higher than any previous tests, with values ranging from 0.91 to 1.84 psi.

The acoustic flameholder (0.125-inch diameter Helmholtz resonators) was mounted in the rig and four tests conducted. Tests 22 and 23 were run at fuel-air ratios of 0.054 and 0.064, respectively. Again no high frequency instability was observed, but average peak-to-peak amplitudes (0.21 to 0.37 psi) were below baseline values at the frequency range of 210-290 Hz. By removing the downstream splitter, the rig was changed to the configuration designed to produce the 250 Hz tangential mode, and test 24 (fuel-air ratio of 0.068) and test 25 (fuel-air ratio of 0.056) were completed. Splitter removal had no effect on the observed natural frequency, with test results from tests 24 and 25 nearly identical to tests 23 and 22, respectively, i. e., no high frequency instability was obtained.

From the preliminary results of tests 13 through 25 it was observed that (1) spontaneous high frequency instability was inherent in the augmentor when operating at stoichiometric conditions with a standard V-gutter flameholder and (2) the high frequency instability could be eliminated by replacing the standard flameholder with either the porous or the acoustic flameholder.

For tests prior to 17, analysis of pressure perturbation decay rates, produced by firing pulse guns, was not providing conclusive results because of initial negative pressure spikes followed by considerable signal drift. On test 17 the passage from the No. 2 Kistler transducer to the combustion chamber was welded closed to determine if the transducers were sensitive to the acceleration caused by the pulse guns firing, which would produce the above results. As shown in figure 61, the negative pressure spike generated by the pulse guns on the No. 2 Kistler trace was similar to the other three transducer signals, indicating a definite acceleration sensitive problem.

As discussed earlier, a survey of alternative dynamic pressure transducers revealed that the 0.190-inch diameter semiconductor strain gage pressure transducers manufactured by Kulite Semiconductor Products, Inc. should be significantly less affected by acceleration because of the extremely small mass of the sensing element. Two of the Kulite transducers were installed in the No. 2 and 4 positions, and two static augmentor tests, i. e., with no flow, were conducted to investigate the feasibility of using the devices. Two pulse guns of 40-grain charge each were simultaneously fired during the first test. A high speed oscillograph trace of the test (figure 62) shows that the Kulite transducers do not have the acceleration sensitivity problem of the Kistler Model 606A transducers.

Because the pulse guns are mounted radially, firing directly across the annulus toward the centerbody, a nondirectional 40-grain bomb was used on the second test to determine if a uniformly directional pulse would minimize the acceleration effect on the Kistler transducers. The bomb (figure 54) was mounted through the No. 1 Kistler location (figure 53) so that the encased charge was completely inside the combustion chamber. The oscillograph trace from this test (figure 63) indicates that the bomb firing caused the Kistler transducer to record the initial negative pressure spike; however, no such effect is evident in the Kulite data. From the results of the static tests, it was concluded that (1) either pulse guns or bombs could be used to disturb combustion, but only the Kulite probes would provide acceptable pressure decay data, (2) either type of transducer could still be used to measure "steady-state" peak-to-peak amplitudes, and (3) all tests in which a pulse gun had been used should be repeated.

The rig in which the acoustic flameholder was still mounted was set up with Kulite transducers in the No. 2 and 4 locations and with Kistler Model 606A transducers in the No. 1 and 3 locations; tests 26, 27, and 28 were conducted with fuel-air ratios of 0.053, 0.066, and 0.064, respectively. Two 40-grain guns were fired during each test. Stand oscillograph data indicated that the Kulite transducers were recording successfully under hot conditions because peak-to-peak amplitudes were approximately the same as those of tests 23 and 25, which were conducted previously with the same rig configuration.

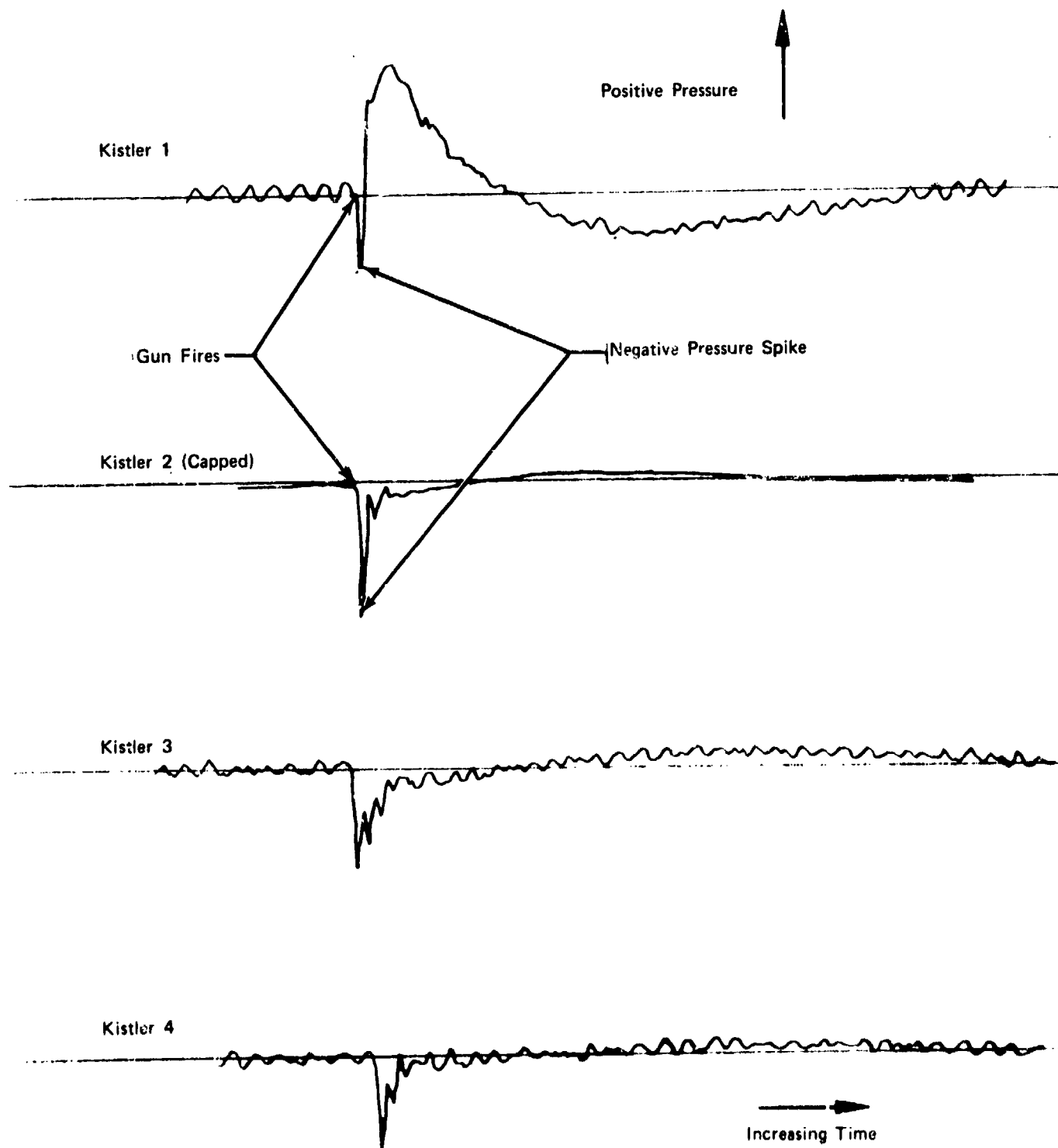


Figure 61. Kistler Oscillograph Trace of Pulse Gun Firing, Test 17

FD 65618

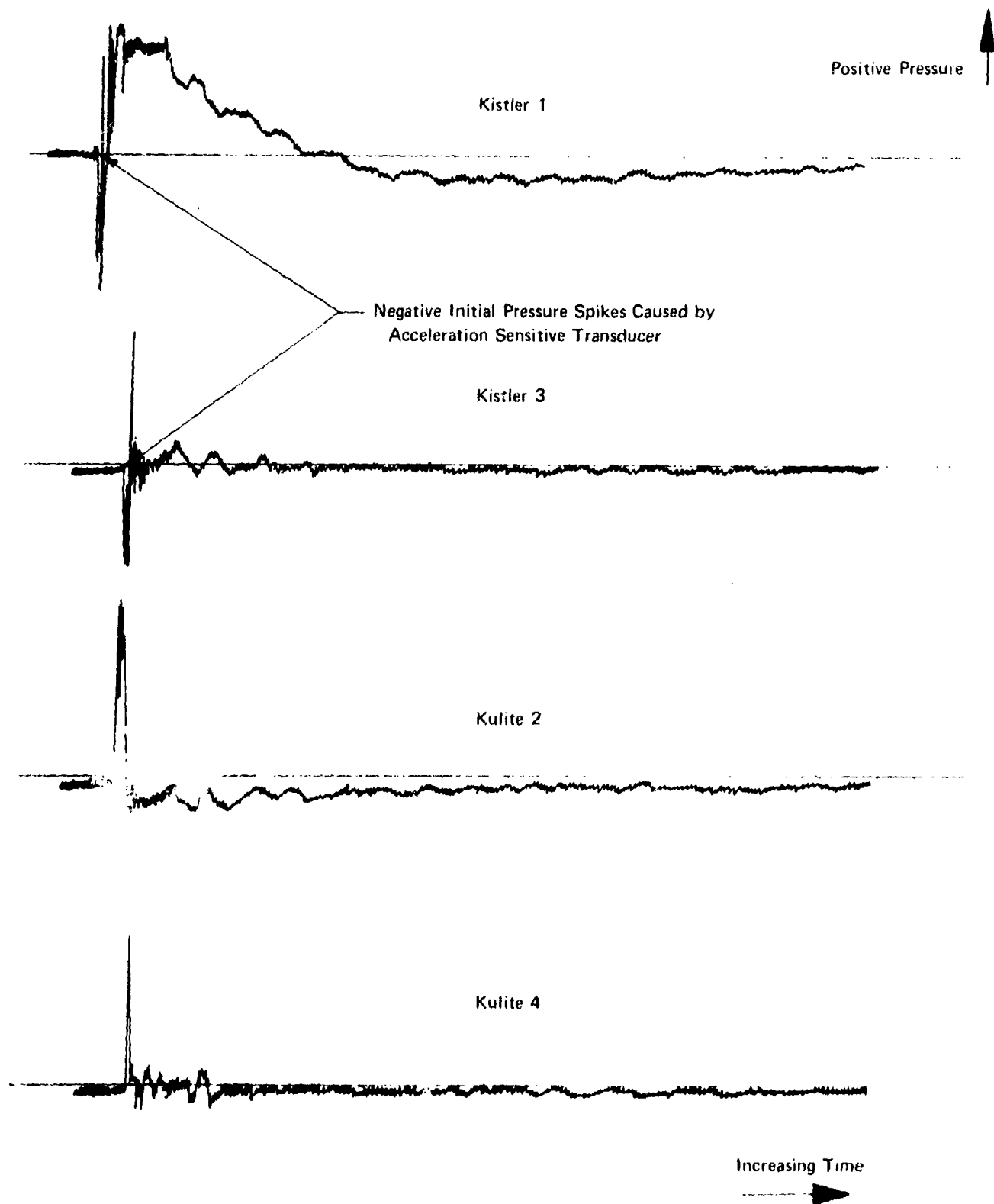


Figure 62. Oscilloscope Trace of Kulite and Kistler Dynamic Pressure Data From Static Pulse Firing Test

FD 65619

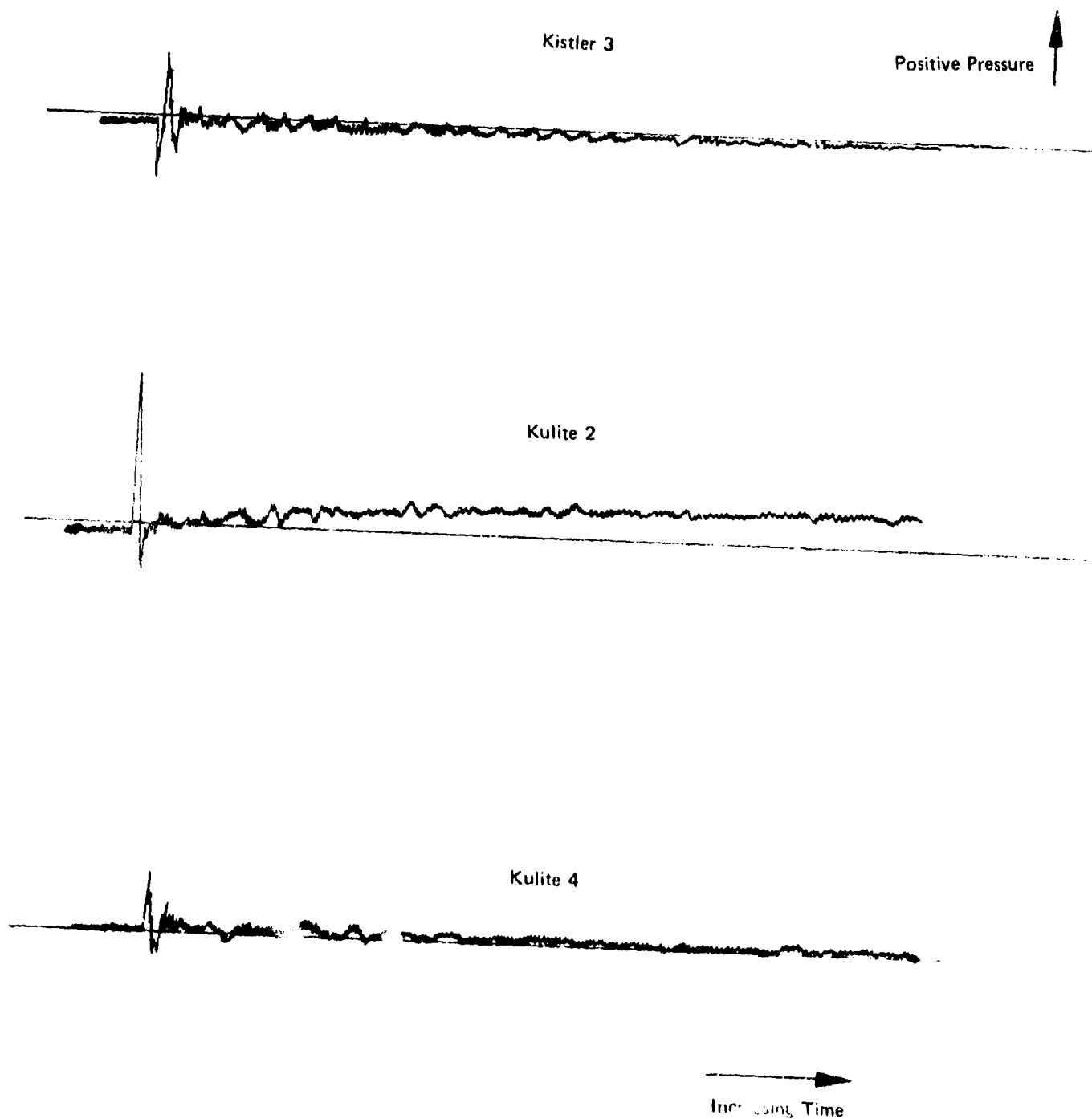


Figure 63. Oscillograph Trace of Static Bomb Firing Test

FD 65620

The complex-porous flameholder was installed in the rig and four tests conducted; tests 29 and 32 at a fuel-air ratio of 0.053 and tests 30 and 31 at fuel-air ratios of 0.064 and 0.065, respectively. Spectrum analysis showed that average peak-to-peak amplitudes from all four transducers at a frequency of 230 Hz ranged from 0.43 psi at the high fuel-air ratios to 1.50 psi at the 0.053 fuel-air ratio, with the highest amplitude of any test to date occurring during test 29 with a value of 6.48 psi. No high frequency instability occurred.

The porous flameholder was mounted in the rig and four tests conducted. Tests 34 and 36 were run at a fuel-air ratio of 0.052; average peak-to-peak amplitudes of 2 psi were recorded at 230 Hz. Peak-to-peak amplitudes of 1.55 and 1.06 psi occurred during tests 35 (fuel-air ratio of 0.062) and 37 (fuel-air ratio of 0.066), respectively. These amplitudes were higher than previous porous flameholder tests (19-21) because data from Kistler transducer No. 2, which had been capped during the earlier tests, was included in the averaged results.

The dimpled liner was installed in the augmentor to determine its low frequency suppression characteristics at the higher amplitude levels obtained with the porous flameholder. Four tests (38-42) were completed. Average peak-to-peak amplitudes were 0.7 psi on test 41 (fuel-air ratio of 0.056) and 0.91 psi and 0.59 psi on tests 40 and 42 (fuel-air ratio of 0.068), respectively. On test 42, a bomb was mounted in the No. 1 Kistler transducer location to produce the pressure perturbations. The Teflon casing containing the explosive (figure 54) was coated with RTV as a heatshield; however, the bomb detonated prematurely while the rig inlet temperature was being set. No further attempts to use bombs instead of pulse guns were made.

The porous flameholder was then replaced with the standard (baseline) flameholder and five tests (45-49) of the dimpled liner were conducted. A third Kulite transducer was added in the No. 3 location prior to test 47. Stand oscillograph data showed a high frequency (above 2000 Hz) instability occurred during every test after test 46. It was observed that, during adjustment of prerun airflow set points, approximately 40% higher preheater fuel flow was required to obtain the desired rig air inlet temperature of 1000°F. The stand run lines were checked for leakage and the flow measuring devices and other instrumentation were verified for accuracy, but no appreciable errors were found. Although the thermocouple used to measure the inlet temperature had checked out acceptably, it was replaced and the rig changed to the baseline configuration. Six tests (50-55) were completed and again the high frequency instability occurred during every test.

An additional inlet air thermocouple was installed in the rig 180 deg from the existing probe and the rig changed to the porous liner configuration. During airflow setup for test 56, the new thermocouple was found to read 150°F higher, and, in addition, when the inlet temperature was adjusted using this probe as the reference, the required preheater fuel flow returned to previous normal levels. The test was conducted at a fuel-air ratio of 0.05 using the new thermocouple as the reference; no high frequency instability occurred. Tests 57-59 were run with inlet temperature referenced similarly, and the high frequency instability appeared only at the high fuel-air ratio, which was the case during original tests. Test 60 was conducted referencing inlet temperature at the original position, with a fuel-air ratio of 0.052. The high frequency instability reappeared, verifying that high inlet air temperature had caused the problem. It is believed that damage

to the burner can of the preheater caused localized inefficient combustion in the area of the old reference probe, which caused the actual inlet temperature on tests 47-55 to be 1150°F rather than the desired 1000°F. The higher inlet temperature resulted in increased reaction rates and the high frequency instability at low fuel-air ratios.

### C. ANALYSIS OF DATA

An analysis of dynamic pressure data was performed to determine the effectiveness of the damping devices for suppressing low frequency combustion instability. The effectiveness of each device was determined by comparing amplitudes and perturbation decay data with similar data from the augmentor in the baseline configuration. Amplitudes were obtained from spectrum analysis of Kistler and Kulite data from each test. A Federal Scientific Model UA6B Real Time Spectrum Analyzer was used to prepare the amplitude-frequency diagrams; typical diagrams are shown in figure 64. Decay rates were determined manually from high speed (40 ips) oscillograph displays of the Kulite data and damping coefficients;  $\lambda_D$  was computed using the method illustrated in figure 65. This parameter is more meaningful than decay time alone for comparing damping effectiveness because it is dependent on both the amplitude of the perturbation spike and the decay time.

#### 1. Pressure Amplitude Data

Amplitude data from the spectrum analyses were averaged for each transducer over the time interval from 4 to 6 sec after ignition and from 8 sec after ignition to shutdown. Data between 6 and 8 sec after ignition were omitted because pulse gun firings occurred during this time. The resulting amplitudes are listed in table 6, along with the cumulative average amplitude from each transducer for each test and the maximum amplitude that occurred during the above time intervals.

The maximum amplitudes of the low frequency (210-290 Hz) instabilities measured with each rig configuration are shown in figure 66. The most effective of all devices tested for suppressing the low frequency instability was the porous liner, which reduced the baseline amplitude levels by approximately one-half to 0.7 psi or slightly less than 5% of combustion pressure. The dimpled liner was almost as effective with a maximum amplitude of 0.8 psi. In figure 67 the averaged amplitudes from all transducers have been graphed as a function of mixture ratio for both liners and the baseline configuration; these data show that the liners were equally effective at all mixture ratios tested.

As shown in figure 66, combustion was most unstable at low frequencies with the complex-porous flameholder and a solid liner. The other two absorbing flameholders also caused maximum amplitudes to be higher than those of the baseline tests. However, all of the absorbing flameholders were extremely effective in eliminating high frequency instability that occurred with an inlet temperature of 1000°F when the baseline configuration was tested at stoichiometric conditions. The instabilities were the result of longitudinal modes set up in the 18-inch long combustion chamber between the flameholder and the nozzle and a complex mixed mode; they occurred at 1100 and 1470 Hz, respectively. The acoustic, porous, and complex-porous flameholders all completely eliminated these instabilities.



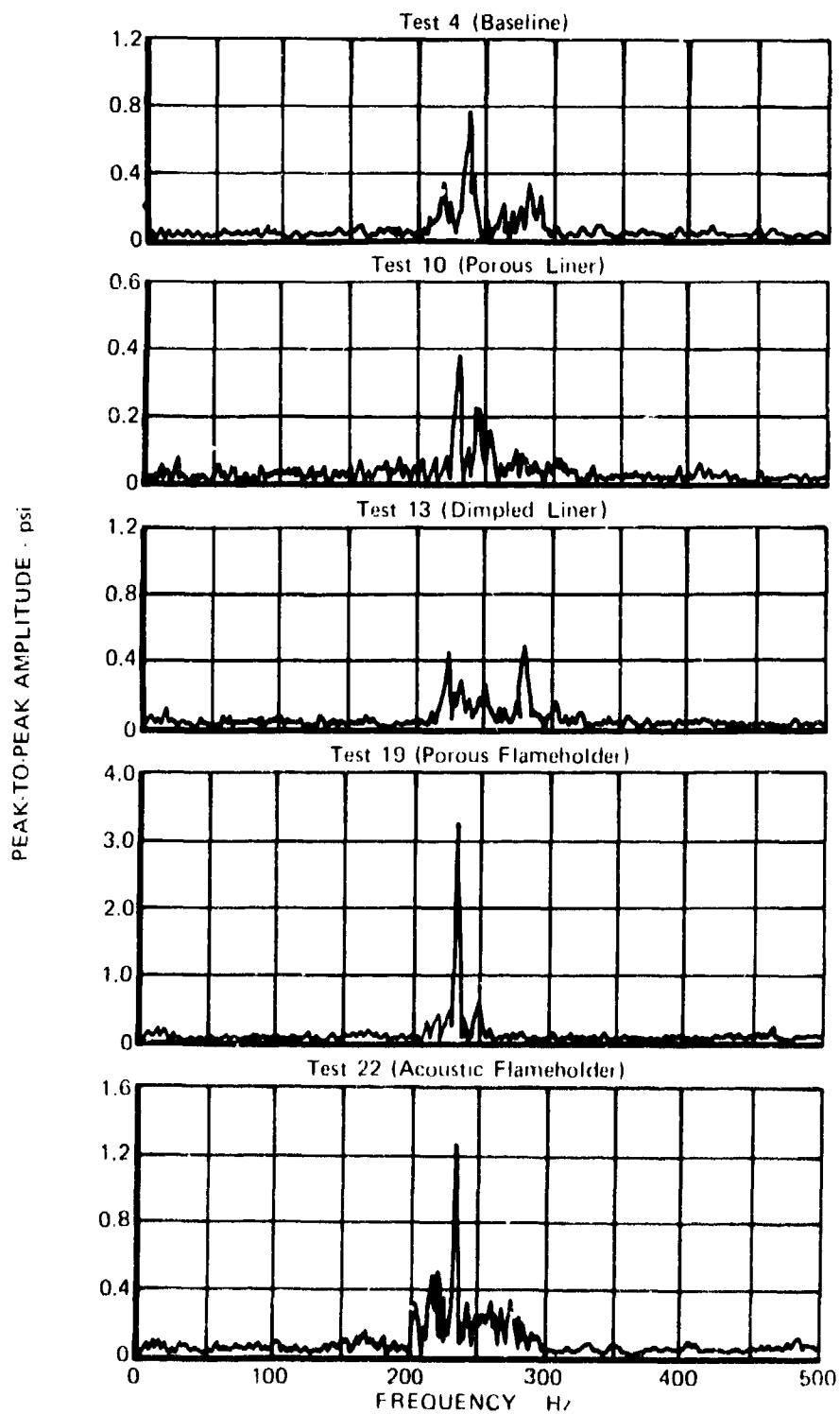
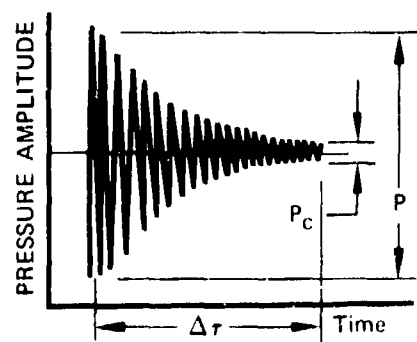
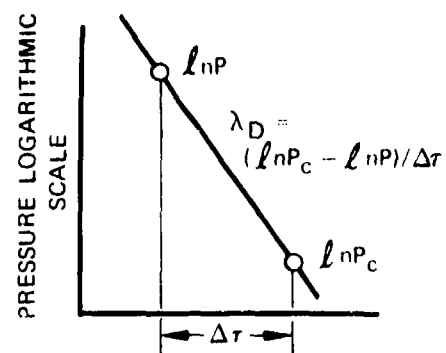


Figure 64. Typical Results From Real Time  
Spectrum Analysis - Frequency  
Range 0-500 Hz, Kistler No. 1

FD 65621



Typical Pressure vs Time Oscillograph Trace for Augmentor Response to an Induced Transient Pulse



Method of Computing Damping Coefficient

Figure 65. Method for Determining Experimental Damping Coefficient ( $\lambda_D$ ) From the Dynamic Pressure Decay Trace

FD 65622

Table 6. Augmentor Simulator Instability Data

| Test No. | Test Type                             | Fuel-Air Ratio | Frequency, Hz | Average Peak-to-Peak Amplitude, psi |            |            |            | Maximum Peak-to-Peak Amplitude, psi |                   |
|----------|---------------------------------------|----------------|---------------|-------------------------------------|------------|------------|------------|-------------------------------------|-------------------|
|          |                                       |                |               | Location 1                          | Location 2 | Location 3 | Location 4 |                                     | All Locations 1-4 |
| 4        | Baseline                              | 0.058          | 210-290       | 0.57                                | 0.43       | 0.37       | 0.53       | 0.48                                | 1.36              |
| 6        |                                       | 0.053          |               | 0.58                                | 0.49       |            | 0.35       | 0.46                                | 0.78              |
| 7        |                                       | 0.061          |               | 0.28                                | 0.32       |            | 0.29       | 0.31                                | 0.65              |
| 17       |                                       | 0.056          |               | 0.21                                | a          | 0.13       | 0.13       | 0.15                                | 0.28              |
| 18       |                                       | 0.064          |               | 0.49                                | a          | 0.13       | b          | 0.31                                | 0.70              |
|          |                                       |                | 1100          | 1.52                                | a          | 1.76       | b          | 1.64                                | 2.97              |
| 8        | Porous Liner                          | 0.055          | 1470          | 0.58                                | a          | 0.90       | b          | 0.74                                | 2.06              |
|          |                                       |                | 210-290       | 0.32                                | 0.30       | 0.22       | 0.28       | 0.28                                | 0.52              |
| 9        |                                       | 0.054          |               | 0.34                                | 0.37       | 0.28       | 0.41       | 0.35                                | 0.70              |
| 10       |                                       | 0.055          |               | 0.22                                | 0.24       | 0.20       | 0.27       | 0.23                                | 0.63              |
| 13       | Dimpled Liner                         | 0.057          |               | 0.33                                | 0.31       | 0.28       | 0.44       | 0.34                                | 0.60              |
| 14       |                                       | 0.066          |               | 0.30                                | 0.32       | 0.19       | 0.28       | 0.27                                | 0.56              |
|          |                                       |                | 1100          | 0.73                                | 0.41       | 0.64       | 0.74       | 0.63                                | 3.2               |
|          |                                       |                | 1470          | 0.93                                | 0.44       | 1.52       | 0.59       | 0.87                                | 2.76              |
| 19       | Porous Flameholder                    | 0.054          | 210-290       | 2.98                                | a          | 0.46       | 2.09       | 1.84                                | 3.95              |
| 20       |                                       | 0.064          |               | 1.15                                | a          | 0.84       | 0.73       | 0.91                                | 1.58              |
| 21       |                                       | 0.065          |               | 1.12                                | a          | 1.27       | 1.08       | 1.16                                | 1.76              |
| 22       | Acoustic Flameholder                  | 0.055          |               | 0.53                                | a          | 0.22       | 0.35       | 0.37                                | 1.27              |
| 23       |                                       | 0.070          |               | 0.27                                | a          | 0.16       | 0.19       | 0.21                                | 0.35              |
| 24       |                                       | 0.069          |               | 0.25                                | a          | 0.19       | 0.19       | 0.21                                | 0.56              |
| 25       |                                       | 0.057          |               | 0.50                                | a          | 0.32       | 0.39       | 0.40                                | 0.80              |
| 26       |                                       | 0.053          |               | 0.91                                | 0.93       | 0.19       | 0.48       | 0.63                                | 1.88              |
| 27       |                                       | 0.066          |               | 0.21                                | 0.16       | 0.21       | 0.18       | 0.19                                | 0.37              |
| 28       |                                       | 0.064          |               | 0.41                                | 0.33       | 0.24       | 0.29       | 0.32                                | 0.63              |
| 29       | Complex-Porous Flameholder            | 0.053          |               | 1.19                                | 2.76       | 0.31       | 1.74       | 1.50                                | 6.48              |
| 30       |                                       | 0.064          |               | 0.28                                | 0.55       | 0.26       | 0.64       | 0.43                                | 1.00              |
| 31       |                                       | 0.065          |               | 0.29                                | 0.54       | 0.24       | 0.64       | 0.43                                | 1.21              |
| 32       |                                       | 0.053          |               | 0.79                                | 1.92       | 0.32       | 1.56       | 1.15                                | 5.58              |
| 34       | Porous Flameholder                    | 0.052          |               | 2.85                                | 2.61       | 0.55       | 1.82       | 1.96                                | 3.58              |
| 35       |                                       | 0.062          |               | 2.04                                | 1.95       | 0.86       | 1.35       | 1.55                                | 2.90              |
| 36       |                                       | 0.052          |               | 2.94                                | 2.65       | 0.68       | 2.06       | 2.08                                | 3.65              |
| 37       |                                       | 0.066          |               | 1.34                                | 1.11       | 0.94       | 0.84       | 1.06                                | 2.55              |
| 38       | Porous Flameholder With Dimpled Liner | 0.054          |               | b                                   | b          | 0.44       | b          |                                     |                   |
| 40       |                                       | 0.068          |               | b                                   | 1.25       | 0.92       | 0.65       | 0.94                                | 2.08              |
| 41       |                                       | 0.056          |               | b                                   | 1.15       | 0.42       | 0.52       | 0.70                                | 1.80              |
| 42       |                                       | 0.068          |               | b                                   | 0.70       | 0.51       | 0.37       | 0.59                                | 1.19              |

|    |       |      |      |      |      |      |      |
|----|-------|------|------|------|------|------|------|
| 42 | 0.068 | b    | 0.70 | 0.51 | 0.37 | 0.59 | 1.19 |
| 45 | 0.062 | 0.61 | 0.40 | 0.25 | 0.26 | 0.38 | 0.88 |
| 46 | 0.051 | 0.35 | 0.25 | 0.18 | 0.24 | 0.26 | 0.48 |
| 47 | 0.063 | 0.10 | 0.10 | 0.08 | 0.09 | 0.09 | 0.14 |
|    |       | 0.36 |      | 0.42 |      | 0.39 | 0.88 |
|    |       | 0.70 |      | 1.09 |      | 0.90 | 2.32 |
|    |       |      |      |      |      |      | 1.05 |
| 48 | 0.062 | 0.11 | 0.09 | 0.09 | 0.09 | 0.09 | 0.14 |
| 49 | 0.051 | 0.10 | 0.10 | 0.10 | 0.10 | 0.10 | 0.12 |
| 50 | 0.050 | 0.09 | 0.12 | 0.08 | 0.09 | 0.10 | 0.12 |
|    |       | 0.52 |      | 0.46 |      | 0.49 | 1.08 |
|    |       | 0.26 |      | 0.50 |      | 0.38 | 1.17 |
|    |       |      |      |      |      |      | 0.83 |
| 51 | 0.053 | 0.10 | 0.11 | 0.09 | 0.10 | 0.10 | 0.14 |
| 52 | 0.053 | 0.10 | 0.12 | 0.10 | 0.10 | 0.10 | 0.16 |
|    |       | 0.37 |      | 0.26 |      | 0.32 | 0.55 |
|    |       | 0.54 |      | 0.78 |      | 0.66 | 1.19 |
|    |       |      |      |      |      |      | 1.60 |
| 53 | 0.064 | 0.12 | 0.12 | 0.09 | 0.09 | 0.10 | 0.14 |
|    |       | 0.45 |      | 0.46 |      | 0.46 | 0.96 |
|    |       | 1.21 |      | 1.57 |      | 1.39 | 2.08 |
|    |       |      |      |      |      |      | 0.64 |
| 54 | 0.064 | 0.11 | 0.11 | 0.09 | 0.08 | 0.10 | 0.15 |
| 55 | 0.053 | 0.11 | 0.12 | 0.10 | 0.11 | 0.11 | 0.15 |
| 56 | 0.053 | 0.23 | 0.23 | 0.15 | 0.20 | 0.20 | 0.44 |
| 57 | 0.063 | 0.44 | 0.39 | 0.27 | 0.16 | 0.32 | 0.75 |
|    |       | 0.10 |      | 0.05 |      | 0.08 |      |
|    |       | 0.06 |      | 0.06 |      | 0.06 |      |
|    |       |      |      | 0.47 |      | 0.47 |      |
| 58 | 0.052 | 0.27 | 0.33 | 0.17 | 0.36 | 0.28 | 0.52 |
| 59 | 0.062 | 0.34 | 0.35 | 0.14 | 0.18 | 0.25 | 0.60 |
|    |       |      |      | 0.35 |      | 0.35 | 0.55 |
| 60 | 0.052 | 0.10 | 0.13 | 0.06 | 0.13 | 0.11 | 0.18 |
|    |       | 0.09 |      | 0.04 |      | 0.06 |      |
|    |       | 0.07 |      | 0.04 |      | 0.06 |      |
|    |       |      |      |      |      |      | 0.69 |

<sup>a</sup> Passage from transducer to combustion chamber plugged to determine acceleration effects.

<sup>b</sup> Transducer did not

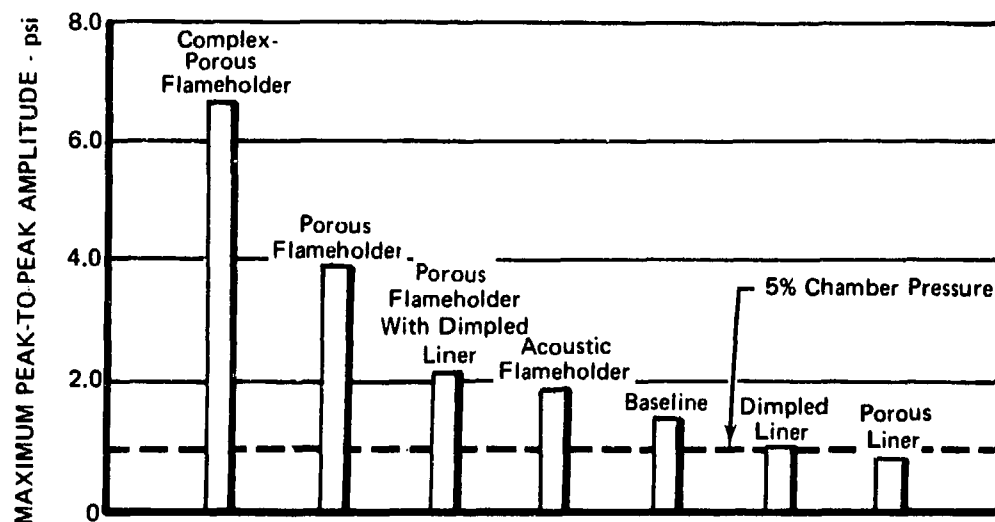


Figure 66. Maximum Low Frequency Amplitudes Measured With Each Augmentor Configuration

FD 65623

Reproduced from best available copy.

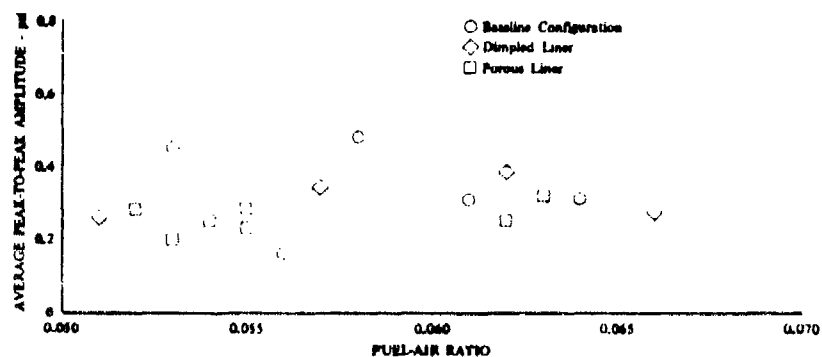


Figure 67. Average Low Frequency Instability Data From Liner and Baseline Tests

DF 92937

A comparison of all averaged amplitudes obtained with the absorbing flameholders, figure 68, shows that the low frequency effectiveness of the porous and complex-porous devices was sensitive to mixture ratio variations with effectiveness increasing as stoichiometric was approached. Instability of the baseline and acoustic flameholder configurations was also less severe as fuel-air ratio approached stoichiometric; however, the increasing stability was not as pronounced as with the porous and complex-porous devices.

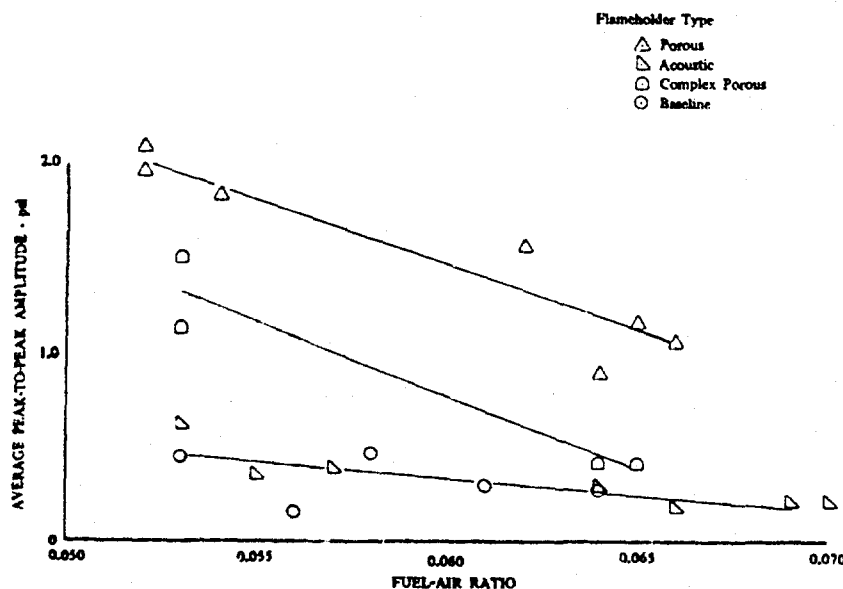


Figure 68. Comparison of Low Frequency Instability Data From Absorbing Flameholder Tests With Baseline Results DF 92938

The most severe test of liner effectiveness occurred when the dimpled liner was used with the porous flameholder. As shown in figure 66, the maximum amplitudes were reduced by the liner from 4 to 2.1 psi. In addition, as shown in figure 69, the effectiveness of the liner was again independent of mixture ratio.

Both of the liners were only quarter annular sections, thus were only one-quarter as effective as a full annular liner such as used in flight augmentors. If the liners had been full annular sections, all maximum low frequency amplitudes recorded in the test program would have been reduced to insignificant levels.

The dimpled and the complex-porous liners were also effective for suppressing high frequency instability, even though they were not designed for good high frequency absorption. The dimpled liner reduced the average amplitude at 1100 Hz from 1.64 psi to 0.63 psi but appeared to have no effect on the 1479 Hz instability. The above longitudinal and complex modes did not appear when the porous liner was tested at fuel-air ratios close to stoichiometric; however, a mode believed to be the first radial did occur at 5400 Hz with an average peak-to-peak amplitude of 0.41 psi. Only data from the Kistler transducer at location 3 were available for analysis of this mode because the other transducers were Kulites, in which signal amplification was possible because of the resonant characteristics of the adapters.

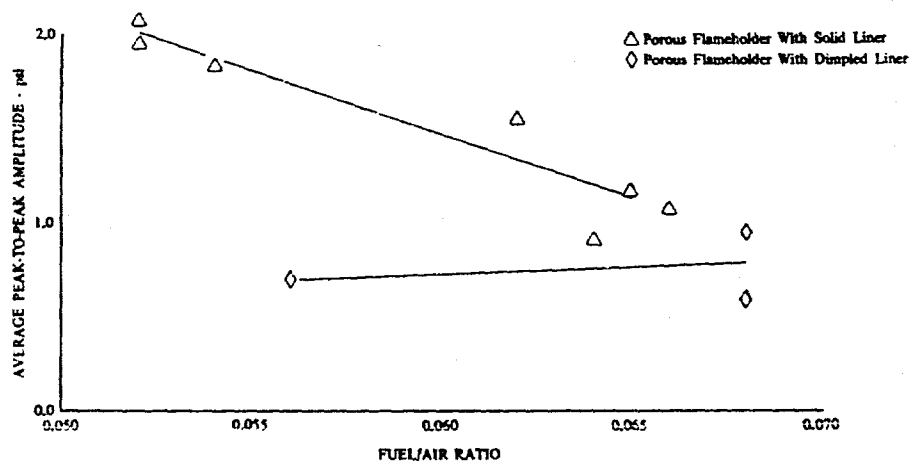


Figure 69. Comparison of Low Frequency Instability Data From Porous Flameholder Tests DF 92939

When rig inlet temperatures were increased to approximately 1100°F (test 47-55), high frequency instabilities occurred with the baseline and dimpled liner configuration regardless of fuel-air ratio. Analysis indicated that longitudinal, mixed, and radial modes were present. The dimpled liner reduced the amplitudes at 1100 Hz from 0.40 psi to 0.16 psi at a fuel-air ratio of 0.052 and from 0.46 psi to 0.39 psi at a fuel-air ratio of 0.063. Amplitudes at 1470 Hz decreased from 0.52 psi to 0.38 psi (fuel-air ratio of 0.052) and from 1.57 psi to 0.90 psi (fuel-air ratio of 0.063). The dimpled liner had almost no effect on the 5200-5800 Hz radial mode. One test at a rig inlet temperature of 1100°F (test 60) was conducted with the porous liner configuration. No longitudinal or mixed modes appeared in this test; however, a radial mode was present with a maximum amplitude of 0.69 psi at 5800 Hz.

## 2. Perturbation Decay Data

As discussed earlier, perturbation decay data were obtained only from Kulite transducers because of the acceleration sensitivity of the Kistler Model 606A transducers. Typical oscillograph records used in the perturbation analysis are shown in figure 70; data shown are from test 30 (complex-porous flameholder) and from test 35 (porous flameholder). The perturbation amplitudes, decay times, and damping coefficient data from all valid tests are listed in table 7.

The high frequency instability occurring during dimpled liner tests 47 and 48 and during baseline tests 50-55 made measurement of the decay times impossible because the low frequency decay was partially obliterated by the high amplitude instability. The high frequency oscillations were removed by filtering the data with a 500 Hz low pass filter, which allowed the low frequency decay to be determined. However, comparison of the resulting decay coefficients with those from identical tests (45 and 46) in which no high frequency instability occurred indicated that the coefficients computed from the filtered data were significantly greater.

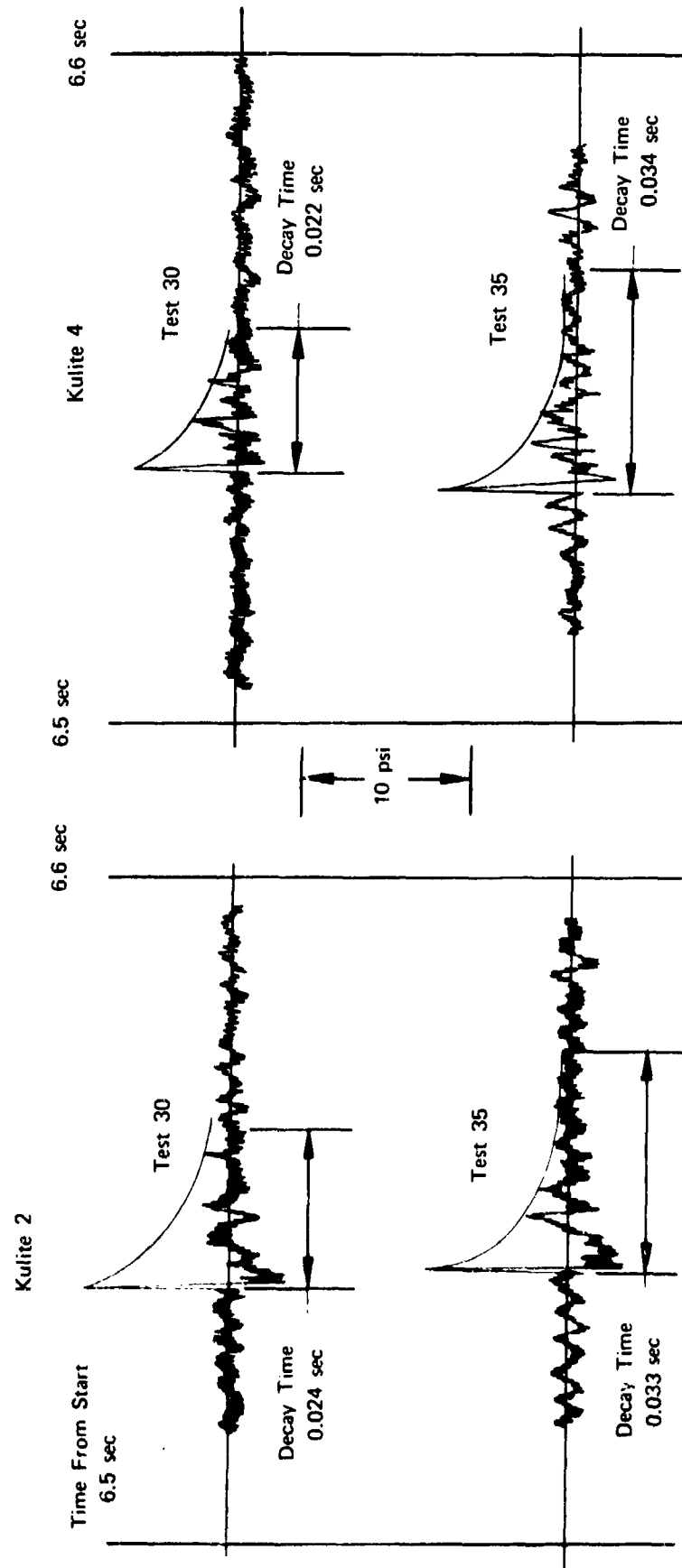


Figure 70. Typical Oscillograph Traces of Pulse Gun Firings

FD 65624



Table 7. Augmentor Pressure Decay Data

| Test No. | Test Type                                  | Kulite Location | Decay Time, sec | Peak-to-Peak Amplitude, psi |                | Damping Coefficient $\lambda D$ |
|----------|--|-----------------|-----------------|-----------------------------|----------------|---------------------------------|
|          |  |                 |                 | P                           | P <sub>c</sub> |                                 |
| 26       | Acoustic Flameholder<br>↓                  | 2               | 0.018           | 13.8                        | 4.0            | 68.8                            |
|          |  | 4               | 0.017           | 14.0                        | 2.0            | 103.8                           |
| 27       |  | 2               | 0.018           | 18.8                        | 2.8            | 105.8                           |
|          |  | 4               | 0.016           | 16.0                        | 2.8            | 108.9                           |
| 28       |  | 2               | 0.017           | 10.8                        | 1.6            | 112.4                           |
|          |  | 4               | 0.019           | 12.0                        | 2.8            | 76.6                            |
| 29       | Complex-Porous Flameholder<br>↓            | 2               | 0.030           | 8.2                         | 2.0            | 47.0                            |
|          |  | 4               | 0.019           | 9.0                         | 1.6            | 91.0                            |
| 30       |  | 2               | 0.024           | 12.4                        | 2.2            | 72.1                            |
|          |  | 4               | 0.022           | 8.0                         | 2.0            | 63.0                            |
| 31       |  | 2               | 0.020           | 17.8                        | 2.4            | 100.3                           |
|          |  | 4               | 0.021           | 8.8                         | 1.6            | 78.9                            |
| 32       | Porous Flameholder<br>↓                    | 2               | 0.020           | 14.4                        | 2.4            | 89.5                            |
|          |  | 4               | 0.023           | 9.2                         | 2.2            | 62.2                            |
| 35       |  | 2               | 0.033           | 9.4                         | 1.8            | 41.3                            |
|          |  | 4               | 0.034           | 15.4                        | 1.6            | 66.6                            |
| 36       |  | 2               | 0.034           | 8.4                         | 2.4            | 36.9                            |
|          |  | 4               | 0.026           | 10.4                        | 2.8            | 40.0                            |
| 37       | Porous Flameholder With Dimpled Liner<br>↓ | 2               | 0.030           | 12.2                        | 2.2            | 57.0                            |
|          |  | 4               | 0.036           | 15.0                        | 2.7            | 47.6                            |
| 40       |  | 2               | 0.022           | 13.6                        | 1.4            | 103.4                           |
|          |  | 4               | 0.023           | 6.6                         | 0.8            | 91.7                            |
| 41       |  | 2               | 0.024           | 13.2                        | 1.6            | 87.9                            |
|          |  | 4               | 0.024           | 13.5                        | 1.5            | 91.6                            |
| 45       | Dimpled Liner<br>↓                         | 2               | 0.028           | 13.0                        | 1.7            | 72.6                            |
|          |  | 4               | 0.017           | 9.8                         | 1.0            | 134.2                           |
| 46       |  | 2               | 0.022           | 13.8                        | 2.0            | 87.8                            |
|          |  | 4               | 0.020           | 11.4                        | 2.0            | 87.0                            |
| 47*      |  | 1               | 0.016           | 19.0                        | 1.6            | 154.4                           |
|          |  | 4               | 0.019           | 13.0                        | 1.0            | 134.7                           |
| 48*      | Baseline<br>↓                              | 1               | 0.018           | 12.0                        | 1.6            | 111.7                           |
|          |  | 4               | 0.019           | 8.5                         | 1.2            | 103.2                           |
| 50*      |  | 1               | 0.015           | 9.1                         | 1.0            | 147.3                           |
|          |  | 2               | 0.017           | 9.0                         | 0.6            | 159.4                           |
|          |  | 4               | 0.021           | 4.7                         | 1.0            | 73.8                            |
| 52*      |  | 1               | 0.028           | 14.8                        | 1.0            | 92.8                            |
|          |  | 2               | 0.030           | 6.9                         | 0.8            | 71.7                            |
| 53*      |  | 1               | 0.021           | 14.8                        | 1.6            | 105.7                           |
|          |  | 2               | 0.021           | 5.7                         | 0.4            | 126.7                           |
|          |  | 4               | 0.016           | 4.7                         | 0.5            | 140.0                           |

\*Data from tests 47-54 were filtered (500 Hz low pass).

Table 7. Augmentor Pressure Decay Data (Continued)

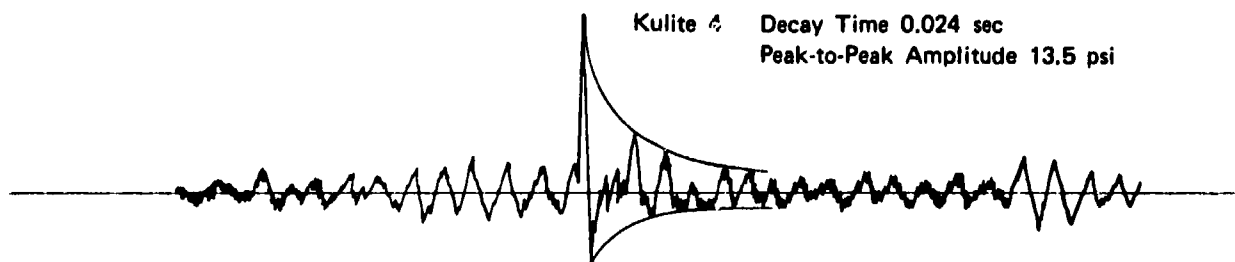
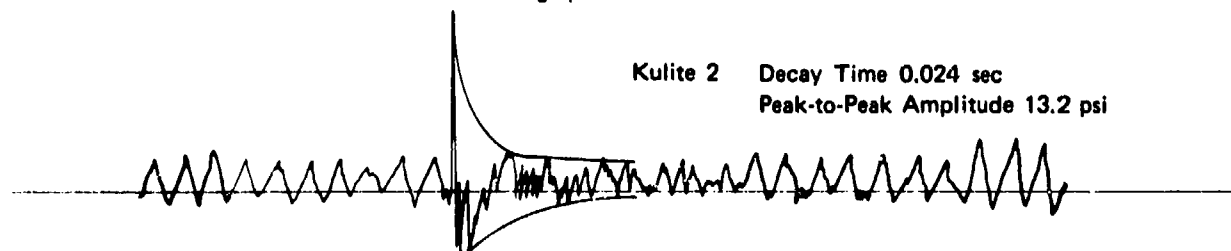
| Test No. | Test Type         | Kulite Location | Decay Time, sec | Peak-to-Peak Amplitude, psi |                | Damping Coefficient $\lambda D$ |
|----------|-------------------|-----------------|-----------------|-----------------------------|----------------|---------------------------------|
|          |                   |                 |                 | P                           | P <sub>C</sub> |                                 |
| 54 *     | Baseline<br>↓     | 1               | 0.015           | 6.5                         | 1.2            | 112.7                           |
|          |                   | 2               | 0.019           | 6.0                         | 0.8            | 105.8                           |
|          |                   | 4               | 0.016           | 4.1                         | 0.6            | 120.0                           |
| 56       | Porous Liner<br>↓ | 1               | 0.020           | 14.2                        | 2.0            | 98.0                            |
|          |                   | 2               | 0.017           | 14.5                        | 1.9            | 119.5                           |
|          |                   | 4               | 0.017           | 8.9                         | 1.0            | 128.6                           |
| 57       | ↓                 | 1               | 0.017           | 20.0                        | 2.3            | 127.2                           |
|          |                   | 2               | 0.032           | 13.9                        | 1.8            | 102.2                           |
|          |                   | 4               | 0.017           | 15.0                        | 1.7            | 128.1                           |
| 58       | ↓                 | 1               | 0.016           | 10.7                        | 1.0            | 148.1                           |
|          |                   | 2               | 0.016           | 20.8                        | 1.0            | 189.7                           |
|          |                   | 4               | 0.022           | 8.8                         | 1.2            | 117.2                           |
| 59       | ↓                 | 1               | 0.018           | 19.8                        | 1.6            | 139.8                           |
|          |                   | 2               | 0.018           | 22.4                        | 1.6            | 164.9                           |
|          |                   | 4               | 0.015           | 10.4                        | 2.0            | 109.9                           |

\*Data from tests 47-54 were filtered (500 Hz low pass)

Similar filtering was conducted on data from test 41 (which had no high frequency instability) to determine reasons for the data inconsistencies. Figure 71 is a comparison of filtered and unfiltered oscillograph data from test 41. It shows that decay times were unaffected by filtering, but the amplitude of the initial pressure spike was significantly reduced from 13.2 and 13.5 psi to 5.4 and 9.2 psi when frequencies above 500 Hz were eliminated. The resulting damping coefficient is increased from 89.8 to 104.1 by the filtering process. For this reason, coefficients from filtered data were excluded from further analysis.

The results of the perturbation analysis in the form of averaged damping coefficients for each rig configuration and fuel-air ratio are summarized in table 8. The configuration with the highest coefficient, and thus the most stable at low frequencies, was the porous liner followed by the dimpled liner, which is consistent with the results from the analysis of the amplitude data. The most unstable configuration based on damping coefficients was the porous flameholder, while amplitude data showed the complex-porous flameholder to be most unstable. Except for the porous liner, the damping coefficients for each configuration from tests with near stoichiometric conditions were greater than those run at lower fuel-air ratios.

Test 41 Oscillograph Trace - Unfiltered



Test 41 Oscillograph Trace - 500 Hz Low Pass Filter

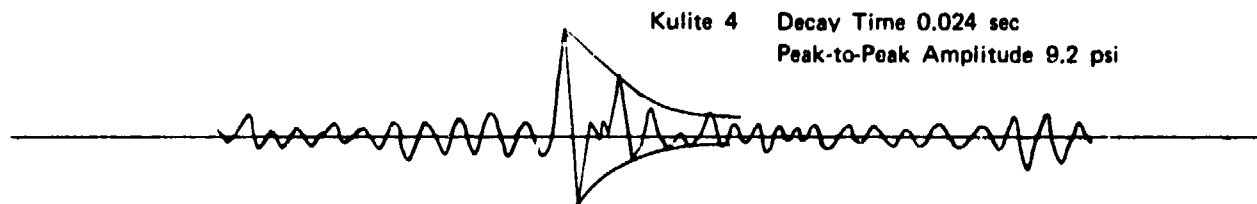
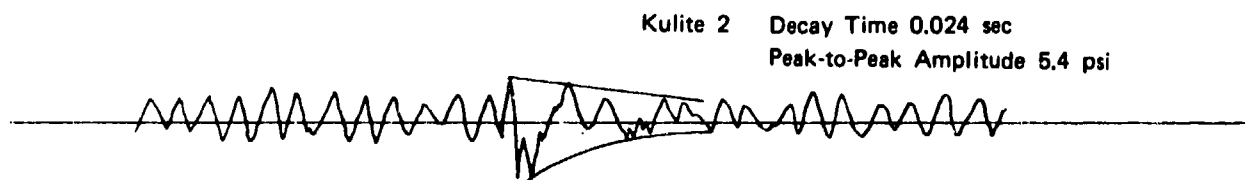


Figure 71. Comparison of Effects of Frequency Filtering on Decay Time and Peak Amplitude

FD 65789

Table 8. Average Damping Coefficients From Perturbation Analysis

| Rig Configuration                     | Fuel-Air Ratio, Nominal |       |
|---------------------------------------|-------------------------|-------|
|                                       | 0.054                   | 0.065 |
| Acoustic Flameholder                  | 86                      | 101   |
| Complex-Porous Flameholder            | 72                      | 79    |
| Porous Flameholder                    | 39                      | 53    |
| Porous Flameholder With Dimpled Liner | 90                      | 98    |
| Dimpled Liner                         | 87                      | 103   |
| Porous Liner                          | 134                     | 129   |

### 3. Liner Cavity Gas Temperatures

Liner cavity gas temperatures are generally found to be strongly affected by the stability of the combustion process. In unstable systems the cavity temperature quickly approaches that of the combustion gases, while in stable systems it is always much lower, the actual value depending on the amount and type of cooling employed. Results from the augmentor liner tests were no exception. As shown in figure 72, the porous liner (the most stable configuration) had the lowest temperatures, while the dimpled liner (the next most stable) had higher temperatures and the porous flameholder/dimpled liner configuration (the most unstable liner configuration) had the highest temperatures. The data indicate that with either liner no supplementary cooling would be necessary.

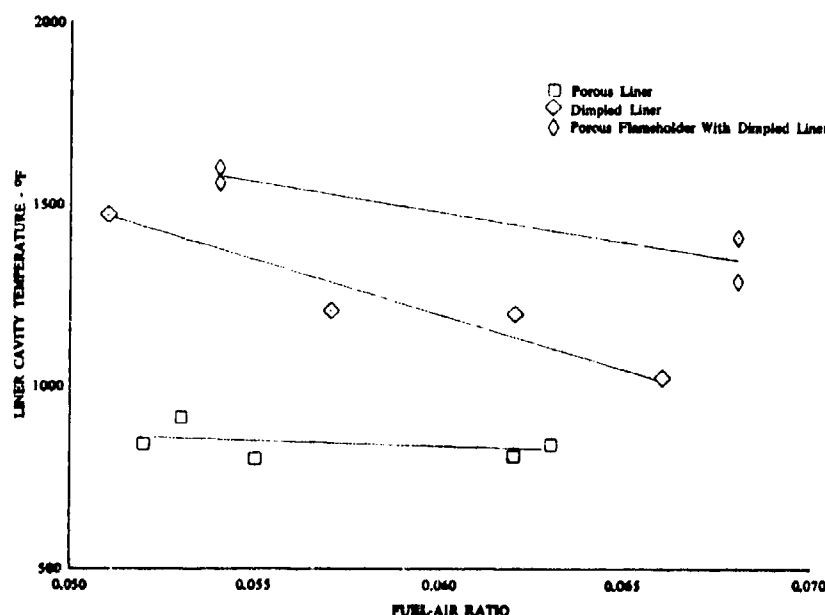
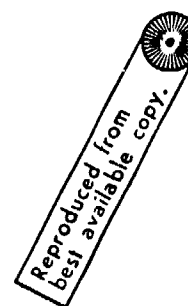


Figure 72. Comparison of Liner Cavity Gas Temperature

DF 92940



The porous liner cavity temperatures were independent of fuel-air ratio, but all dimpled liner temperatures were lower near stoichiometric. This indicates, as did the amplitude and decay coefficient data, that the augmentor was more stable at the higher mixture ratios.

#### 4. Conclusions and Recommendations

Analysis of the augmentor test data shows that the rig was spontaneously unstable with frequencies less than 300 Hz when operated at design point conditions with no damping devices. Both the dimpled liner and the complex-porous liner significantly reduced the amplitudes of the instability. Data from pulse gun firings and cavity temperature probes confirmed the effectiveness of the liners. Augmentor combustion was also unstable in several modes having frequencies in the range 1000 to 1500 Hz. The liners, although not designed to do so, were also effective in reducing the amplitude of these modes. The high frequency instability was completely eliminated by each of the three absorbing flameholders that were tested in place of the standard V-gutter of the baseline configuration. The absorbing flameholders were not effective for suppressing the low frequency instability; the devices actually made the amplitudes of the low frequency instability higher than that of the baseline configuration.

As noted during the test program, reaction rates were a significant factor affecting levels of instability. It is believed that in an augmentor, instability is propagated by pockets of unburned fuel and air along the flame front that are detonated prematurely when excited by impinging pressure waves. The igniting pockets produce new pressure waves that reflect off chamber walls to propagate, and if in phase, amplify the condition. If a centrifugal component can be imparted to the gas stream before it enters the combustion zone, the pockets of unburned reactants will be dissipated by the improved mixing, possibly resulting in a more inherently stable combustor. It is recommended that effects of centrifugal force fields on augmentor combustion stability characteristics be investigated; one method of accomplishing this might be to install turning vanes in the augmentor simulator and conduct additional tests. It is also suggested that the range of study be extended to investigate the effects on stability of chamber pressures typical of augmentor operation at sea level, i. e., 30 psia with a choked nozzle.

Reproduced From  
Best Available Copy

## REFERENCES

1. Beranek, Leo L., "Acoustic Impedance of Porous Materials," Journal of the Acoustical Society of America, Volume 13, page 248, 1942.
2. "Acoustic Liner Design and Demonstration," Final Report, Pratt & Whitney Aircraft, AFRPL-TR-71-75, 28 August 1971.
3. Fisher, J. I. and A. R. Erickson, "Properties of Fiber Metal Acoustically - Resistive Materials," Huyck Metals Company, November 1966.
4. "A Study of the Suppression of Combustion Oscillations With Mechanical Damping Devices," Phase II Summary Report, Pratt & Whitney Aircraft, PWA FR-1922, 15 July 1966.
5. "A Study of the Suppression of Combustion Oscillations With Mechanical Damping Devices," Summary Report of Tasks III through VI, Pratt & Whitney Aircraft, PWA FR-1115, 28 November 1964.
6. "Suppression of Combustion Oscillations With Mechanical Damping Devices," Phase II Interim Report, Pratt & Whitney Aircraft, PWA FR-3880, June 1970.
7. "A Study of the Suppression of Combustion Oscillations With Mechanical Damping Devices," Final Report, Pratt & Whitney Aircraft, PWA FR-2596, November 1967.
8. "Suppression of Combustion Oscillations With Mechanical Damping Devices," Final Report, Pratt & Whitney Aircraft, PWA FR-4993, June 1972.
9. Ingard, U., "On the Theory and Design of Acoustic Resonators," Journal of the Acoustical Society of America, Volume 25, No. 6, November 1953.